University of Tennessee, Knoxville

TRACE: Tennessee Research and Creative Exchange

Doctoral Dissertations

Graduate School

8-2009

Forecasting Dose and Dose Rate from Solar Particle Events Using Locally Weighted Regression Techniques

Theodore Franklin Nichols
University of Tennessee - Knoxville

Follow this and additional works at: https://trace.tennessee.edu/utk_graddiss

 Part of the Nuclear Engineering Commons

Recommended Citation

Nichols, Theodore Franklin, "Forecasting Dose and Dose Rate from Solar Particle Events Using Locally Weighted Regression Techniques. " PhD diss., University of Tennessee, 2009.
https://trace.tennessee.edu/utk_graddiss/77

This Dissertation is brought to you for free and open access by the Graduate School at TRACE: Tennessee Research and Creative Exchange. It has been accepted for inclusion in Doctoral Dissertations by an authorized administrator of TRACE: Tennessee Research and Creative Exchange. For more information, please contact trace@utk.edu.

To the Graduate Council:

I am submitting herewith a dissertation written by Theodore Franklin Nichols entitled "Forecasting Dose and Dose Rate from Solar Particle Events Using Locally Weighted Regression Techniques." I have examined the final electronic copy of this dissertation for form and content and recommend that it be accepted in partial fulfillment of the requirements for the degree of Doctor of Philosophy, with a major in Nuclear Engineering.

L. W. Townsend, Major Professor

We have read this dissertation and recommend its acceptance:

J. W. Hines, T. Handler, J. P. Hayward

Accepted for the Council:

Carolyn R. Hodges

Vice Provost and Dean of the Graduate School

(Original signatures are on file with official student records.)

To the Graduate Council:

I am submitting herewith a dissertation written by Theodore Franklin Nichols entitled "Forecasting Dose and Dose Rate from Solar Particle Events Using Locally Weighted Regression Techniques." I have examined the final electronic copy of this dissertation for form and content and recommend that it be accepted in partial fulfillment of the requirements for the degree of Doctor of Philosophy, with a major in Nuclear Engineering.

L. W. Townsend, Major Professor

We have read this dissertation
and recommend its acceptance:

J. W. Hines

T. Handler

J. P. Hayward

Accepted for the Council:

Carolyn R. Hodges, Vice Provost and Dean
of the Graduate School

(Original signatures are on file with official student records.)

Forecasting Dose and Dose Rate from Solar Particle Events Using Locally Weighted Regression Techniques

A Dissertation
Presented for the
Doctor of Philosophy
Degree
The University of Tennessee, Knoxville

Theodore Franklin Nichols
August 2009

Copyright © 2009 by Theodore Franklin Nichols.

All rights reserved.

Dedication

This dissertation is dedicated to my parents, Trent and Sally Nichols, who always believed in me and worked hard to give me this opportunity and to my wife, Stacey, for her love.

Acknowledgments

Without the help of many individuals, this research would not of been possible. I would like to thank Dr. Thomas Handler of the University of Tennessee Department of Physics and Dr. Jason Hayward of the University of Tennessee Department of Nuclear Engineering for agreeing to be on my dissertation committee. A special thanks to Dr. Wesley Hines, also of the Nuclear Engineering Department, for his assistance and expertise in locally weighted regression and modeling techinques in general. I would also like to thank Dr. Lawrence Townsend, my committee chair and faculty advisor, for his guidance of my graduate studies and for providing me the opportunity to work on this research. A thank you to my parents Trent and Sally Nichols and my sister Frances whose constant love, support, and encouragement helped me to strive for exellence. My wife Stacey, for her love, support, and unwavering belief in me. To God and Jesus Christ for being the foundation of my life. There are many other friends and family members who have helped me to make this dissertation possible.

Abstract

Continued human exploration of the solar system requires the mitigating of radiation effects from the Sun. Doses from Solar Particle Events (SPE) pose a serious threat to the health of astronauts. A method for forecasting the rate and total severity of such events would give time for the astronauts to take actions to mitgate the effects from an SPE. The danger posed from an SPE depends on dose received and the temporal profile of the event. The temporal profile describes how quickly the dose will arrive (dose rate). Previously developed methods used neural networks to predict the total dose from the event. Later work added the ability to predict the temporal profiles using the neural network approach. Locally weighted regression (LWR) techniques were then investigated for use in forecasting the total dose from an SPE. That work showed that LWR methods could forecast the total dose from an event. This previous research did not calculate the uncertainty in a forecast. The present research expands the LWR model to forecast dose and temporal profile from an SPE along with the uncertainty in these forecasts.

Forecasts made with LWR method are able to make forecasts at a time early in an event with results that can be beneficial to operators and crews. The forecasts in this work are all made at or before five hours after the start of the SPE. For 58 percent of the events tested, the dose-rate profile is within the uncertainty bounds. Restricting the data set to only events less than 145 cGy, 86 percent of the events are within in the uncertainty bounds. The uncertainty in the forecasts are large, however the forecasts are being made early enough into an SPE that very little of the dose will have reached the crew. Increasing the number of SPEs in the data set increases the accuracy of the forecasts and reduces the uncertainty in the forecasts.

Contents

List of Tables

List of Figures

1 Introduction

Space exploration whether manned or unmanned requires understanding of the space weather environment. Continued excursions into the Solar System have resulted in Astronauts being in space for longer periods of time. On April 12, 1981 NASA launched the first Space shuttle [21]. Since then there have been more than 126 shuttle flights [21]. The International Space Station (ISS) has a minimum crew of two and a maximum crew of three with plans to expand the crew to a maximum of seven. On March 3, 2009 the cumulative crew time was over 3043 person-days [20]. Longer shuttle missions and longer time aboard the ISS have increased the amount of time astronauts are exposed to the space weather environment. Soon NASA and the other world wide space agencies will not be to be the only ones concerned with the risks of space flight. Space Tourism is starting to become a reality. Companies like Virgin Galactic are currently preselling tickets for space flights [41]. The start of space tourism will lead to more people entering space and flight crews logging more time in space. As more people enter space, especially civilians, the demand to make space travel safe will increase.

People and astronauts spending longer periods of time in space increase the probability of exposure to radiation released from a Solar Particle Event(SPE), sometimes referred to as Solar Energetic Particles (SEP). The term SPE will be used over SEP for the remaining of this paper. Starting in October 2000 to May 2002 there were six expeditions launched to the ISS [11]. The crew stay times varied during this time period with a minimum time of 128 days (expedition three) and a maximum time of 195 days (expedition four). During this time span there were four significant SPEs (Nov. 8, 2000, Sept. 24, 2001, Nov. 4, 2001 and Nov. 21, 2001) and two smaller SPEs (Oct. 1, 2001 and April 21, 2002) [11].

During the August 1972 SPE the dose rate behind one g cm^{-2} of aluminum shielding exceeded the

ICRP low-dose-rate limit of 10 cGy per hour [12] for 18.9 hours to the skin and eight hours for the bone marrow [34]. During the same time period that dose rates were exceeded the skin would have received 14.8 Gy and the bone marrow 0.6 Gy [34]. Even during solar maximum the likelihood of a large event or multiple large events is small; however, they do occur and with an intensity that could pose health threats [11, 44]. Currently determining what actions to take when the detection of SPE occurs is done by relying on the decision of NASA analysts. Giving these analysts a tool for forecasting the dose-time profiles and total dose with some knowledge of the uncertainties would greatly increase NASA's abilities to protect astronauts.

1.1 Past Work in SPE Forecasting

Initially, forecasting sunspot number and geomagnetic indices were explored. While these values give a good idea of how active the sun is, they are not required to accurately predict space weather [7]. Proton and heavy ion fluences are important for SPE forecasts when radiation protection is the focus. Therefore, past and current research focuses on the forecasting of doses caused by protons emitted from an SPE. It was believed that most of the hazardous particles from an SPE came with the initial shock from a coronal mass ejections (CME) [35]. Reames estimated that there was a window of approximately 12 hours to predict the intensity of the event before the shock wave reached Earth's orbit [35]. Therefore, intial attempts to forecast SPEs focused on predicting the dose from the shock wave. Further research indicates that predicting when the shock wave will arrive would not always prevent the astronauts from receiving a dose that exceeds the 30-day limit [24]. Therefore, forecasters will need to give information about the dose prior to the shock to space mission planners in order to provide adequate radiation protection. Forecasting the dose-time profile is important in providing all the information needed by space mission planners.

Past research and this work are based on flux data obtained from Geostationary Operational Environmental Satellites (GOES). The reason for using flux data is that there are currently no

dosimeters in positions to obtain dose readings from SPEs in deep space. Figure 1 shows the fluxes from an SPE starting on April 21, 2002 (All figures and tables are located in the appendix). This plot only shows fluxes for protons above 10 MeV. Although the proton flux is much larger for protons with energies below 10 MeV (for this event the maximum flux for protons with energy less than 5 MeV was 4350 ions/(cm^2 s sr)) protons above 30 MeV present the larger radiation threat. Protons with energies below 10 MeV will not penetrate a typical space craft. Looking at Figure 1 a peak is very noticeable, this peak is usually associated with the CME shock arrival.

In current and previous research, one uses the fluxes/fluence to calculate the dose. Actual measurement of the dose values would have been used if they were available. Determining the dose from proton fluxes requires the use of a transport code. The code used in this work is BRYNTRN. BRYNTRN is a deterministic transport code that was developed by NASA at Langley Research Center [43]. BRYNTRN is one-dimensional code capable of transporting protons, neutrons, deuterons, tritons, helions, and alphas [43]. The code was developed primarily to make dose calculations from SPEs [43]. BRYNTRN calculates dose by analytically solving the Boltzmann transport equation in one dimension.

Past research started with the parameterization of the dose profiles from a SPE [45]. thus allowing the temporal relationships in the data to be more accurately modeled. A TDNN has a constant time delay between each input. Figure 3 shows a diagram of generalized TDNN. Note that each input D(t) is delayed by n-1 time steps.

TDNN techniques have been used in several studies for predictions of solar observables [6] and for recognition of sequence patterns [5]. Conway et al, used a month as the delay constant for their feed-forward multi-layer network which predicted sunspot numbers.

Another type of TDNN is a sliding time delay neural network (STDNN). A STDNN has a varying time delay between each input [8, 39]. This allows the STDNN to make new predictions each time a new input arrives. The prediction is made with the new input plus a few of the past inputs. Since the time delay is variable, the network is able to make a prediction each time an input is received. Recall that the dose function is given as D(t). Allowing for n input neurons in the network and a delay time of τ, and given the dose function, the first input neuron acquires data from D(t), the second from D(t-τ) and so forth until the final input neuron which acquires data from D(t-(n-1)τ) [8, 39]. Figure 4 shows a diagram of a sliding time delayed neural network.
The ability of an STDNN to handle temporal data is the reason it was chosen as the type of neural network to predict dose time-profiles. The architecture for the network used is as follows:

- 1 input layer with 5 input neurons
- 1 hidden layer with 10 neurons and a hyperbolic tangent activation function
- 1 output layer with 1 neuron and a linear activation function

These choices were used because previous work had shown this architecture to be the most effective [11]. However, the number of neurons in the hidden layer was changed depending on the events used to train the network. The number of neurons used was determined by optimizing the networks to produce the best results. The user did the optimization of the network. The STDNN method was improved to provide dose profiles before a certain dose level was reached [27]. The STDNN method, still had some speed and accuracy issues. Therefore, a locally weighted regression (LWR) technique was developed to predict the parameter D_∞ [27].

1.2 Objective

In this work, for the first time, LWR techniques are applied to the forecasting of dose-time profiles from a solar particle event. Uncertainty of the forecast of the dose-time profiles is calculated with each forecast. The MATLAB software package is used for programming the LWR techniques.

The work herein includes the methods for calculating dose from fluences, parameterizing the time-dose profile with a Weibull function, the LWR method for predicting each of the three Weibull parameters, and the uncertainty in the forecast. Appendix A contains plots of 60 SPEs with forecasts made at 50 minutes, 1.67, 2.5, 3.33, 4.167, and 5 hours from the start of the event. The forecasts were made with a "leave-one-out" testing method. Appendix B contains plots of 49 SPEs with forecasts made at 50 minutes, 1.67, 2.5, 3.33, 4.167, and 5 hours from the start of the event. The SPEs used for making these forecasts were only SPEs that had a total dose less than 145 cGy. The forecasts were made using a leave one out method on the reduced data set.

1.3 Impact and Originality

Forecasting or predicting of dose-time profiles from a SPE has been accomplished previously with neural networks and Bayesian inference techniques [11, 25, 27]. Past work using LWR methods focused only on forecasting the total dose received from a SPE. Predicting the dose rate from an event is just as important as predicting the total dose received. Uncertainties in the forecasts give a good idea of how accurately the method is able to forecast the dose-profile from a particular event.

This research is an extension of research on using LWR methods for forecasting the total dose from a SPE. This work differs from previous work in that it forecasts the overall dose-time profile and gives the uncertainty in the forecast [27–29]. The forecasting of the dose-time profile gives operators information about both the length of time from the start of an SPE until the maximum dose from that SPE is received, and it gives them knowledge of the dose-rate along with an uncertainty estimate in the forecast. This knowledge will allow activities such as space walks to be better planned and executed. Potentially as the age of space tourism starts, this knowledge will help in the planning of trips to provide better safety for space tourists.

2 Space Radiation Environment

When astronauts leave Earth to explore the solar system, there are many threats known and unknown that they must face. Most of these threats are manageable either by the crew or by ground based mission control. There is a threat, however, that neither mission control nor the crew can control: bombardment by energetic space radiation. People on the Earth are protected from these energetic heavy charged particles by the Earth's magnetic field and a thick atmosphere. Astronauts usually only have the shielding provided by their spacecraft or, on space walks, only the protection of their space suit. Neither offers much shielding to high energy ions. Near Earth there are three naturally occurring sources of space radiation: the Van Allen belts, galactic cosmic rays (GCR), and solar particle events (SPEs). Table 1 shows relevant information about the particles and energies constituting space radiation [37]. In the table, HZE is an ancronym for high-Z, high-energy particles and LET is Linear Energy Transfer. Outside of Earth's magnetic field GCR and SPEs remain potential radiation hazards.

2.1 Van Allen Belts

Van Allen belts were discovered in 1958 by James Van Allen and collaborators using detectors on Explorer I [2]. The belts are composed of protons and electrons trapped by the Earth's magnetic field. The Van Allen belts are composed of two belts aligning the radiation with the magnetic field lines of the Earth [26]. Figure 5 shows a depiction of the Van Allen belts. The inner radiation belt is primarily where protons are trapped. The energy range for particles trapped by the Van Allen Belts are shown in table 1 under the trapped column. Electrons are trapped in the outer radiation belt. The energy range of the trapped charge particles range from a few thousand electron volts to a few million electron volts. Appreciable charged particle flux begins between approximately 300 km to 1000 km above Earth's surface [26]. However, the maximum intensity occurs around 4000 km for the inner belt and 16000km for the outer belt. The outer belt extends to about 55,000 km

above the Earth's surface [26]. The radiation trapped in the Van Allen belts comes from the solar wind, SPEs, and the decay of albedo neutrons. The radiation trapped in the Van Allen belts is what produces the Aurora Borealis and the Aurora Australis [31].

2.2 Galactic Cosmic Rays

Galatic Cosmic Ray (GCR) refers to radiation that originates somewhere outside of the solar system, possibly from supernova explosions. The GCR was first discovered in 1912 by Victor Hess. Hess discovered that an electroscope discharged quicker when ascending in a balloon. He attributed the effect to radiation entering the atmosphere from space and received the 1936 Nobel prize for his discovery [15].

The flux from the GCR is isotropic throughout the solar system. All known naturally occurring elements have been found in the GCR. The elemental composition of cosmic rays are: 89% hydrogen, 10% helium, and about 1% heavier ions [15]. These elemental isotopes account for about 98% of the cosmic rays. The remaining 2% is composed of electrons and positrons [11]. The GCR is a constant source of radiation and therefore, doses received from the GCR remain fairly constant over time.

2.3 Solar Particle Events

Humans probably saw the effects of solar particle events (SPEs) many years ago when they noticed changes in the size and color of the aurora borealis. Scientists, in the 1940s, conducting experiments in ionization chambers, noticed a change in the background noise of their experiments [13]. The connection was made that changes in the number of charged particles in the ionization chambers were due to charged particles being released from the sun [13]. The concern caused by a SPE is that some SPEs have particles with intensities several orders of magnitude higher than the GCR [9].

There are two known sources for SPEs: solar flares and coronal mass ejections (CME). Solar flares emit light over a large part of the electromagnetic spectrum and typically emit a high gamma flux [19]. They occur when built up magnetic energy is suddenly released [19]. Figure 6 shows a solar flare image taken by the Solar and Heliospheric Observatory (SOHO) spacecraft. An image of Earth relative to the size of the solar flare is shown to give a perspective about size. CMEs are large pockets of gas threaded with magnetic field lines [16]. The gas is ejected from the Sun over the course of several hours. The first observations of CMEs were made using a coronagraph on the seventh Orbiting Solar Observatory (OSO7) between 1971 and 1973 [16]. Figure 7 is a picture of a CME taken from SOHO. Analysis of SPEs from different sources has concluded that CMEs are the prime source of events where there are major intensity increases of accelerated particles [3].

When ionizing radiation is emitted from a SPE, protons and heavy ions that have high enough fluxes and energies can pose a serious health risk to astronauts. Most SPEs are of no radiation protection concern. This is due to a low peak flux, a soft energy spectrum or because the particles are emitted in a trajectory away from any manned spacecraft. Here, soft energy spectrum refers to a distribution where the flux of higher energy particles decreases quickly with increasing particle energy. However, some SPEs are very large events, which create a radiation protection concern [36]. SPEs are related to the approximate 11-year cycle of activity of the sun and usually occur near maximum solar activity. However, they have also occurred during periods of minimum solar activity. Empirical data dating back to the mid 1700's have indicated evidence of such a cycle (see Figure 8). Sunspots represent a local change in the magnetic field of the sun. Sunspots appear typically as two spots, one representing the north side and the other the south side of the magnetic field. Solar flares typically occur along the neutral line that divides the magnetic field lines of north and south. Therefore, increases in the number of sunspots leads to an increase in the number of solar flares [19]. The frequency of CME occurance is also related to the sunspot cycle. Near solar maximum an average of 2 to 3 CMEs per day are observed and at solar minimum the rate drops to

an average of 1 per week [16]. The next solar maximum is expected to occur in 2011 give or take one year [19].

Specifically this research deals with how to forecast the resulting dose produced from a Solar Particle Event (SPE). Protons and heavy ions pose a large threat to the health and safety of astronauts. During a SPE large numbers of these particles can be released. Therefore, the goal of forecasting the dose-profile is to give an accurate enough prediciton to allow ground-based mission control to make a determination of the potential health threat a SPE poses.

3 Health Risks from Ionized Particles

The concern arising from a SPE is to estimate what kind of an effect the charged particles will have on a astronaut. Interactions of ionized particles cause different types of biological effects depending on different attributes of the charged particles. Energy, number of particles (flux), length of exposure and type of particle all contribute to the damage caused to tissue. Further complicating matters, certain cells are more radiosensitive than other cells.

The goal of space radiation protection is to enable long-term or permanent human presence in space without incurring unacceptable health risks [37]. The accomplishment of this goal requires: (1) predicting health risk accruing due to exposure of humans to radiation in space; (2) identifying risks not seen or not seen at comparable doses, with exposure to terrestrial sources of occupational exposure; (3) predicting these health risks with sufficient accuracy to enable space missions to proceed with substantial assurance that radiation limits will not be exceeded; and (4) reducing radiation risk by operational measures, radiation shielding, and discovery of biological countermeasures [37]. Meeting the above goals requires an understanding of what the threats are. This chapter is a brief overview of what threats to crews are posed by radiation from solar particle events.

3.1 Biological Effects

Radiation is assumed to effect biological systems through both direct and indirect interactions [40]. Direct effects are caused by the initial physical interaction between the radiation and the biological material. Indirect effects are caused by the chemical interactions of free radicals, which were formed by the interaction of tissue with radiation [40]. DNA is considered to be the primary target of concern for either type of radiation [32]. Damage to DNA occurs as either a single-strand or double-strand break. A single-strand break is where only one side of the DNA is broken, the other side remains intact. Cells are better able to successfully repair damage caused by a single-strand

break [1]. Double-strand breaks are were both strands of DNA are broken. A double strand break results in at least two fragments of DNA. Double-strand breaks are more difficult for a cell to correctly repair since the repair mechanisms have the possibility of repairing DNA in the wrong order. If the cell puts the DNA back together in the wrong order this will lead to either apoptosis (cell death), inactivation of the cell, or the creation a of cancerous cell.

Ionizing radiation is thought to produce 1000 single-strand and 25-40 double-strand breaks per diploid per gray [32]. Diploid, is defined as a cell that has the full number of chromosomes for a particular species. Human diploid cells have 46 chromosomes. Table 2 shows the physical and biological stages of ionizing radiation along with the approximate time scale of each process. Physical and chemical stages are completed as early as $\sim 10^{-12}$s and as late as $\sim 10^{-6}$s after an interaction with ionizing radiation has occurred. The biological stages happen over a much longer period of time. Stochastic biological effects: cataracts, cancer, and genetic effects in offspring, do not show symptoms until years after exposure [40]. A persons genetic predisposition contributes to what stochastic effects exposure to ionizing radiation may have on a particular individual [37].

3.2 Radiation Protection

The National Council on Radiation Protection and Measurements (NCRP) defines the goal of radiation protection as:

> The goal of radiation protection is to prevent the occurrence of serious radiation-induced conditions (acute and chronic deterministic effects) in exposed persons and to reduce the stochastic effects in exposed persons to a degree that is acceptable in relation to the benefits to the individual and to society from the activities that generate such exposures. *[23]*

This statement separates radiation-induced effects into two broad categories: deterministic and stochastic. A deterministic effect is defined as a somatic effect which increases in severity with increasing radiation dose above a threshold dose [23] . The increasing severity is caused by an increasing number of cells being damaged. A large dose of radiation is necessary to cause deterministic effects. Deterministic effects may occur "early", within a few hours or days; or "late" effects, occurring months or years after exposure (see Table 2 [40]).

Stochastic effects occur in a statistical manner and usually take many years after the time of exposure develop [40]. In this case the probability of occurrence, but not the severity of the effect increases with increasing dose. Cancers, cataracts and genetic effects in offspring are types of stochastic effects. The statistical nature of stochastic effects makes determining who will contract a disease from a particular exposure to radiation and who will not impossible [40]. Complicating the issue is that there are other sources of carcinogens along with a natural incidence of cancer. Cancer risks varies with geographic location and/or lifestyle [33]. Therefore, it is difficult to determine the risk caused by a particular exposure to radiation.

3.3 Exposure Limits

Exposure limits for space operations are defined by NASA. The space-permissible exposure limit (SPEL) is design to prevent in-flight risks that jeopardize mission success and limit chronic risks to acceptable levels [22]. Acceptable levels are based on moral, ethical, financial, and legal concerns. Balancing these concerns by reducing the radiation risks is accomplished using the As Low As Reasonably Achievable (ALARA) principle. The ALARA principle is a legal requirement, designed to ensure astronaut exposures do not approach radiation limits and that such limits are not considered as "tolerance values" [22]. The career exposure limit is set so as to not exceed 3% Risk of Exposure-Induced Death (REID) for fatal cancer [22]. Table 3 lists different orgrans with their coresponding 30 day, 1 year, and career non-cancer effects dose limits. The abbreviations BFO and CNS are for blood forming organs and central nervous system respectively.

4 Dose Calculations

Currently there is no easy access to direct dosimetric measurements in space. Therefore, this work will depend on doses calculated from flux values. The flux values are obtained from the Geostationary Operational Environmental Satellite (GOES) satellites. The resulting dose values are calculated using BRYNTRN, a transport code developed by NASA.

4.1 Flux Data

Flux data are obtained from GOES via the Space Physics Interactive Data Resource (SPIDR) [38]. SPIDR is maintained by National Geophysical Data Center (NGDC) which is part of National Oceanic and Atmospheric Administration (NOAA). GOES satellites are in geosynchronous orbit at the equatorial plane of the Earth [30]. The satellites are approximately 22,000 miles above the surface of the Earth and are used for atmospheric measurements along with measuring Space Environmental Monitor (SEM) [30]. The SEM instrument package has the capabilities to provide magnetometer, energetic particle and soft x-ray data. This research only uses the energetic particle data.

The proton fluence provided by GOES has a sampling rate of five minutes. The proton fluence is given in units of [ions/cm^2-sec-ster]. The flux data were downloaded as an ASCII file from SPIDR with the following energy channels: >1 MeV, >5 MeV, >10 MeV, >30 MeV, >50 MeV, >60 MeV, and >100 MeV. If there is an error in one of the measurements a value of $1x10^{33}$ is assigned for the sampling interval. The first step in processing the flux data is to "smooth" out these errors. Typically there is only a few of these detector errors together. A cubic spline interpolation with the last good value before and after the points of error as endpoints is used here. For example an event on February 6, 1986 had the following flux values around one of these type errors: 394, $1x10^{33}$, $1x10^{33}$, $1x10^{33}$, $1x10^{33}$, 409. After applying the cubic spline interpolation the values were:

394, 397, 400, 403, 406, 409. These detection errors do not occur often. In the event used here the number of missing values were 0.43% of the data points.

The flux values in the >10 MeV, >30 MeV, >50 MeV, and >100 MeV channels are integrated. The fluxes are then integrated over the five-minute sampling time and multiplied by the spherical 4π steradians. This yields a cumulative omnidirectional (isotropic) proton fluence, for each energy channel, with units of ions per cm^2. This cumulative fluence is used for the calculation of the dose-time profiles.

Let J be the values for the isotropic integral fluence as obtained from GOES. Each five-minute time interval is parametrized using an exponential rigidity function with the following form:

$$J = J_0 e^{-R/R_0} \tag{1}$$

$$R = \frac{(E^2 + 2mc^2E)^{\frac{1}{2}}}{e} \tag{2}$$

Where J_0 has units of ions per cm^2, R is the proton rigidity (2) with units of momentum per unit charge and R_0 has units of (GV). The J_0 and R_0 values are fitting parameters obtained using least-squares regression. J_0 and R_0 describe the input spectra in a way that enables the BRYNTRN code to calculate the resulting dose.

4.2 Charged Particle Transport

Obtaining dose values for a given fluence of protons requires the use of computer code. All doses in this research were transported through 1 g/cm^2 of water. Water was chosen since human tissue is primarily water. The value 1 /cm^2 was chosen because it is the lowest thickness of water BRYNTRN will handle, this speeds up the calculation of the dose. Since the research is only concerned if the methods are able to forecast the dose, more shielding would just increase calculation time without

adding any benefit. Therefore, the dose calculated should be close to what the dose would be in tissue. Second, the calculation of dose for this research was done using codes based on charged particle transport theory.

The transport code chosen was BRYNTRN. BRYNTRN is a baryon transport computer code which uses a straight ahead approximation of the Boltzmann equation for which energy changing processes are handled, but all propagation occurs along a fixed path [42]. The use of BRYNTRN was just to obtain doses similar to doses that would be measured if proper dosimetry were available to make the input dose measurements. The dose-time profile has the general form seen in Figure 2.

4.3 Dose Parameterization

This research uses a Weibull function to parameterize the dose-time profile. This is the same parameterization used in past research [11, 27, 45]. The parameterization works well for many different types of SPEs though it does not characterize all of them well [46]. However, since only one parameterization can be used with the LWR methods at a given time, the Weibull function was chosen since it parmeterizes more SPEs events than other functions explored. The Weibull function used has the following form:

$$D(t) = D_\infty(1 - e^{-(\alpha t)^\gamma}) \tag{3}$$

Where:

D(t) $\equiv$ Dose at time t

$D_\infty \equiv$ Asymptotic dose which is equal to the cumulative dose received from a SPE [cGy]

$\alpha \equiv$ Fitting parameter [inverse time]

$\gamma \equiv$ Fitting parameter [dimensionless]

The Weibull parameter D_∞ is the asymptotic dose for the event, which is taken to be the maximum dose+0.2 cGy. The other two parameters (α, γ) are calculated by using a curve fit. The curves are fitted by linearizing the functional form for the cumulative dose equation (4).

$$ln(-ln(1 - \frac{D}{D_\infty})) = \gamma ln(t) + ln(\alpha) \tag{4}$$

The intercept is $ln(\alpha)$ and the slope is γ. With the 3 parameters a smooth dose profile curve is created. Figure 9 shows the Weibull fit for an SPE on April 21, 2002.

5 Locally Weighted Regression Model

Locally Weighted Regression (LWR) is a memory-based algorithm and is a non-parametric model [10]. The "locally" part of the name indicates that this regression model does not use a global model, but rather relies on local models created as the algorithm runs [14]. When a query is made, past data exemplars are recalled. The algorithm locates similar training exemplars, then performs a weighted regression only with the local observations [10]. Local here is determined by how close the observations are to the query point.

The LWR model starts with the following linear regression model:

$$\overrightarrow{Y} = \mathbf{X}\overrightarrow{\beta} + \overrightarrow{\epsilon} \tag{5}$$

Where:

$\overrightarrow{Y}$ is a (n x 1) vector containing the response variable

$\mathbf{X}$ is a (n x p) matrix containing predictor variables where the columns are the variables and the rows are the samples

$\overrightarrow{\beta}$ is a (p x 1) vector containing the regression coefficients that linearly combine the predictors to form the response

$\overrightarrow{\epsilon}$ is a (n x 1) vector containing the prediction errors

$\overrightarrow{Y}$ is defined as the forecasted value for one of the three Weibull parameters at time t: D_∞(t), α(t), or γ(t). The input matrix $\mathbf{X}$ consists of the sliding-time delayed doses from previous SPEs.

Each of the Weibull parameters has its own LWR model as defined in equations (6), (7), and (8).

$$\overrightarrow{D_\infty}(t)_{forecast} = \mathbf{D}\overrightarrow{\beta}_{D_\infty} + \overrightarrow{\epsilon}_{D_\infty} \tag{6}$$

$$\overrightarrow{\alpha}(t)_{forecast} = \mathbf{D}\overrightarrow{\beta}_{\alpha} + \overrightarrow{\epsilon}_{\alpha} \tag{7}$$

$$\overrightarrow{\gamma}(t)_{forecast} = \mathbf{D}\overrightarrow{\beta}_{\gamma} + \overrightarrow{\epsilon}_{\gamma} \tag{8}$$

For brevity, only the method using the notation for α, will be derived. It should be understood that the equivalent methods are applied in forecasting the other two parameters. Optimal estimators for the regression coefficients, β, are calculated by minimizing the sum of squares of the errors (SSE) between the model prediction and the actual response.

$$SSE = \sum_{i=1}^{n}(\alpha_i - \hat{\alpha}_i)^2 \tag{9}$$

Where $\hat{\alpha}_i$ contains the estimates of α_i. Solving equation (7) for ϵ and then substituting into equation (9) results in equation (10).

$$SSE = \sum^{n}(\alpha - \mathbf{D}\hat{\beta}_{\alpha})^2 \tag{10}$$

Solving for $\hat{\beta}_{\alpha}$:

$$\hat{\beta}_{\alpha} = (\alpha - \sqrt{SSE})(D)^{-1} \tag{11}$$

Assuming that SSE is zero, solve for $\hat{\beta}_{\alpha}$. $\mathbf{D}^{-1}$ is calculated using a Moore-Penrose pseudo-inverse where m>n for a (m x n) matrix (12).

$$\mathbf{D}^{-1} = (\mathbf{D}^T\mathbf{D})^{-1}\mathbf{D}^T \tag{12}$$

Solving for $\hat{\beta}_{\alpha}$

$$\hat{\beta}_{\alpha} = (\mathbf{D}^T\mathbf{D})^{-1}\mathbf{D}^T\alpha \tag{13}$$

The estimator for α at a query point q can be written as:

$$\hat{\alpha}(q) = q\hat{\beta}_{\alpha} = q(\mathbf{D}^T\mathbf{D})^{-1}\mathbf{D}^T\alpha \tag{14}$$

Up to equation (14) the derivation has been a traditional linear regression. LWR is a method which relies on a weighted regression. Therefore, the model is weighted by minimizing a weighted SSE function (15).

$$SSE(q) = \sum_{i=1}^{n} (\alpha_i - \mathbf{D}_i \hat{\beta})^2 K(d(x_i, q)) \tag{15}$$

Where:

D_i are training points

q is the query point

x_i are doses

d is a euclidean distance function

K is a kernel weighting function

The euclidean distance function used is shown in equation (16).

$$d(x, q) = \sqrt{\sum_{j} (x_j - q_j)^2} \tag{16}$$

In equation (16) j is the dimension of the vector. The kernel function K used in this work is a Gaussian function (17). σ is the kernel bandwidth.

$$K(d) = e^{-\left(\frac{d(x,q)^2}{\sigma^2}\right)} \tag{17}$$

Solving equation (15) for $\hat{\beta}$:

$$\hat{\beta} = (\mathbf{D}^T \mathbf{W}^T \mathbf{W} \mathbf{X})^{-1} \mathbf{D}^T \mathbf{W}^T \alpha \tag{18}$$

$$w_{ii} = \sqrt{K(d(x_i, q))} \tag{19}$$

Therefore, the weighted solution for the estimator $\hat{\alpha}$ at a query point q is found using equation

(20).

$$\hat{\alpha}(q) = q\hat{\beta} = q(\mathbf{D}^T\mathbf{W}^T\mathbf{W}\mathbf{X})^{-1}\mathbf{D}^T\mathbf{W}^T\alpha \tag{20}$$

Implementing an LWR method requires: optimizing the kernel bandwidth σ, selecting training data, and testing on a known event. The kernel bandwidth determines how close a training point needs to be to a query point to allow it to influence the predicition. Figure 10 is a graphical representation of the LWR technique. If the kernel is too large, then non-linear points will be included in the fit. If the kernel is too small then some points that are part of the local linearity will be excluded from the fit. The kernel is optimized to find the best "width" by finding a value for σ that results in a kernel of the right size.

Take equation (20) and apply it to each of the three Weibull parameters (D_∞, α, and γ), resulting in equations (21),(23), and (22):

$$\hat{D}_\infty(q) = q(\mathbf{D}^T\mathbf{W}^T\mathbf{W}\mathbf{X})^{-1}\mathbf{D}^T\mathbf{W}^T\mathbf{D}_\infty \tag{21}$$

$$\hat{\gamma}(q) = q(\mathbf{D}^T\mathbf{W}^T\mathbf{W}\mathbf{X})^{-1}\mathbf{D}^T\mathbf{W}^T\gamma \tag{22}$$

$$\hat{\alpha}(q) = q(\mathbf{D}^T\mathbf{W}^T\mathbf{W}\mathbf{X})^{-1}\mathbf{D}^T\mathbf{W}^T\alpha \tag{23}$$

$\hat{D}_\infty(q)$, $\hat{\alpha(q)}$, and $\hat{\gamma(q)}$ are the forecasted values of respective parameter at a query point q. Here q is at a some time from the beginning of the event. Each forecast at a specific q, corresponds to a forecast made a certain time from the beginning of the event. Letting q=T, where T=0 is the start of the SPE, the forecast of the dose-time profile and dose is made using equation (24).

$$\hat{D}(t) = \hat{D}_\infty(T)\left(1 - e^{-(\hat{\alpha}(T)t)^{\hat{\gamma}(T)}}\right) \tag{24}$$

The resulting $\hat{D}(t)$ is the forecast of the dose-time profile made at some time T from the start of

the event.

5.1 Uncertainty in Forecasts

Knowing the uncertainty in the forecast of the dose-time profile is important. First, it allows a method of estimating just how accurate are the forecasts. Second, in a real world use, it allows an operator to make a more informed decision. This research is working toward a system that will be used with inputs from a dosimeter. Therefore, the errors in flux measurements and calculation of dose values is not taken into consideration. The uncertainty of concern is how uncertain is the prediction of each Weibull parameter and from that obtain the uncertainty in the forecast of the dose-time profile.

The standard deviations for D_∞, α, and γ are calculated based on a Gaussian normal distribution. Since each parameter has a unique standard deviation, calculating the total uncertainty for the forecast must take the error of each parameter into consideration. We use a Monte Carlo method to simulate 10,000 forecasts with the values of D_∞, α, and γ chosen randomly from a distribution of possible values. Taking the average of all the simulations is then used as the uncertainty in the forecast, thereby allowing the plotting of error bars for a given forecast.

6 Results

The data set used to make forecasts contains 60 historical SPE events. Plotting the 60 SPEs on one graph shows how the size, dose-rate, and total dose varies between SPEs (see Figure 11). The largest total dose for any of these events is 1436.1 cGy and the smallest is 1 cGy. Looking at the plot, it is apparent that the dose rate does not correlate to the size of an event. Some events with a large total dose, start with a small dose rate. Figure 12 is a histogram showing the distribution of D_∞ values for the data set. The histogram shows that the majority of events are less than 145 cGy. There is also a gap between 570 and 1000 cGy were there are no representative SPEs in the data set. That gap combined with the small number of large events makes forecasting SPEs over 145 cGy difficult. There are 49 SPEs out of the 60 that have a total dose less than 145 cGy.

6.1 Forecasts with 60 Past Events

Looking at a SPE that occured on April 21, 2002. Figure 13 shows the dose received from the SPE. The dose for this event rises to a total dose of 223.1 cGy. It takes about 64 hours from the start of the event for the dose to reach its maximum value. Figure 14 is a plot showing six forecasts made for this SPE. The first forecast shown is made 50 minutes from the start of the event. Table 4 has the predicted value for each parameter and the associated percent error. Fifty minutes from the start of the event the predicted D_∞ is 155.94 cGy. This value is 30% different than the actual D_∞. However, 50 minutes from the start of the event the received dose is 1.99 cGy. This means that the method is forecasting that the event will be significant, but the forecast is made before enough particles have arrived to give a significant dose. A significant dose is one that would be close to or over the NASA limits (see Table 3) [22]. The 30 day dose limit for skin is 1500 mGy-Eq, this limit is reached 22 hours from the start of this SPE. Therefore, the method would give the crew 21 hours and 10 minutes to take actions to mitigate exposure before reaching the 30 day dose limit for skin. The forecast closest to the actual dose-time profile was made 3.33 hours from the start of

the event. The prediction of D_∞ at this time is 234.87 cGy or just 2% from the actual value. The other two parameters have errors of approximately 1% and 7% for α and γ respectively. Again at 3.33 hours from the start of this event the received dose is 15 cGy or 150 mGy, well below the 30 day dose limit for skin. Also, the forecasts at 1.67, 2.5, 3.33, 4.167, and 5 hours all have dose rate profiles that closely match the actual dose rate profile. This gives crews knowledge of how fast the dose is arriving from a particular event. Forecasts of the dose-rates are because the percent error for the α and γ parameters with one exception is below 10% (see Table 4). The parameters α and γ control the dose rate of the forecasts.

Figure 15 plots the forecast calculated 50 minutes from the start of the event along with the uncertainty of the forecast. The uncertainty is calculated for a 95% confidence interval. The uncertainty in this forecast, while large, does contain the actual dose-time profile within its range. The forecast made at 50 minutes only included about 2 cGy, or less than 0.89% of the total dose, as input. Figure 16 is a plot of the forecast and uncertainty made 3.33 hours from the start of the event. Of the forecasts made within the first 5 hours of this event, the one made at 3.33 hours was the closest to accurately forecasting the dose-rate and the total dose. Looking at the plot, the uncertainty in the forecast is still large. Note though that the lower bound is around 75 cGy for the total dose, which is a significant dose. Therefore, even with large uncertainties, warning to operators could have been given. Figure 17 plots the forecast made 5 hours from the start of the event along with the uncertainty. The uncertainty for the SPE is still large, however the lower bound has gotten a little closer to the actual value. Though for all the forecasts shown here had large uncertainties, each forecast indicates that the event will be significant. Therefore, the operators and crew would have an indication that this event will pose a potential health risk with time to take mitigating actions.

The SPE on April 21, 2002 was a relatively large event, but the ability to forecast small events, especially ones that pose no health threats, is just as important as correctly forecasting a large

event. This is because any mitigating actions cost time and money. therefore a false positive will result in a loss of productivity and time. The SPE that took place on November 4, 1997 was a small event having a total dose of 2.67 cGy. The dose rate for this event is also small averaging 0.7 mGy per hour. Figure 18 shows the dose-rate time profile along with six forecasts at different times from the start of the event. The forecast made at 2.5 hours from the start of the event is the closest forecast to the actual dose-time profile. The forecasts made at 50 minutes, 1.667 hours, and 5 hours have steeper dose rates and larger total dose than the actual dose-rate time profile. While the forecasts made at 3.333 hours and 4.1667 hours were below the actual dose-rate time profile. However, all of the forecasts indicate that this event will be a small event with a low dose rate. Table 5 lists the actual values, the predicted values, and the percentage error associate with the each parameter. The percentage errors are much higher for this event than they were for the April 21, 2002 SPE. The error for D_∞ ranges from approximately 320% to 8%. The percent error for α and γ are lower and more consistent. Predictions for α all have an error around 30%. Similarly the error for the γ prediction ranged from approximately 12% to 28%.

Looking at the uncertainty in the forecast for the worst performing forecast will indicate what the worst case scenario would be for these forecasts. The worst performing forecast was made 1.67 hours from the start of the event, having a average dose rate of 3.67 mGy per hour and a total dose of 11.15 cGy. This forecast has a dose rate that is 5 times larger than the actual dose rate and total dose that is 4 times larger than the actual total dose. Figure 19 is a plot of the dose, the forecast made at 1.67 hours and the uncertainty in the forecast. The lower uncertainty curve dips down into the negative dose. Although there can not be a negative dose the curve is left in to indicate how large the range of the uncertainty is for the forecast. The upper curve reaches nearly a total dose of 25 cGy. The actual dose curve does lie within the uncertainty bounds. Taking the worst forecast out of the six and within the uncertainty of the forecast the LWR technique gives the operators and crew the knowledge that this SPE will be a small event.

6.2 Forecasts for SPEs with Doses Less Than 145 cGy

Referring back to Figure 12, the histogram shows that 49 of the 60 events have a total dose less than 145 cGy. There is a "gap" between about 550 cGy and a 1000 cGy where there are no SPEs in the data set. Since LWR relies on past exemplars, few or no events in part of the data set can reduce performance. Therefore, 11 events with total does larger than 145 cGy were taken out of the data set. Testing with only events having a total dose less than 145 cGy was carried out to see if the forecasts improve. Figure 20 plots the forecasts made with the LWR method with the reduced data set for the November 4, 1997 SPE. The plot shows that the forecasts have improved over the forecasts made with all 60 events in the data set (see Figure 18). Now the forecasts made at 1.667, 2.5, 3.333, and 4.1667 hour appear to be fairly close to the actual dose curve. Table 6 confirms what the plot indicates. The percent error for D_∞ predictions have all dropped significantly. Two forecasts now have a percent error less than ten and four have a percent error less than forty. The prediction error for α did not change significantly and the prediction of γ only showed slight improvement. Since the predictions of α and γ were not significantly better than with all the events, there was little to no improvement in the forecasting of the dose rate compared to before. Next looking at uncertainty in the forecasts. Figure 21 is a plot containing the forecast made at 1.667 hours from the start of the event and the corresponding uncertainty in the forecast. Comparing this plot to the one in Figure 19 it can be determined that there is less uncertainty in the forecast using the data set with SPEs less than 145 cGy. The forecast made at 1.667 hours with all 60 events had an uncertainty that ranged from -5 cGy to 25 cGy for a total range of 30 cGy. The forecast made at 1.667 hours with the events less than 145 cGy ranged from -7 cGy to 12 cGy for a total range of 19 cGy. That is 33% reduction in the uncertainty. The other forecasts for this SPE had a similar reduction in uncertainty.

Looking at an event that occurred on April 3, 2001 which has a D_∞ value of 38.22 cGy shows significant improvement when using the data set containing SPEs less than 145 cGy. Figure 22 has

a plot of the event with forecasts made using both data sets. The top plot are the forecasts made with all 60 events. These forecasts are have very large percent errors (see Table 7). Consistently each forecast is larger than the one before it. Table 7 confirms what is seen graphically. The percent error for D_∞ also increases for each successive forecast. The percent error for the predictions of α and γ is not very different between the data sets. The reason for this is that the dose rates are not highly correlated with the total dose. Therefore, reducing the data set of past events based on total dose will not give any benefit in the ability to predict α and γ since these parameters are determined by the dose rate. The improvement in forecasting gained by reducing the data set of past events indicates that the more representative past events the method has the better its ability to forecast.

6.3 Problem Forecasts

There are three different cases where the LWR method forecasts poorly. The first case is where all of the forecasts under-predict the actual time dose-rate profile. Figure 23 shows a plot of an SPE starting on November 11, 2000. This SPE was a large one with a total dose over 1000 cGy. The plot shows that the forecasts for the event did not get over 300 cGy for the total dose. The forecasts all predicted a smaller dose-rate than the actual dose-rate. A prediction error like this could lead operators and crew to assume that the event will be small when in actuality the event might be significant. Fortunately, this problem tends to occur only for larger events. Therefore, the forecasts are sufficiently large to have crews take mitigating actions. This problem mainly arises due to having very few large events in the historical data. This gives only a few events on which to train the LWRs. Looking back at the histogram in Figure 12 shows that there are only about 4 events that are over 1000 cGy. The other cause of this problem is that the dose-rates for all the events start out very similar the first few hours into an event. More discussion of this will be done later, because this is a cause for all three of the common problems found using LWR to forecast

SPEs.

Over-predicting is a problem on certain SPEs. Here each forecast predicts a steeper dose-rate and a much larger total dose. Figure 24 gives an example of an SPE in which the forecasts are all predict much higher than the actual dose. This SPE the forecasts predict a final dose between 60 and 120 cGy. Though the LWR is correcting itself as each successive forecast is smaller than the previous one. Here the risk is that a forecast will tell operators and crew to take action for a large SPE. However, the event is smaller than predicted and could possibly be small enough that no action is needed to be taken by operators or crew. A false positive, like this one, can cost money and time. Fortunately, this problem diminishes when you have more past events similar to the SPE that the LWR is trying to forecast. Like the first problem this problem relates to not having enough SPEs in the past data set and that the dose-rate for the events start out with very little to distinguish one event from another.

The first two problems are primarly problems related to the prediction of D_∞ or the total dose. If α and/or γ are badly predicted then the forecasts will have the wrong dose-rate. Figure 25 is a plot of an SPE that started on June 4, 1991 along with several forecasts. Notice that none of the forecasts have dose-rates similar to that of the actual dose. All of the forecasts predict a much steeper dose-rate. For this particular event the average percent error in the prediction of α is 401%. This problem arises from the small differences between the dose-rates of SPEs a few hours from the start of the event–A problem which contributes to the all three types of poor forecasts.

Plotting all 60 SPEs on the same plot from the start of each event to five hours into the event gives an idea of the problem in forecasting SPEs early into an event. Figure 26 shows how closely together the dose-rates are in the first few hours an event. Even the very large dose-rate turns out not to be the largest SPE, although it is one of the largest. Therefore, since the LWR method

is a memory based method and it is comparing the new event to the past events it is difficult to distinguish one SPE from another this early into an event.

The uncertainty is calculated to a 95% confidence interval for the prediction of D_∞, α, and γ. The uncertainty for each event is then calculated by building 10000 histories taken randomly from the distribution of parameters. The average of the histories results in the uncertainty in the forecast. For the data set with 60 events, 58% of the dose-rate profiles are within the uncertainty bounds. When only the events less than 145 cGy are used, 86% of the events fall within the uncertainty bounds.

7 Conclusion

The goal of this work was to develop LWR techniques to forecast the dose-rate time profiles from an SPE. The forecasts need to be early, near the beginning of the event, and include the uncertainty in the forecast. The forecasts were to be optimized towards meeting radiation protection requirements. The method performs well on some SPE events; however, it has trouble with others. For many of the events where the LWR technique performs poorly, the forecasts still give useful information for the purposes of radiation protection.

The historical data set contains only a few events compared to the large dose range of the SPEs. This limits the effectiveness of the LWR method in predicting each parameter. Reducing the data set to only events with a total dose less than 145 cGy showed that having more SPEs similar to the one being tested the better the LWR techniques perform. The uncertainties in the forecasts showed improvement with the reduced data set. Also, the number of SPEs that are within the uncertainty of the forecast increases as well. Therefore, it is reasonable to assume that as there are more SPEs added to the data set the better the forecasts will become using a LWR method.

The historical data indicates that early in a SPE, dose-rates between events are similar. A large SPE may have a dose-rate in the first few hours that is almost identical to a dose-rate for a small event. For example a SPE that will have a total dose of 30 cGy after 24 hours may have almost the same dose-rate 5 hours into an event that a SPE that will have a total dose of 120 cGy 48 hours from the start of an event. Since the dose-rate for the two events is almost the same at 5 hours into either event, the LWR method making the forecast will have a difficult time determining what the total dose for the new event will be. This is due to the memory based approach of LWR which compares past exemplar data to current data.

8 Future Work

Future work on this project is to identify another source of information connected to SPEs, which may have a characteristic that will allow for more separation of events earlier from the start of an event. This would help eliminate the problem illustrated in Figure 26 where the dose-rates for different events are all very similar to each other. Perhaps using electron fluences, gamma rays, radio waves, magnetic field fluctuations on the sun or something completely different as another source will add information that will improve the forecasts. Using information other than dose might be able to increase the accuracy of the forecasts.

Another avenue of research is to try and forecast the SPEs without the parametrization. This research used a Weibull parametrization, which fits many events fairly well. However, if forecasts could be made without being parametrized, then the forecasts will not have problems with events which have dose profiles that do not parametrize well.

References

References

[1] J. O. Blaisdell, L. Harrison, and S. S. Wallace. Base Excision Repair Processing Radiation-induced Clustered DNA Lesions. *Radiation Protection Dosimetry*, 97:25–31, 2001.

[2] C. O. Bostrom and D. J. Williams. The space environment. APL Technical Digest Volume 19, Number 1, Johns Hopkins, 1998.

[3] V. Bothmer. Solar corona, solar wind structure and solar particle events. In *ESA Workshop Space Weather*, volume ESA WPP-155, pages 117–126, (Nov. 1998) 1999.

[4] C. E. Campbell, T. M. Miller, T. F. Nichols, J. R. Edwards, H. M. Moussa, and L. W. Townsend. Sensitivity of solar energetic particle event doses to spectral hardness. In *35th International Conference on Environmental Systems (ICES)*, Rome, Italy, 2005.

[5] R. Cancelliere and R. Gemello. Efficient training of time delay neural networks for sequential patterns. *Neurocomputing*, 10:33–42, 1996.

[6] A. J. Conway, K. P. Macpherson, and J.C. Brown. Delayed time series predictions with neural networks. *Neurocomputing*, 18:81–89, 1998.

[7] J. Feynman and S.B. Gabriel. On space weather consequences and predictions. *Journal of Geophysical Research*, 105:10543–10564, 2000.

[8] G. M. Forde, L. W. Townsend, and J. W. Hines. Application of artificial neural networks in predicting astronaut doses from large solar particle events in space. In *1998 ANS Radiation Protection and Shielding Division Topical Conference Proceedings*, Nashville, Tennessee, 1998.

[9] D. Hastings and H. Garrett. *Spacecraft – Environment Interactions.* Cambridge University Press, London, England, 1996.

[10] J. W. Hines, T. F. Nichols, and L. W. Townsend. SPE Dose Prediction Using Locally Weighted Regression. *Radiation Protection Dosimetry*, 116(December 2005):232–235, 2005.

[11] J. L. Hoff. *Prediction of Dose-Time Profiles Events Using Neural Networks.* PhD thesis, University of Tennessee, Knoxville, 2003.

[12] ICRP60. Recommendations of the international commission on radiological protection. publication 60. *Annals of the ICRP*, 21, 1990.

[13] S. W. Kahler. Origin and properties of solar energetic particles in space. *American Geophysical Union*, 2001.

[14] Achim Lewandowski, Michael Tagscherer, Lars Kindermann, and Peter Protzel. Improving the Fit of Locally Weighted Regression Models. *Neural Information Processing, 1999. Proceedings. ICONIP '99. 6th International Conference on*, 1:371–374, 1999.

[15] R. Mewaldt. Cosmic rays. Macmillan Encyclopedia of Physics, 1996.

[16] NASA. Coronal Mass Ejections. `URL=http://solarscience.msfc.nasa.gov/CMEs.shtml`, Accessed on March 26, 2009. Published by Marshall Space Flight Center.

[17] NASA. SOHO-Gallery. `URL=http://sohowww.nascom.nasa.gov/gallery/images/large/20020716c2halo\_prev.jpg`, Accessed on March 26, 2009.

[18] NASA. SOHO-Gallery: Best Of SOHO. `URL=http://sohowww.nascom.nasa.gov/gallery/images/eit99promclose.html`, Accessed on March 26, 2009.

[19] NASA. Solar Flares. URL=http://hesperia.gsfc.nasa.gov/sftheory/flare.htm, Accessed on March 26, 2009.

[20] NASA. HSF - International Space Station. URL=http://spaceflight.nasa.gov/station/index.html, Accessed on March 3, 2009.

[21] NASA. NASA - Shuttle Missions. URL=http://www.nasa.gov/mission_pages/shuttle/shuttlemissions/list_main.html, Accessed on March 3, 2009.

[22] NASA. NASA-STD-3001, NASA SPACE FLIGHT HUMAN SYSTEM STANDARD VOLUME 1: CREW HEALTH, March 5, 2007.

[23] NCRP. *Limitation of Exposure to Ionizing Radiation.* National Council on Radiation protection and Measurements, 7910 Woodmont Avenue, Bethesda, MD 20814, March 31, 1993.

[24] J. S. Neal, T. F. Nichols, and L. W. Townsend. Forecasting dose and dose rate for large solar energetic particle events: Is there time to predict? *2005 IEEE Aerospace Conference, Big Sky, MT*, 2005.

[25] J. S. Neal and L. W. Townsend. Predicting Dose-Time Profiles of Solar Energetic Particle Events Using Bayesian Forecasting Methods. *IEEE Transactions on Nuclear Science*, 48(6):2004–2009, December 2001.

[26] Homer E. Newell Jr. The space environment. *Science*, 131(3398):385–390, 1960.

[27] T. F. Nichols. Using artificial intelligence methods to predict doses from large solar particle events in space. Master's thesis, University of Tennessee, Knoxville, 2005.

[28] T. F. Nichols, J. W. Hines, J. W. Hoff, and L. W. Townsend. *Using Artificial Intelligence Methods to Predict Doses from Large Solar Particle Events in Space.* Colorado Springs, CO, 2004.

[29] T. F. Nichols, L. W. Townsend, and J. W. Hines. Forecasting the dose and dose rate from a solar particle event using localized weighted regression. 2008.

[30] NOAA. Geostationary Operational Environmental Satellite. URL=http://www.oso.noaa.gov/goes/, Accessed on March 26, 2009. National Environmental Satellite,Data, and Information services.

[31] C. R. O'Dell. Aurora. URL=http://www.worldbookonline.com/wb/Article?id=ar038160, 2005.

[32] Peggy L. Olive. The role of single- and double-strand breaks in cell killing by ionizing radiation. *Radiation Research*, 150, 1998.

[33] D. Max Parkin, MD, Freddie Bray, J. Ferlay, and Paola Pisani, PhD. Global cancer statistics, 2002. *CA Cancer Journal for Clinicians*, 55:74–108, 2005.

[34] J. L. Parsons and L. W. Townsend. Interplanetary crew dose rates for the August 1972 solar particle event. *Radiation Research*, 153:729–733, 2000.

[35] D. Reames. Solar energetic particles: Is there time to hide? *Radiation Measurements*, 30:297–308, 1999.

[36] D. Reames. Seps: Space weather hazard in interplanetary space. *American Geophysical Union*, 2001.

[37] W. Schimmerling. Overview of NASA's Space Radiation Research Program. *Gravitational and Space Biology Bulletin*, 16, 2003.

[38] SPIDR. Space Physics Interactive Data Resource. URL=http://spidr.ngdc.noaa.gov/spidr/index.jsp, Accessed on March 26, 2009. Maintained by National Geophysical Data Center (NGDC).

[39] Nazila H Tehrani. *Predicting Astronaut Radiation Doses from Major Solar Particle Events Using Artificial Intelligence*. PhD thesis, University of Tennessee, Knoxville, 1998.

[40] James E. Turner. *Atoms, Radiation, and Radiation Protection second edition*. John Wiley & Sons, Inc., 605 Third Avenue, New York, NY, 1995.

[41] Virgin Galatic. Space Flight Reservations. `URL=http://www.virgingalactic.com/flash.html?language=english`, Accessed on March 3, 2009.

[42] J. W. Wilson, L. W. Townsend, S. Y. Chun, W. W. Buck, F. Khan, and F. A. Cucinotta. BRYNTRN: A Baryon Transport Computer Code. *Computation Procedures and Data Base, NASA Technical Memorandum 4037*, 1988.

[43] J. W. Wilson, L. W. Townsend, J. E. Nealy, S. Y. Chun, B. S. Hong, W. W. Buck, S. L. Lamkin, B. D. Ganapol, F. Khan, and F. A. Cucinotta. Bryntrn: A baryon transport model. *NASA Technical Paper 2887*, 1989.

[44] J. W. Wilson, L. W. Townsend, W. Schimmerling, G.S. Khandelwal, F. Khan, J. E. Nealy, F. A. Cucinotta, L. C. Simonsen, and J. W. Norbury. Transport methods and interactions for space radiations. *NASA Reference Publication 1257*, 1991.

[45] E. N. Zapp. Solar particle event dose distributions: Parameterization of dose time profiles, with subsequent dose-rate analysis. Master of science thesis, University of Tennessee, Knoxville, 1997.

[46] E. Neal Zapp, Chester R. Ramsey, Lawrence W. Townsend, and Gautum D. Badhwar. Solar particle event dose and dose-rate distributions: parameterization of dose-time profiles, with subsequent dose-rate analysis. *Radiation Measurements*, 30:393–400, 1999.

Appendices

A Tables

Table 1: Characteristics of space radiation

Characteristic	SPE	GCR	Trapped
Proton energy range (MeV)	up to several 100	up to several 1000	up to several 100
HZE energy range (MeV/nucleon)	no significant contribution	up to several 1000	no significant contribution
LET range (keV)/μm)	0.25-10	0.25-1000	0.25-10

Source: [37]

Table 2: Time Frame for Effects of Ionizing Radiation

Times	Events
Physical stage $\lesssim 10^{-15}s$	Formation of H_2O^+, H_2O^*, and subexcitation electrons, e^-, in local track regions ($\lesssim 0.1\mu m$)
Prechemical stage $\sim 10^{-15}s$ to $\sim 10^{-12}s$	Three initial species replaced by H_3O^+, OH, e^-_{aq}, H, and H_2
Chemical Stage $\sim 10^{-12}s$ to $\sim 10^{-6}s$	The four species H_3O^+, OH, e^-_{aq}, and H diffuse and either react with one another or become widely separated. Intratrack reactions essentially complete by $\sim 10^{-6}s$
Biological Stages	
$\lesssim 10^{-3}s$	Radical reactions with biological molecules complete
$\lesssim 1s$	Biochemical changes
Minutes	Cell division affected
Days	Gastrointestinal and central nervous system changes
Weeks	Lung fibrosis develops
Years	Cataracts and cancer may appear; genetic effects in offspring

Source: [40]

Table 3: Dose limits for short-term or career non-cancer effects (in mGy-Eq. or mGy). Note RBE's for specific risks are distinct as described below.

Organ	30 Day limit	1 Year Limit	Career
Lens*	1000 mGy-Eq	2000 mGy-Eq	4000 mGy-Eq
Skin	1500	3000	4000
BFO	250	500	Not applicable
Heart**	250	500	1000
CNS***(Z≥10)	-	100 mGy	250 mGy

*Lens limits are intended to prevent early (< 5 yr) severe cataracts (e.g., from a solar particle event). An additional cataract riskexists at lower doses from cosmic rays for sub-clinical cataracts, which may progress to severe types after long latency (> 5 yr) and are not preventable by existing mitigation measures; however, they are deemed an acceptable risk to the program.
**Heart doses calculated as average over heart muscle and adjacent arteries.
***CNS limits should be calculated at the hippocampus. *Source: [22]*

Table 4: The table contains the predicted value for each Weibull parameter (D_∞, α, and γ) with the associated percent error for an SPE occuring on April 21, 2002. The time column is the time from the start of the event i.e. 2.5 hrs means 2.5 hours have past since the SPE started.

Actual Values: D_∞=223.10 cGy α =0.048 γ=1.49

Time	Predicted D_∞	% Error	Predicted α	% Error	Predicted γ	% Error
50 Mins	155.94	30.10	0.053	9.32	1.61	8.20
1.6667 hrs	174.17	21.94	0.055	14.079	1.50	0.48
2.5 hrs	203.41	8.83	0.051	5.80	1.57	5.26
3.3333 hrs	228.49	2.41	0.048	1.035	1.59	6.78
4.1667 hrs	234.87	5.27	0.045	6.83	1.58	5.81
5 hrs	243.70	9.23	0.045	6.42	1.59	6.27

Table 5: The table contains the predicted value for each Weibull parameter (D_∞, α, and γ) with the associated percent error for an SPE occuring on November 4, 1997. The time column is the time from the start of the event i.e. 2.5 hrs indicates that 2.5 hours have past since the SPE started.

Actual Values: D_∞=2.67 cGy α =0.092 γ=1.025

Time	Predicted D_∞	% Error	Predicted α	% Error	Predicted γ	% Error
50 Mins	9.16	243.031	0.061	34.27	1.31	27.60
1.667 hrs	11.15	317.35	0.063	31.34	1.23	20.00
2.5 hrs	2.88	7.63	0.062	32.32	1.23	19.74
3.3333 hrs	0.61	76.99	0.065	29.83	1.14	11.62
4.1667 hrs	1.41	47.40	0.064	30.69	1.16	13.55
5 hrs	4.81	80.00	0.063	31.78	1.18	15.079

Table 6: The table contains the predicted value for each Weibull parameter (D_∞, α, and γ) with the associated percent error for an SPE occuring on November 4, 1997. The forecasts in this table were made with the LWR methods using only events which have a total dose less than 145 cGy. The time column is the time from the start of the event i.e. 2.5 hrs indicates that 2.5 hours have past since the SPE started.

Actual Values: D_∞=2.67 cGy α =0.092 γ=1.025

Time	Predicted D_∞	% Error	Predicted α	% Error	Predicted γ	% Error
50 Mins	7.82	192.73	0.056	39.80	1.32	28.85
1.667 hrs	2.44	8.75	0.068	26.46	1.17	14.36
2.5 hrs	2.62	2.04	0.06	30.26	1.20	16.88
3.3333 hrs	1.66	37.98	0.063	32.21	1.12	9.41
4.1667 hrs	3.52	31.84	0.063	31.89	1.14	10.81
5 hrs	5.85	118.92	0.062	32.75	1.16	13.07

Table 7: The table contains the predicted value for each Weibull parameter (D_∞, α, and γ) with the associated percent error for an SPE occuring on November 4, 1997. The predictions shown in the top part were made using a data set containing all 60 events. The predictions in the second half of the table were made with the LWR methods using only events which have a total dose less than 145 cGy. The time column is the time from the start of the event i.e. 2.5 hrs indicates that 2.5 hours have past since the SPE started.

Actual Values: D_∞=38.22 cGy α =0.049 γ=1.27

Time	Predicted D_∞	% Error	Predicted α	% Error	Predicted γ	% Error
50 Mins	25.50	33.28	0.063	26.77	1.36	6.53
1.667 hrs	74.69	95.39	0.058	17.24	1.36	6.72
2.5 hrs	111.49	191.67	0.053	8.11	1.49	17.23
3.3333 hrs	133.23	248.55	0.053	7.71	1.48	16.62
4.1667 hrs	153.03	300.34	0.052	6.09	1.517	19.13
5 hrs	182.61	377.72	0.048	2.23	1.59	25.23
Results < 145 cGy						
50 Mins	9.16	76.028	0.070	42.60	1.27	0.47
1.667 hrs	17.82	53.37	0.061	22.92	1.31	2.99
2.5 hrs	27.66	27.64	0.057	16.02	1.44	12.83
3.3333 hrs	33.18	13.21	0.053	8.32	1.44	13.42
4.1667 hrs	39.08	2.25	0.048	1.83	1.48	16.43
5 hrs	47.10	25.57	0.044	11.36	1.56	22.70

B Figures

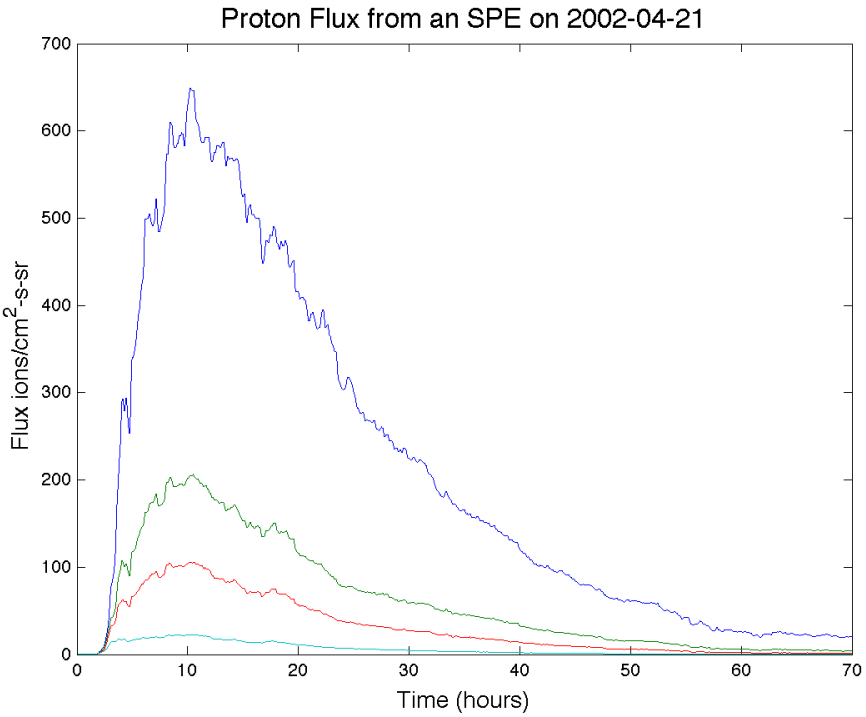

Figure 1: Plot of the proton fluxes above the specific energies received on April 21, 2002. There are 4 energy groups shown >30 MeV, >50 MeV, >60 MeV, and >100 MeV. The fluxes for this plot were collected with five minute sampling interval from GOES-8.

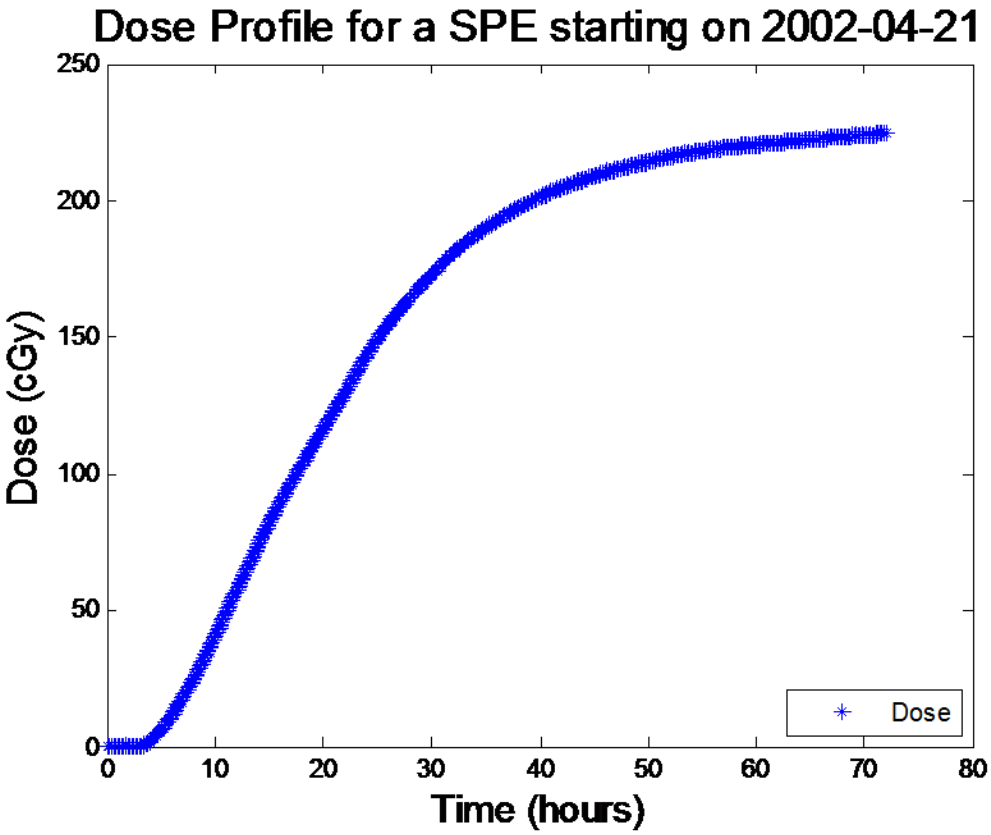

Figure 2: Dose profile for a SPE starting on April 21, 2002. The fluxes were collected at a five minute sampling intervals. Dose was calculated from the flux data using BRYNTRN.

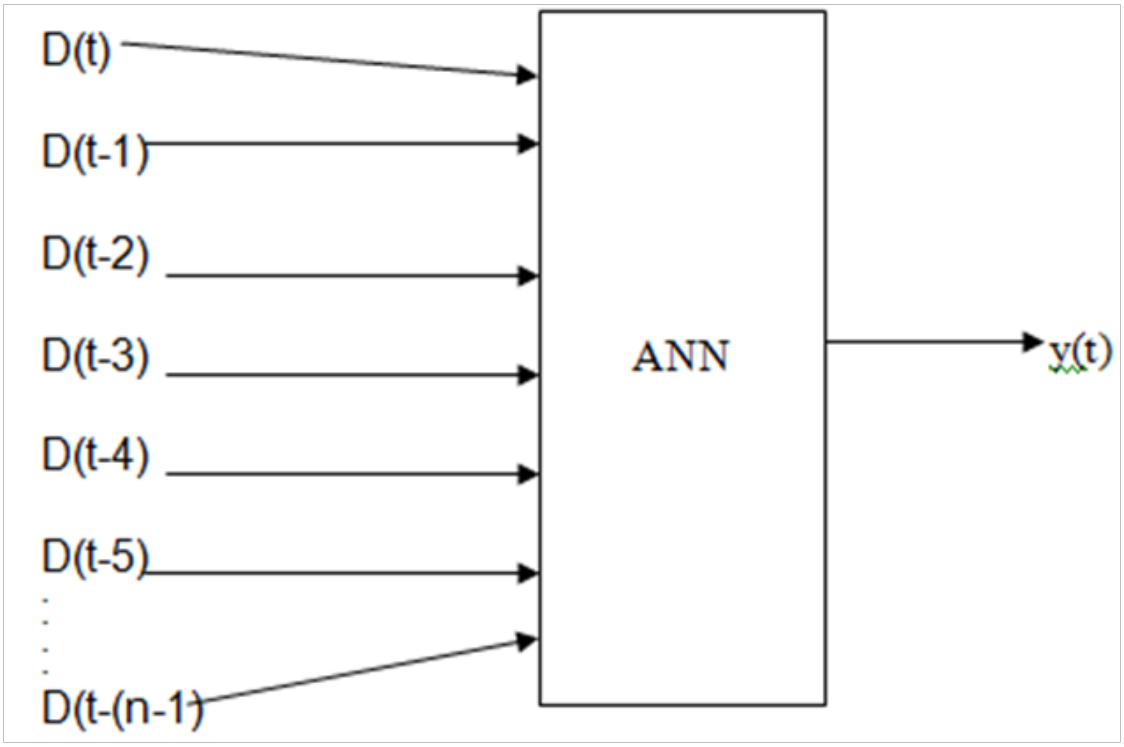

Figure 3: Diagram of a TDNN where time is t and the delay is n-1. Y(t) is the output function.

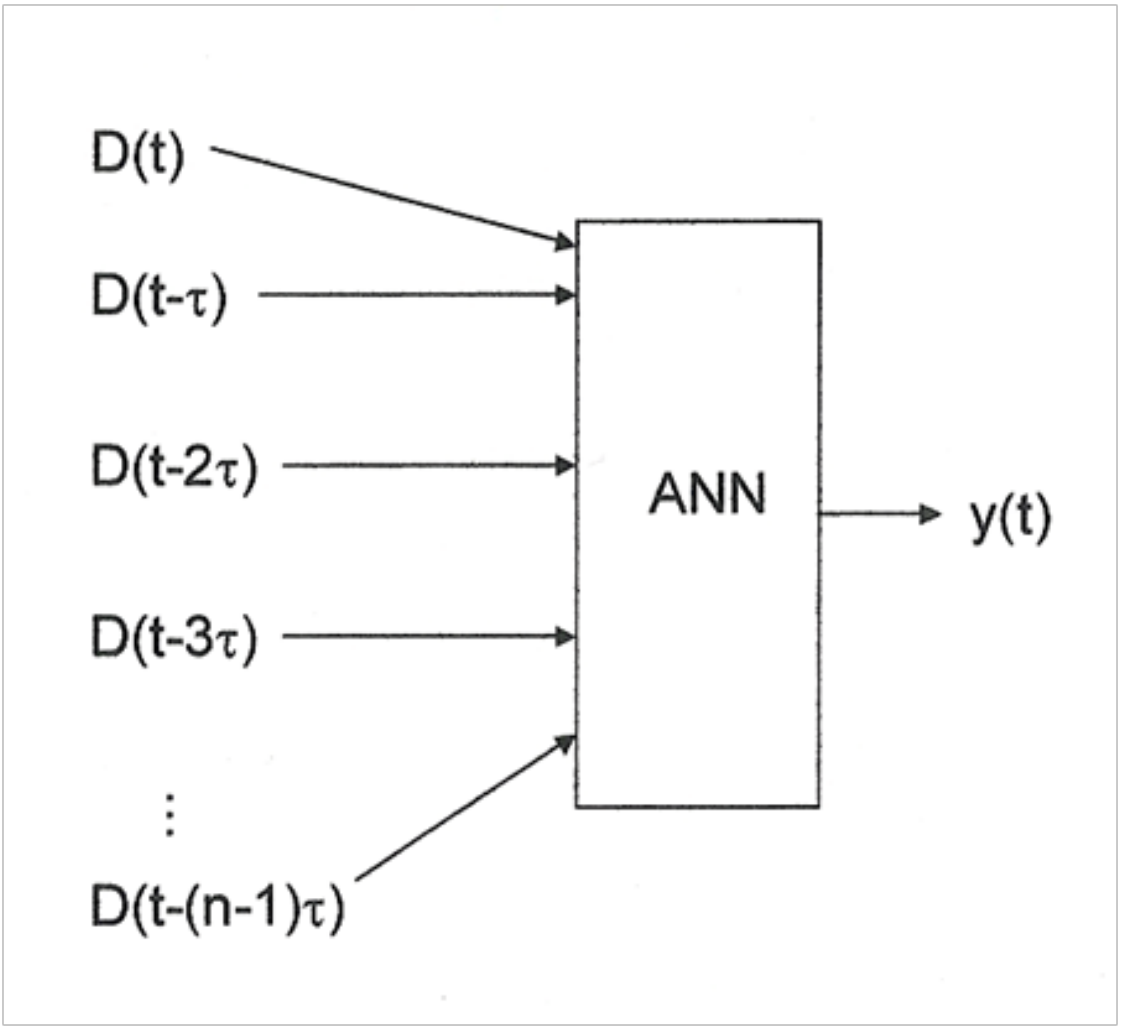

Figure 4: Diagram of an STDNN where time is t and the time delay is τ.

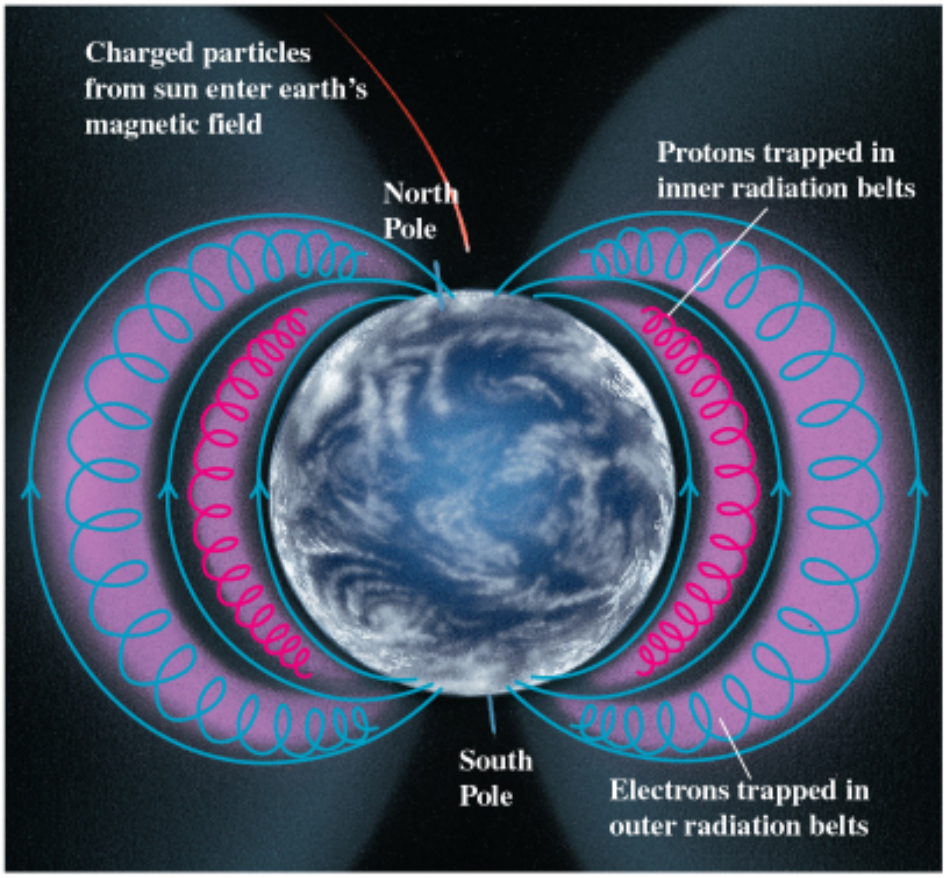

Copyright © Addison Wesley Longman, Inc.

Figure 5: Artist's rendition of the Van Allen belts, showing the inner radiation belts where protons are primarily trapped. The outer radiation belt primarily contains trapped electrons.

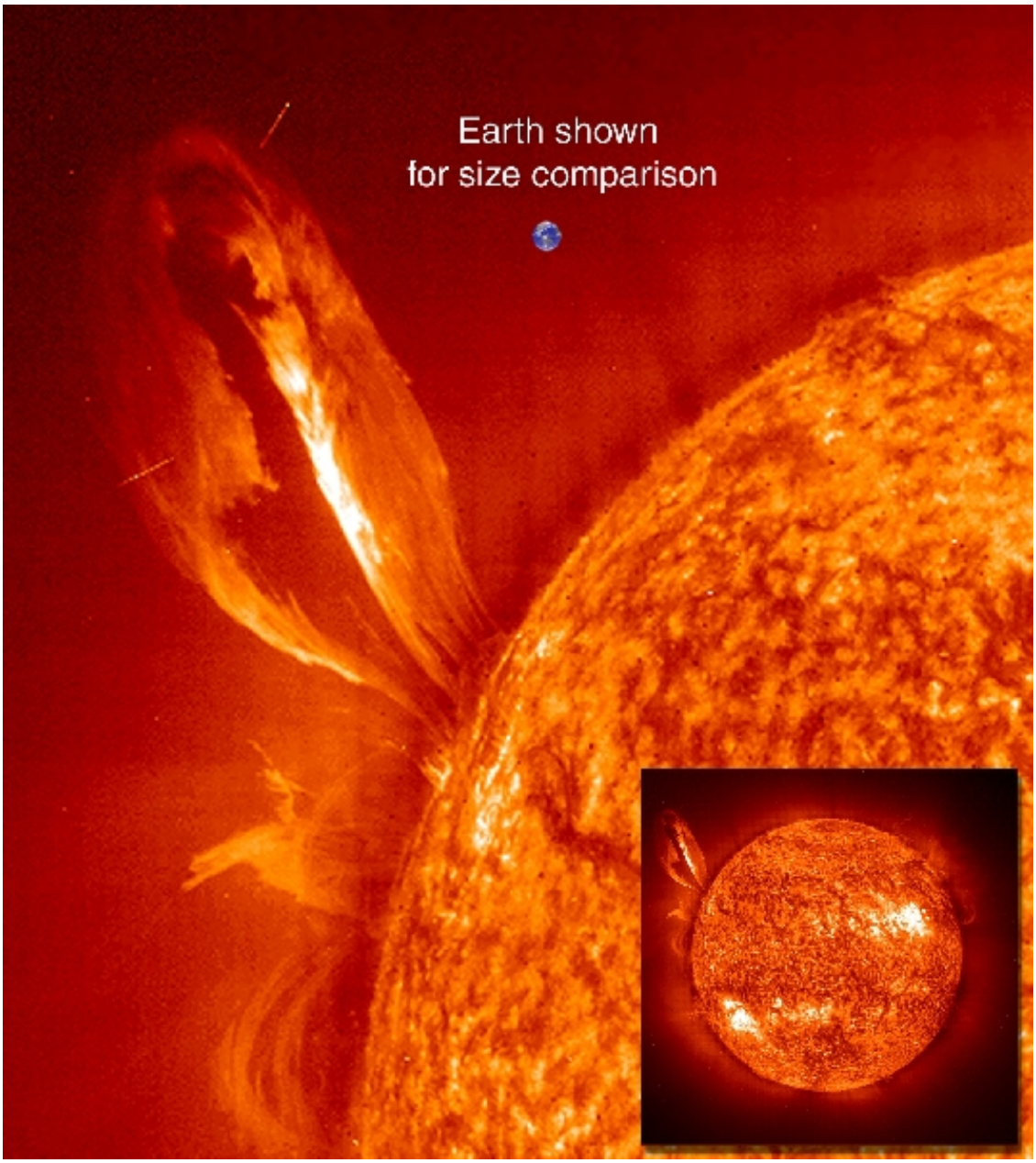

Figure 6: Picture of a solar flare made by SOHO. An image of Earth relative to the size of the solar flare is shown to give an idea about size of these solar flares. Notice how the flare forms a "loop" back to the surface of the sun.SOURCE: [18]

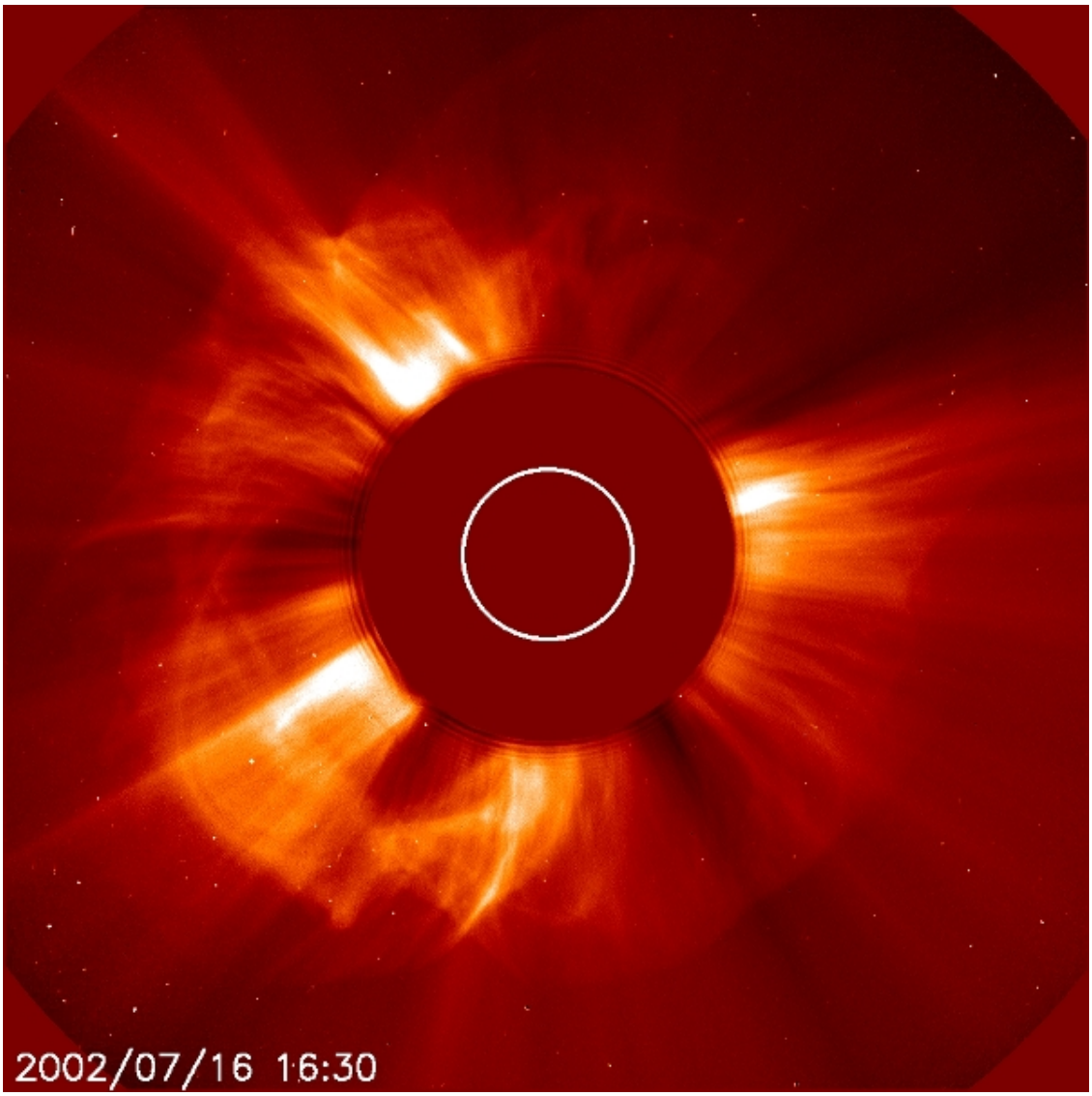

Figure 7: Picture of a CME made by SOHO that occured on July 16, 2002. This CME is coming straight towards the Earth, the occluding disc blocking out the center of the Sun makes it appear that the gases are errupting more to the sides. The "halo" effect where the erupting gases surround the Sun indicates that the CME is directed towards the Earth. SOURCE: [17]

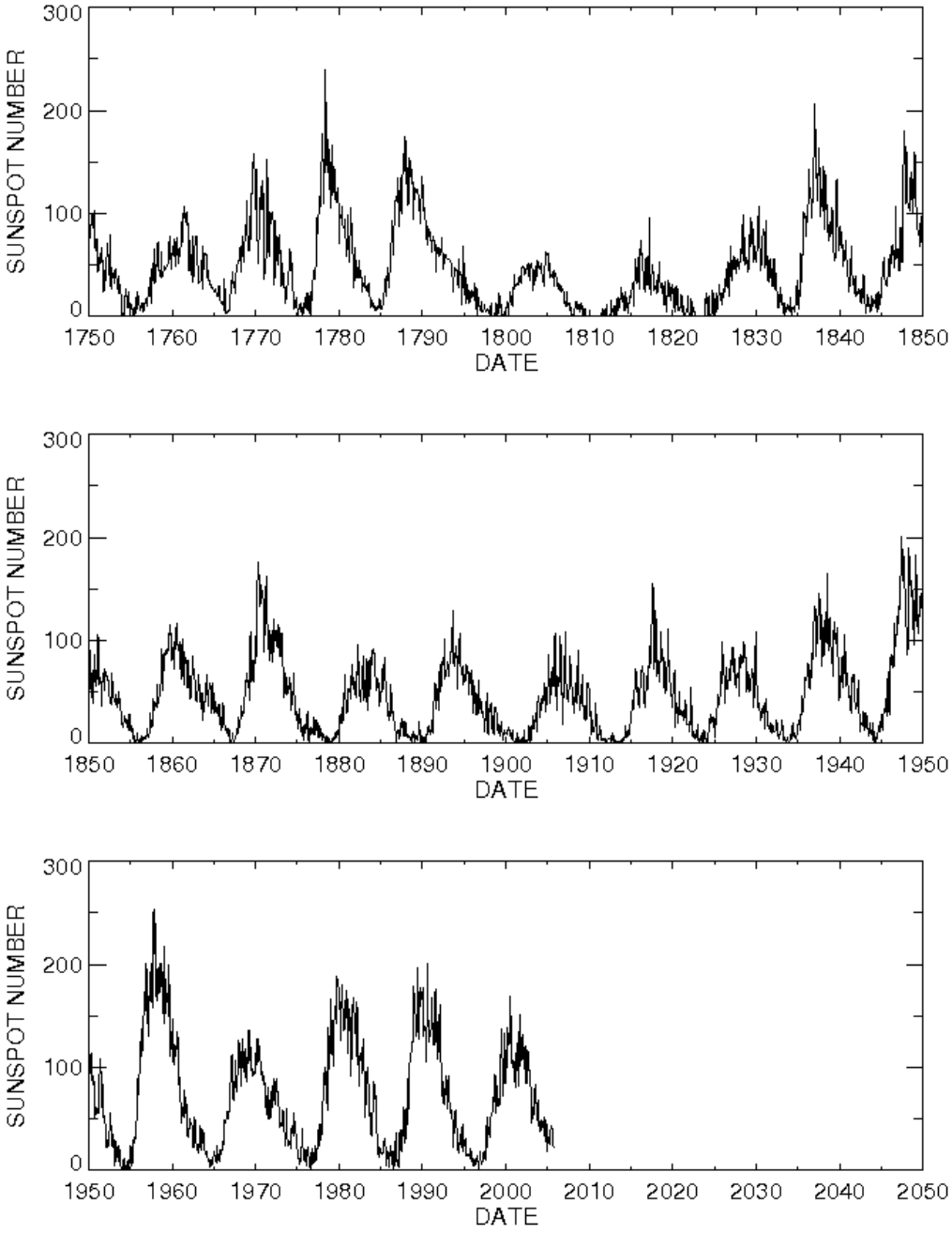

Figure 8: Empirical data recording the number of sunspots, starting in 1750 to the present time. The approximate eleven year cycle is clearly seen on this plot.

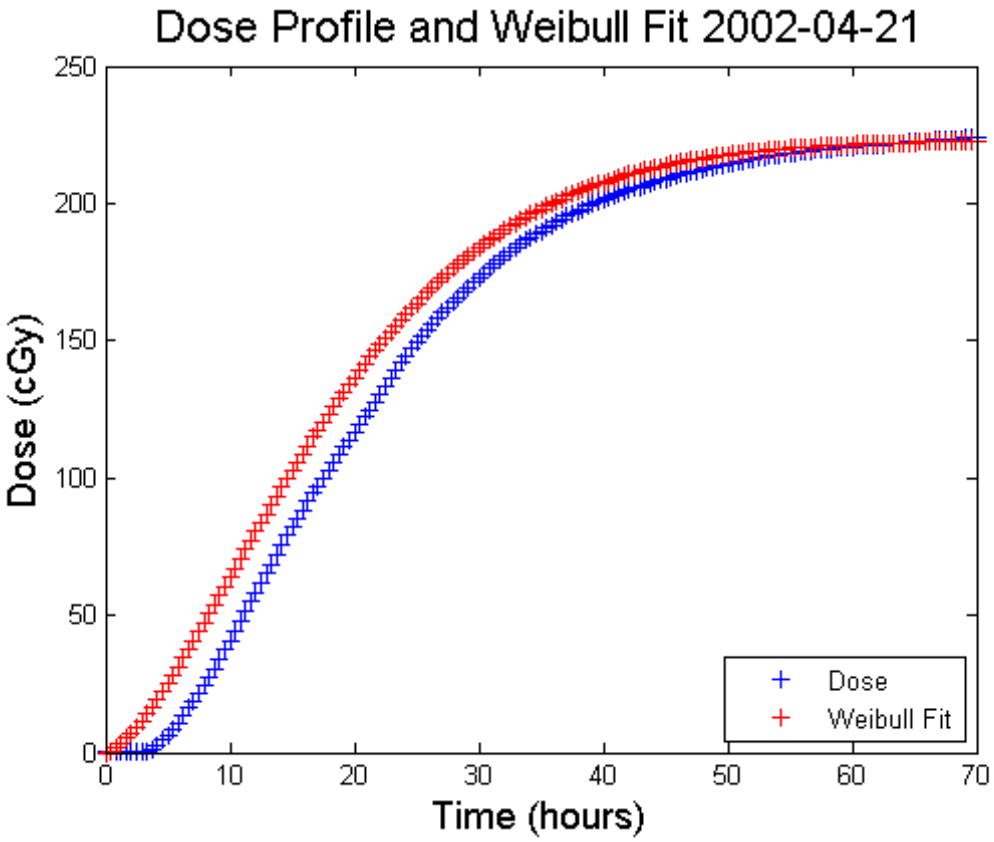

Figure 9: Dose profile and its corresponding Weibull Fit for a SPE starting on April 21, 2002. The flux was collected at a five minute sampling interval. Dose was calculated from the flux data using BRYNTRN.

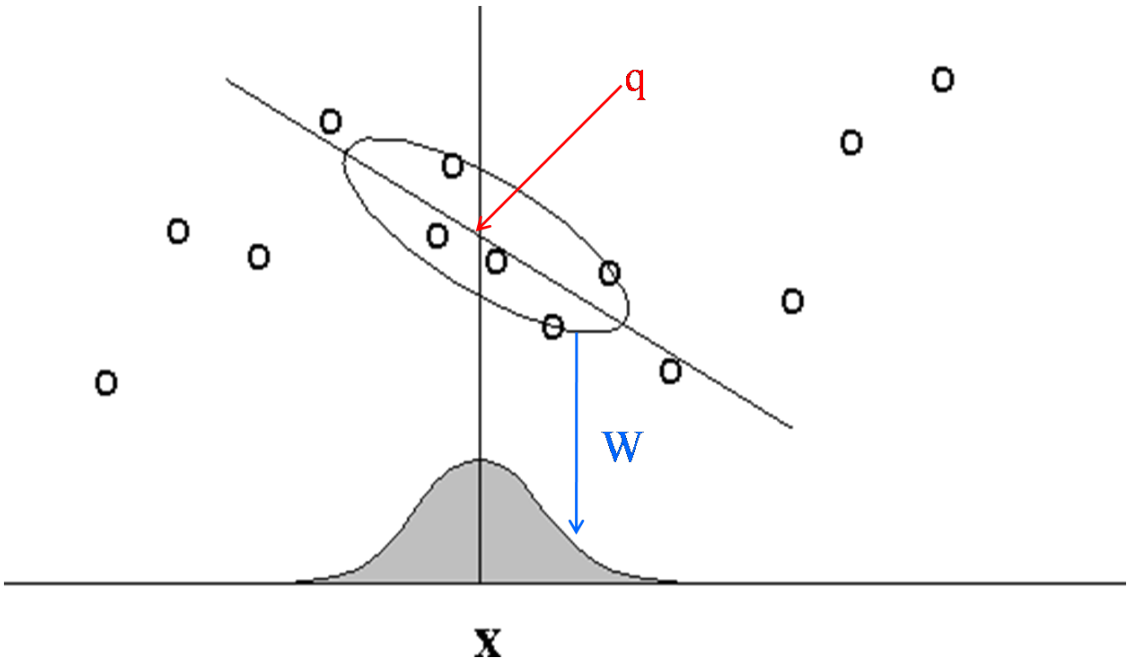

Figure 10: Points are weighted by the proximity to the current q in question using a kernel. A regression is computed using the weighted points. The further away from q the less weight a point has on the regression model. The weight is based on a Gaussian distribution shown at the bottom of the plot.

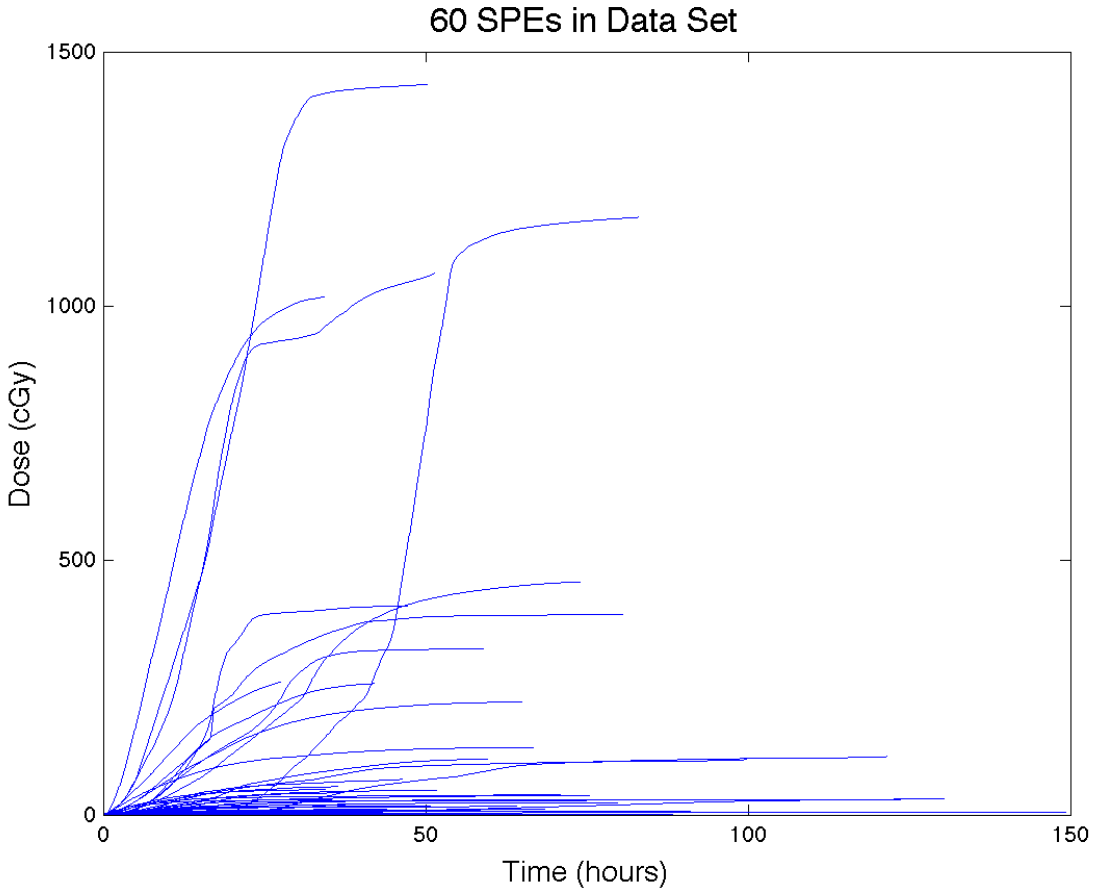

Figure 11: Plot of all 60 events used in training and testing the LWR methods. The "largest" SPE has a total dose of 1436.1 cGy and the "smallest" a total dose of 1 cGy. This gives about a 1500 cGy dose range to be described by 60 events. Note that most events are clustered between a total dose of 0 and 145 cGy

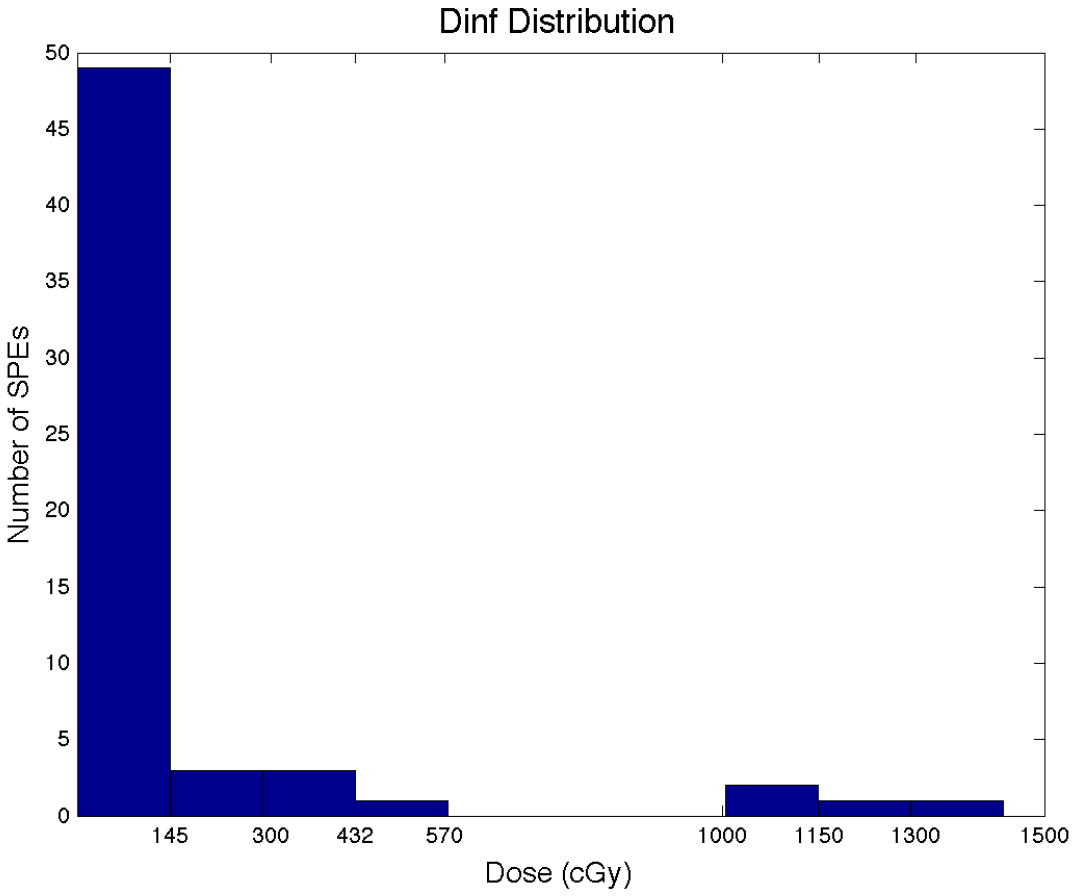

Figure 12: Histogram of the distribution of D_∞ values for the data set. Most D_∞ values are between 0 and 145 cGy. Note that there is a large gap between 570 and 1000 cGy where there are no SPEs covering that dose range. The SPEs with large D_∞ have only a few representative events.

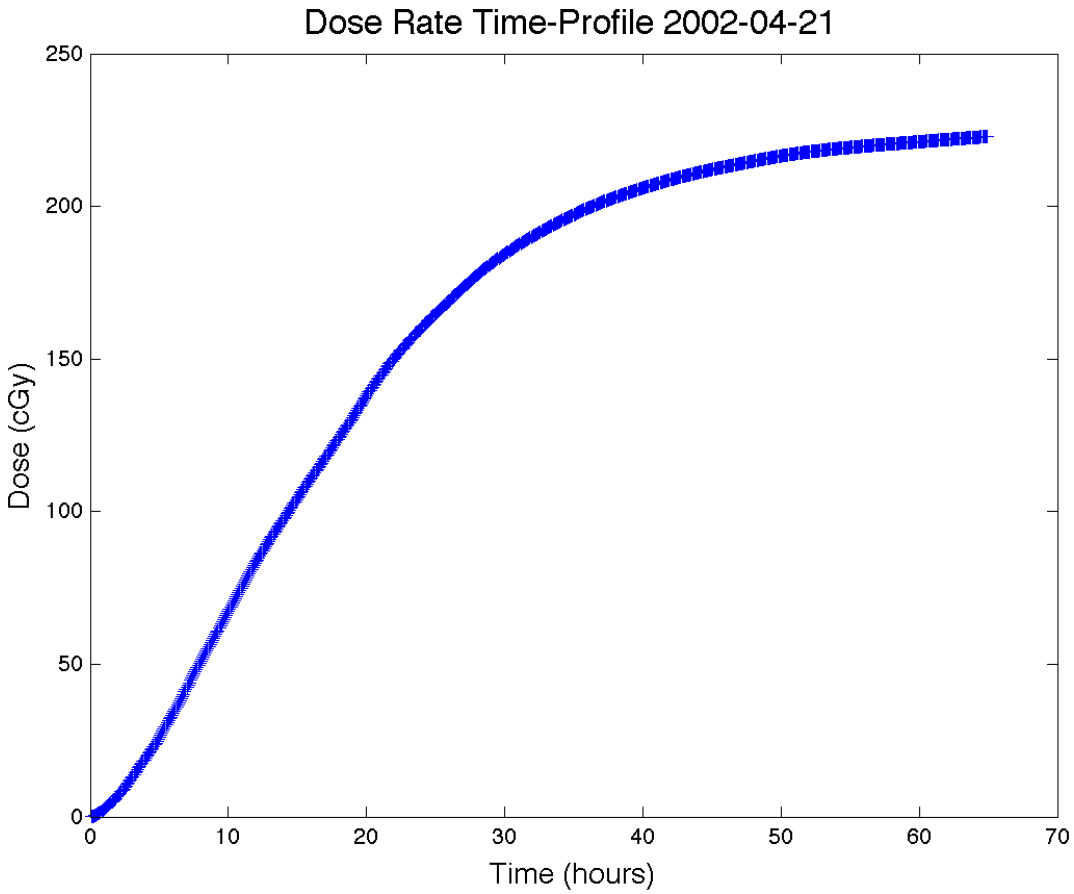

Figure 13: Dose rate time-profile for an event that started on April 21, 2002. The dose reaches its maxiumum value of 223 cGy at approxmately 64 hours from the start of the SPE.

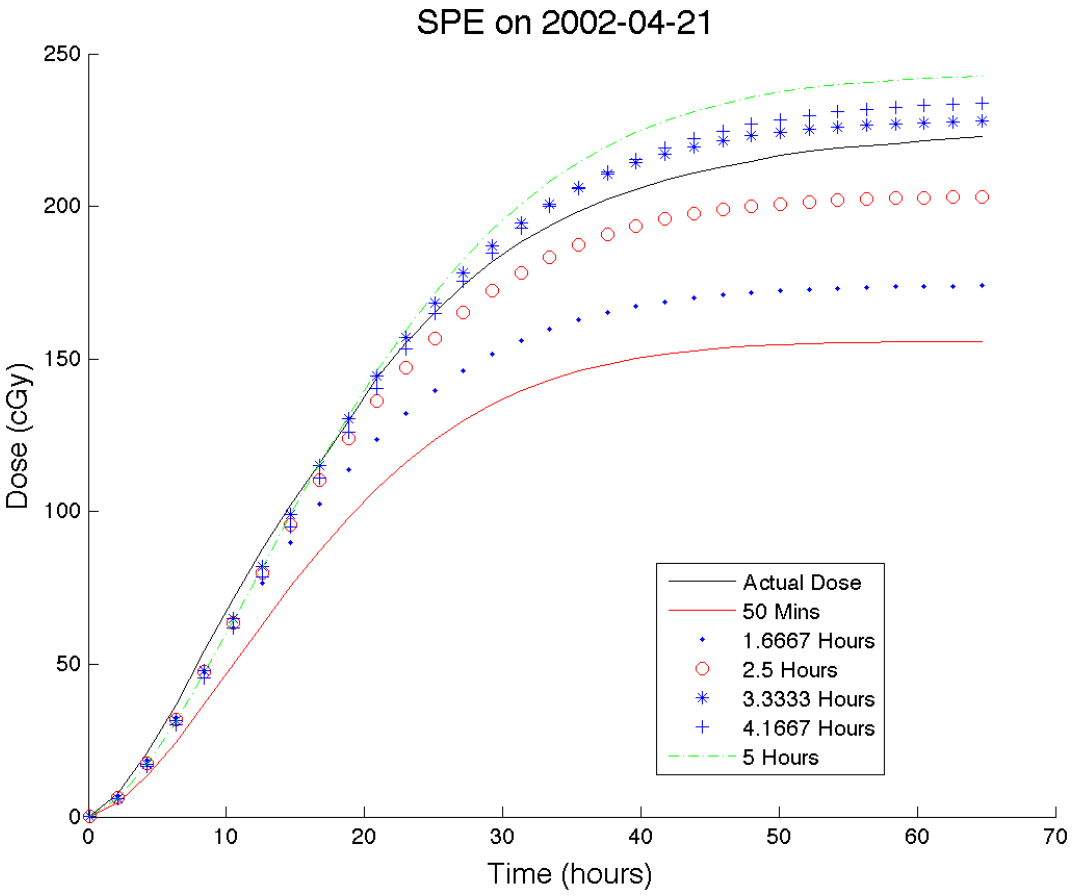

Figure 14: The plot shows six different forecasts each made some time from the start of the event. The time, listed in the legend, is the time from the start of the event. The black line represents the integrated total dose, the smooth red line is the forecast after 50 minutes, the blue diamond is the forecast after 1.6667 hours, the red circle is the forecast after 2.5 hours, the blue asterisk is the forecast after 3.3333 hours, blue plus is the forecast after 4.1667 hours, and the green dashed dot line is the forecast after 5 hours.

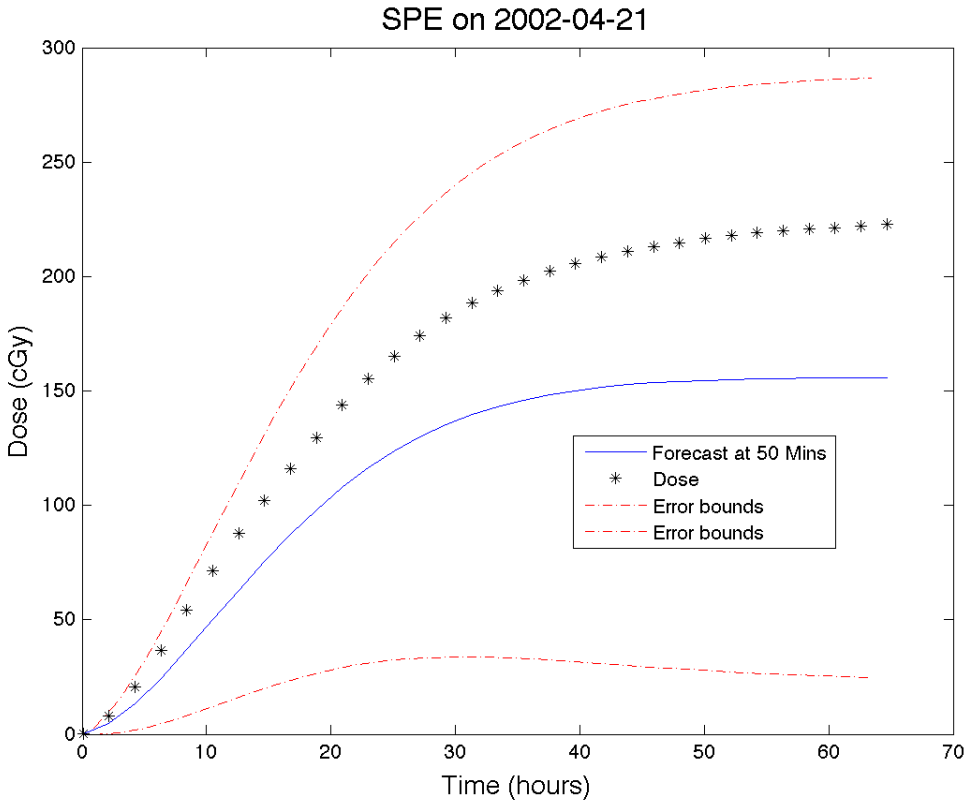

Figure 15: Plot of dose with a forecast and the uncertainty in the forecast for an event that occurred on April 21, 2002. The black asterisks plot the dose-rate time profile. The blue line is the forecast made 50 minutes from the start of the event. The red dot-dash lines are the 95% uncertainty bounds in the forecast.

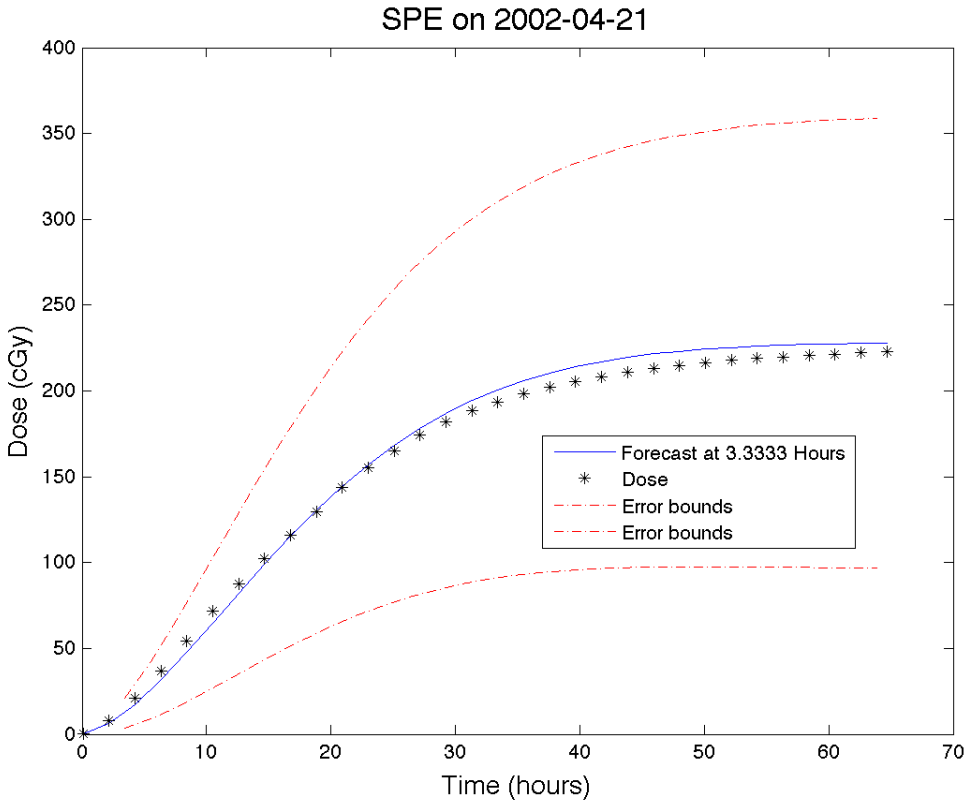

Figure 16: Plot of dose with a forecast and the uncertainty in the forecast for an event that occurred on April 21, 2002. The black asterisks plot the time-dose profile. The blue line is the forecast made 3.333 hours from the start of the event. The red dot-dash lines are the 95% uncertainty bounds in the forecast.

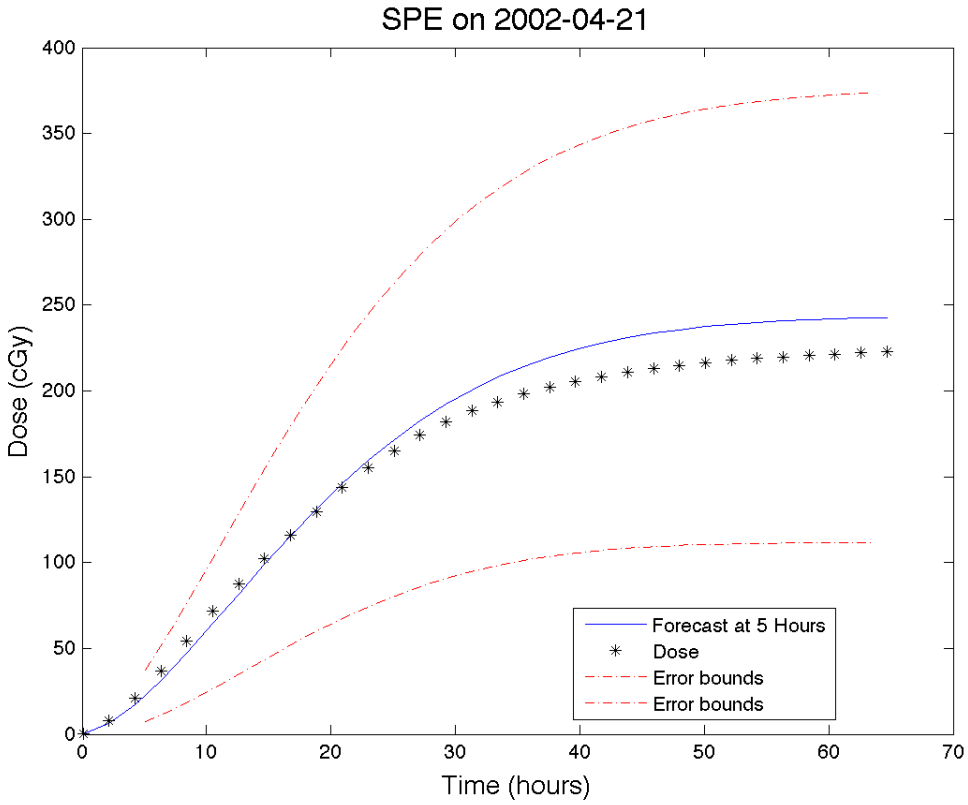

Figure 17: Plot of dose with a forecast and the uncertainty in the forecast for an event that occurred on April 21, 2002. The black asterisks plot the time-dose profile. The blue line is the forecast made 5 hours from the start of the event. The red dot-dash lines are the 95% uncertainty bounds in the forecast.

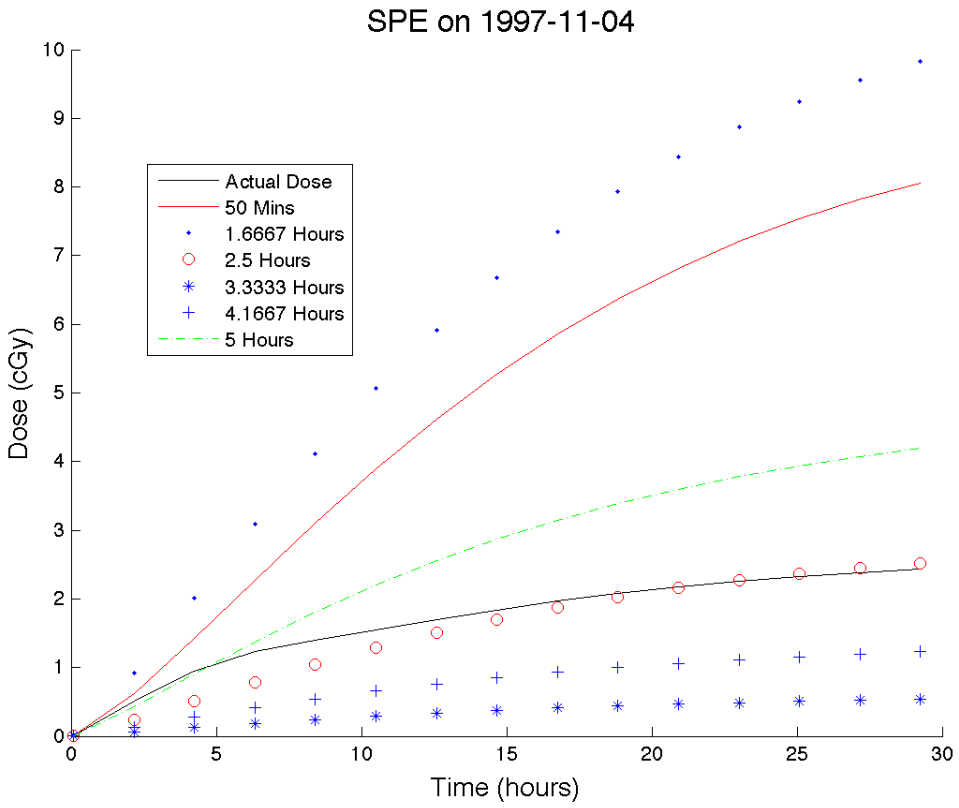

Figure 18: Dose rate time-profile for an event that started on November 4, 1997. The dose reaches its maxiumum value of 2.67 cGy at approximately 30 hours into the event. The black line represents the integrated dose, the smooth red line is the forecast after 50 minutes, the blue diamond is the forecast after 1.6667 hours, the red circle is the forecast after 2.5 hours, the blue asterisk is the forecast after 3.3333 hours, blue plus is the forecast after 4.1667 hours, and the green dashed dot line is the forecast after 5 hours.

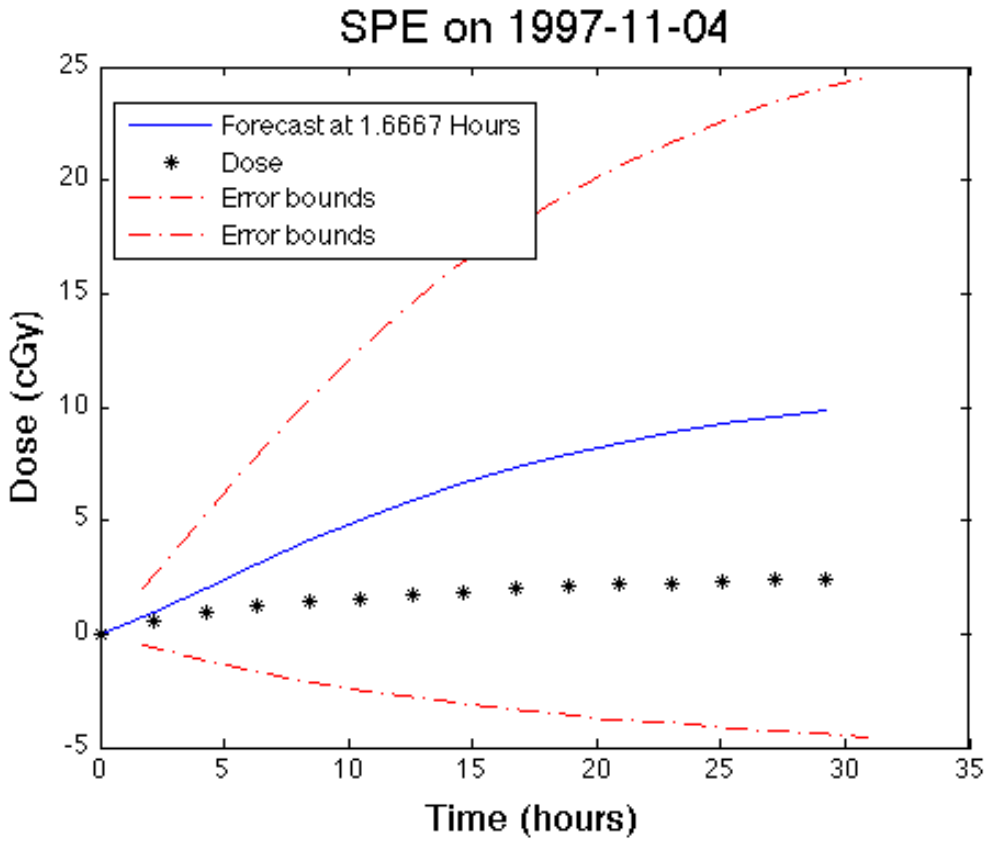

Figure 19: Plot of dose with a forecast and the uncertainty in the forecast for an event that occurred on November 4, 1997 made with a data set containing 60 events. The black asterisks plot the time-dose profile. The blue line is the forecast made 1.6667 hours from the start of the event. The red dot-dash lines are the 95% uncertainty bounds in the forecast.

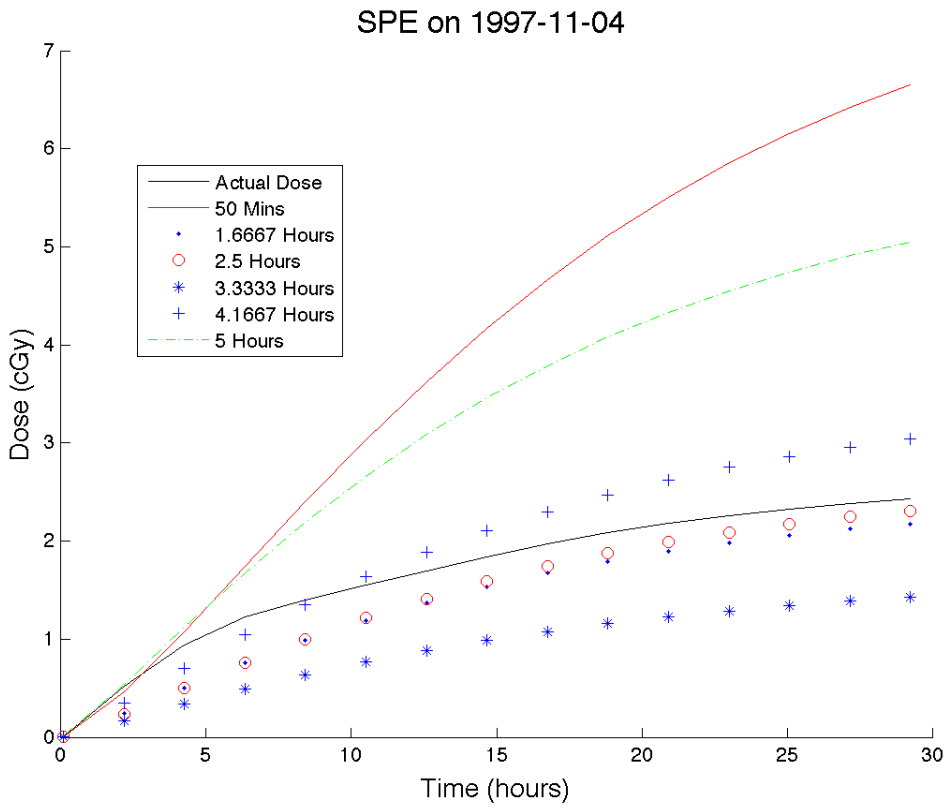

Figure 20: Dose rate time-profile for an event that started on November 4, 1997. The forecasts on this plot were made with the LWR methods using only events which have a total dose less than 145 cGy. The dose reaches its maxiumum value of 2.67 cGy at approximately 30 hours into the event. The black line represents the integrated dose, the smooth red line is the forecast after 50 minutes, the blue diamond is the forecast after 1.6667 hours, the red circle is the forecast after 2.5 hours, the blue asterisk is the forecast after 3.3333 hours, blue plus is the forecast after 4.1667 hours, and the green dashed dot line is the forecast after 5 hours.

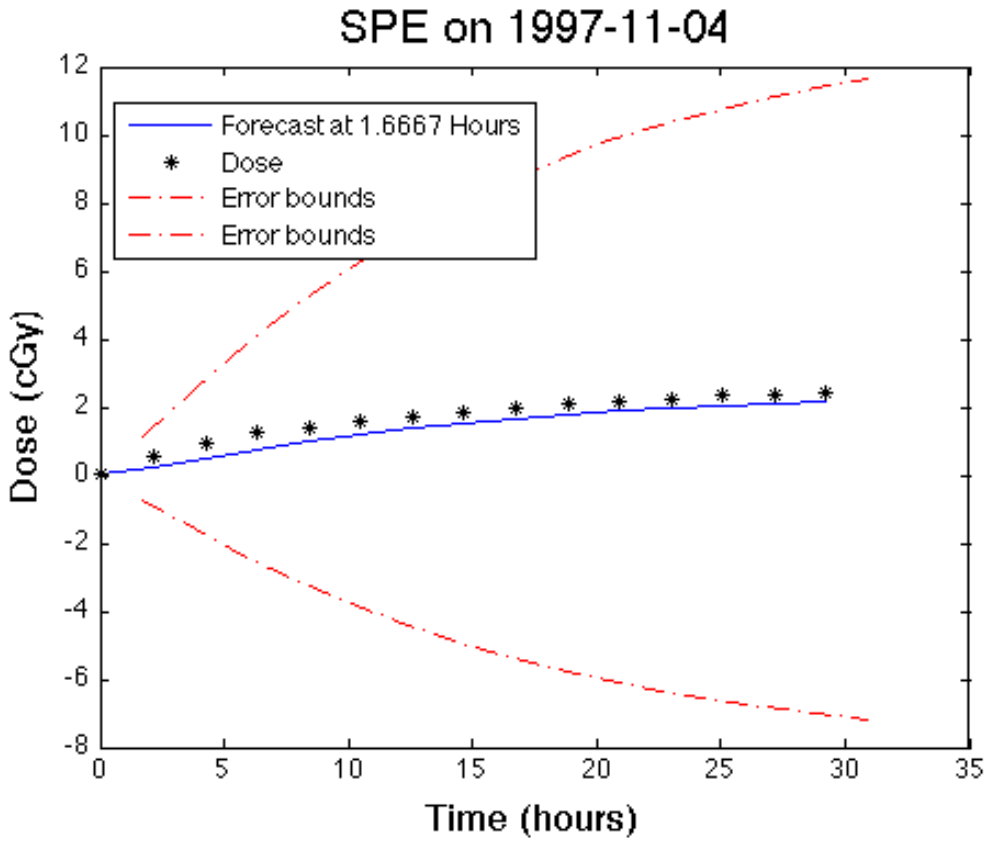

Figure 21: Plot of dose with a forecast and the uncertainty in the forecast for an event that occurred on November 4, 1997 made with a data set only containing SPEs less than 145 cGy. The black asterisks plot the time-dose profile. The blue line is the forecast made 1.6667 hours from the start of the event. The red dot-dash lines are the 95% uncertainty bounds in the forecast.

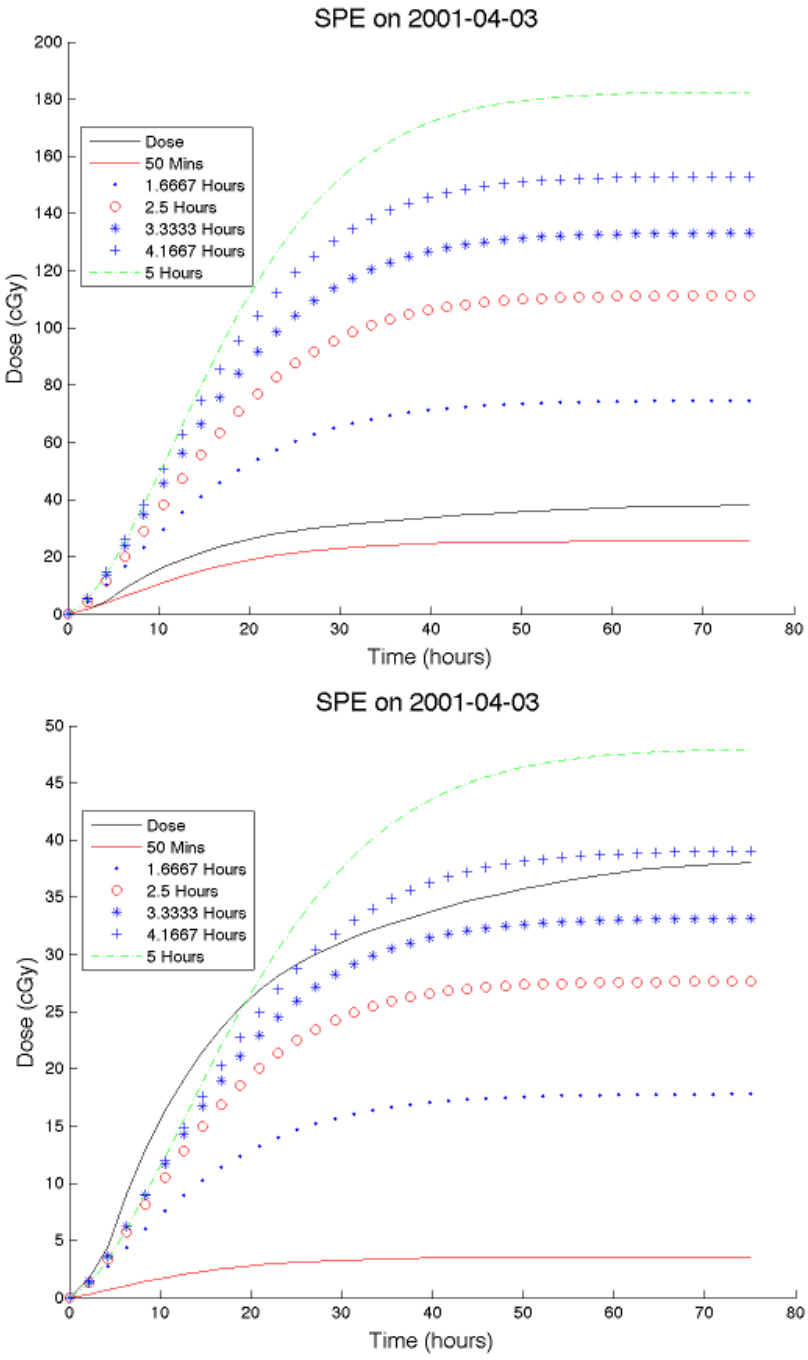

Figure 22: Plots of an SPE on that occurred on April 3, 2001 with forecasts. The top plot the forecasts were made using all 60 SPEs the bottom plot the forecasts were made using only events less than 145 cGy.

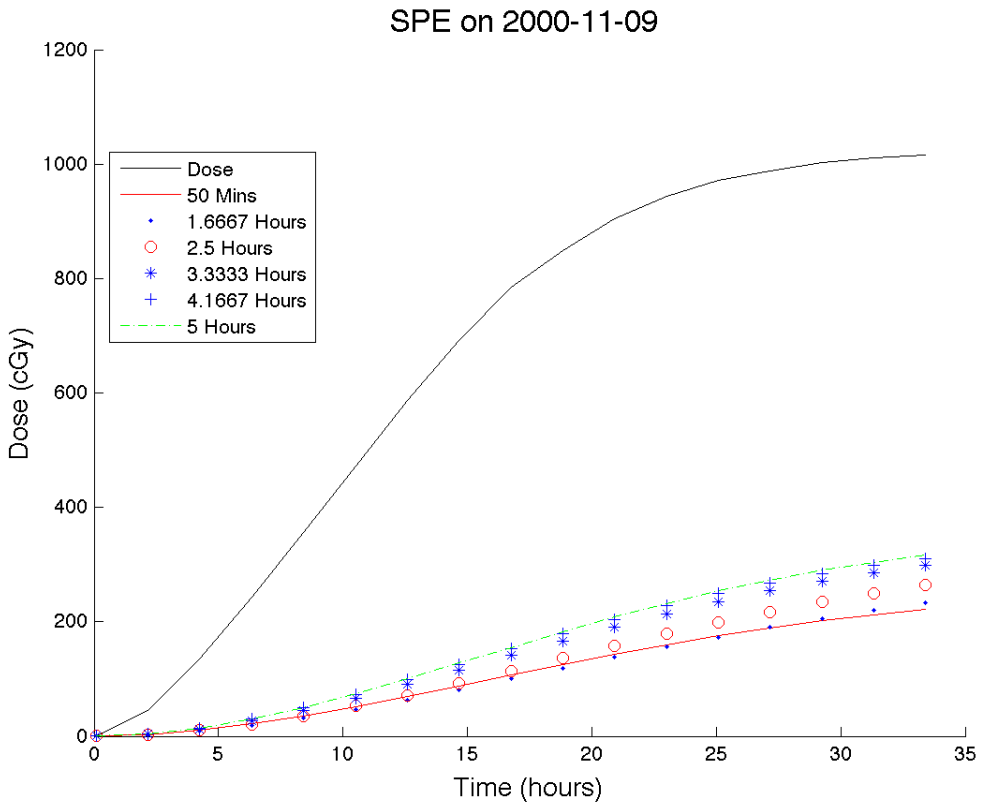

Figure 23: Plot of an SPE that started on November 11, 2000. This was a very large SPE having a total dose above 1000 cGy. The six forecasts all under-predict the dose-rate and the total dose.

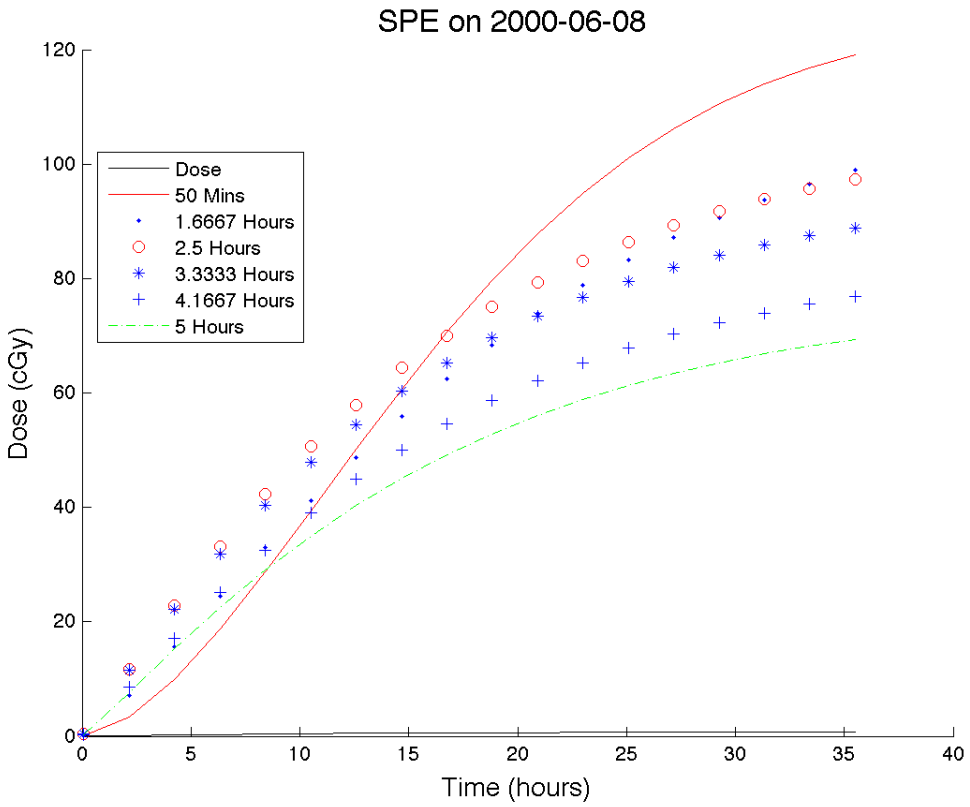

Figure 24: Plot of an SPE that started on June 06, 2000. This was a small SPE having a total dose less than 10 cGy. The six forecasts all over-predict the dose-rate and the total dose.

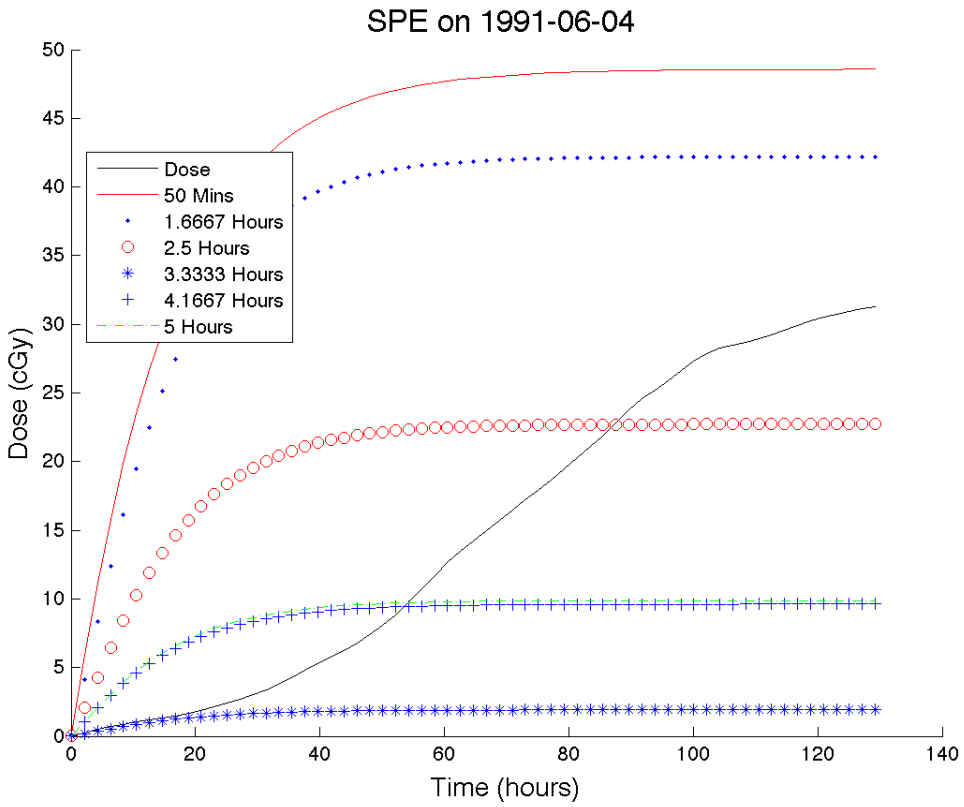

Figure 25: Plot of an SPE that started on November 11, 2000. This was a very large SPE having a total dose above 1000 cGy. The six forecasts all under-predict the dose-rate and the total dose.

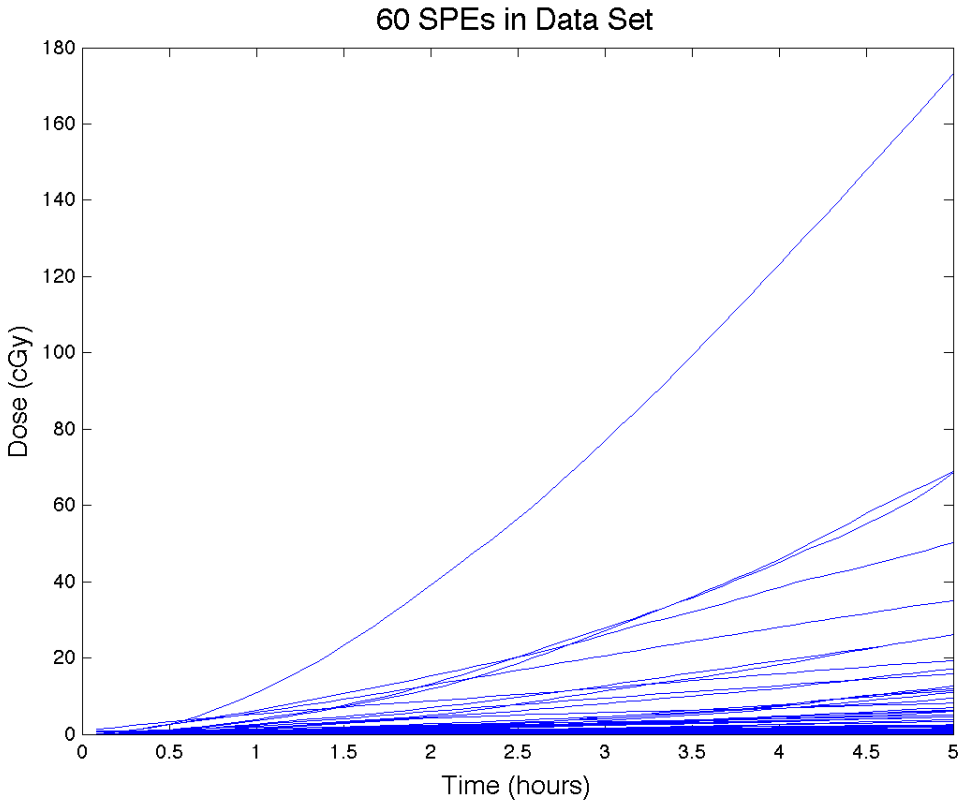

Figure 26: Plot of an SPE that started on November 11, 2000. This was a very large SPE having a total dose above 1000 cGy. The six forecasts all under-predict the dose-rate and the total dose.

C Forecasts for 60 Events in Data Set

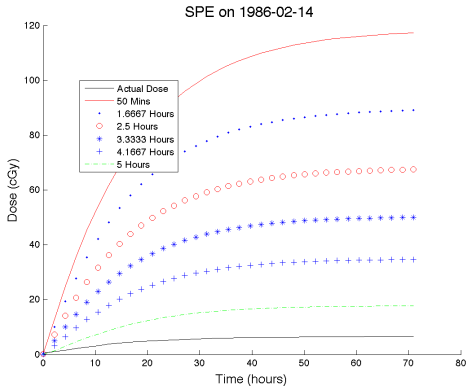

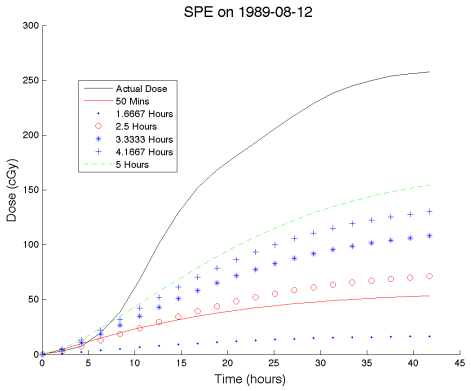

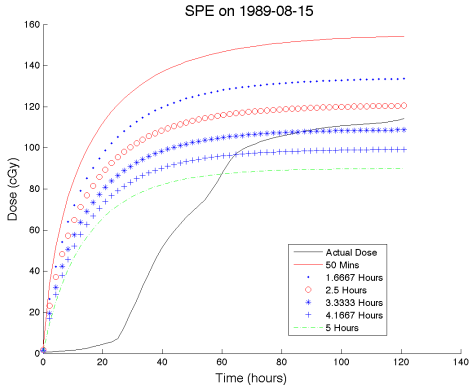

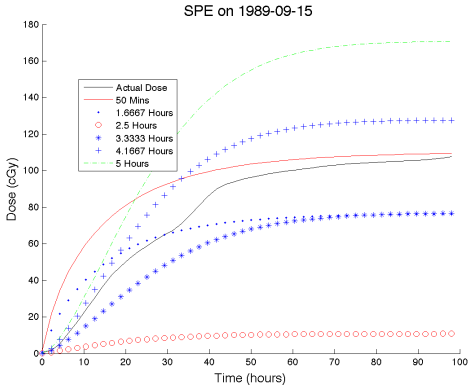

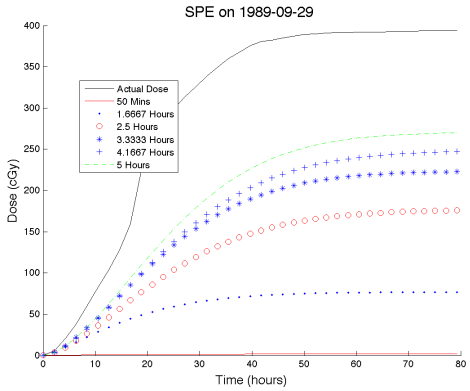

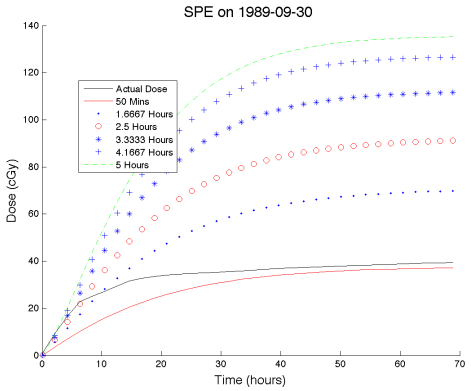

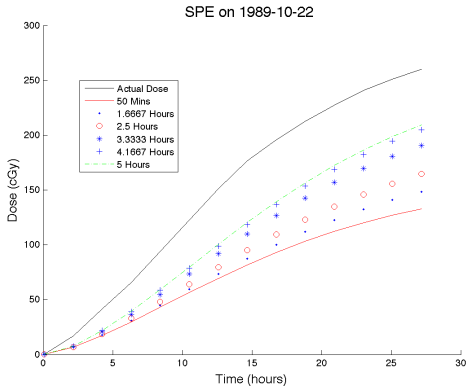
SPE on 1989-10-22
Dose (cGy)
Time (hours)
Actual Dose
50 Mins
1.6667 Hours
2.5 Hours
3.3333 Hours
4.1667 Hours
5 Hours

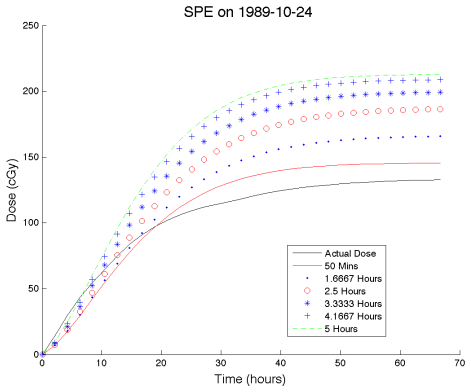
SPE on 1989-10-24
Dose (cGy)
Time (hours)
Actual Dose
50 Mins
1.6667 Hours
2.5 Hours
3.3333 Hours
4.1667 Hours
5 Hours

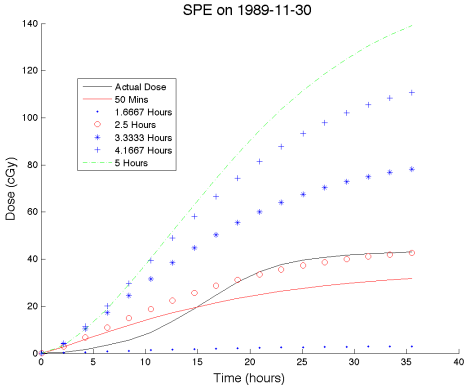
SPE on 1989-11-30
Dose (cGy)
Time (hours)
Actual Dose
50 Mins
1.6667 Hours
2.5 Hours
3.3333 Hours
4.1667 Hours
5 Hours

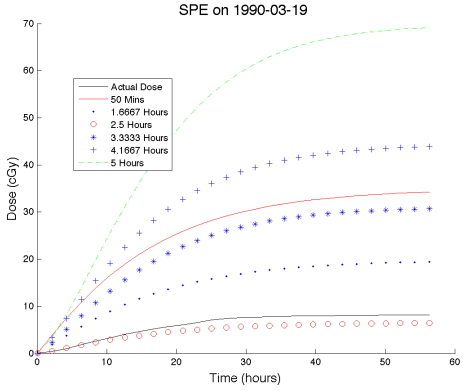
SPE on 1990-03-19
Dose (cGy)
Time (hours)
Actual Dose
50 Mins
1.6667 Hours
2.5 Hours
3.3333 Hours
4.1667 Hours
5 Hours

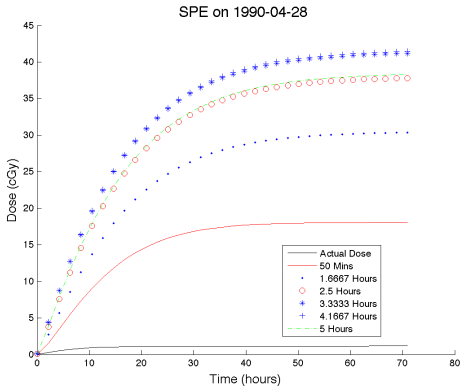
SPE on 1990-04-28
Dose (cGy)
Time (hours)
Actual Dose
50 Mins
1.6667 Hours
2.5 Hours
3.3333 Hours
4.1667 Hours
5 Hours

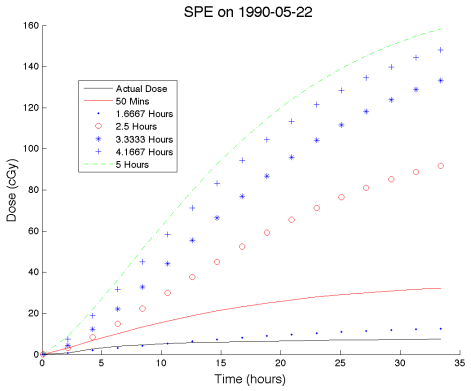
SPE on 1990-05-22
Dose (cGy)
Time (hours)
Actual Dose
50 Mins
1.6667 Hours
2.5 Hours
3.3333 Hours
4.1667 Hours
5 Hours

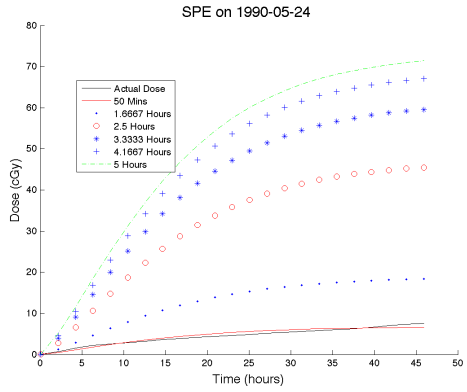
SPE on 1990-05-24
Actual Dose
50 Mins
1.6667 Hours
2.5 Hours
3.3333 Hours
4.1667 Hours
5 Hours
Dose (cGy)
Time (hours)

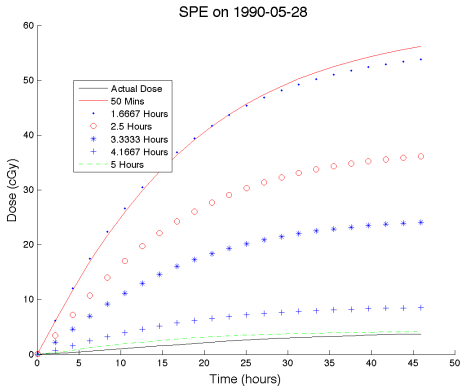
SPE on 1990-05-28
Actual Dose
50 Mins
1.6667 Hours
2.5 Hours
3.3333 Hours
4.1667 Hours
5 Hours
Dose (cGy)
Time (hours)

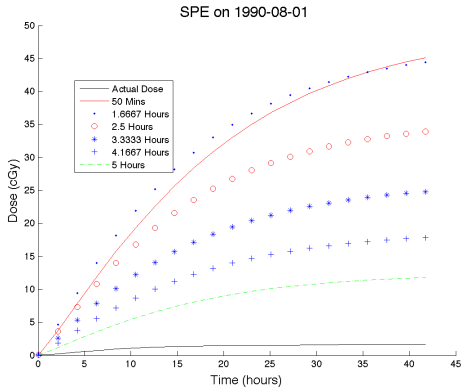
SPE on 1990-08-01
Actual Dose
50 Mins
1.6667 Hours
2.5 Hours
3.3333 Hours
4.1667 Hours
5 Hours
Dose (cGy)
Time (hours)

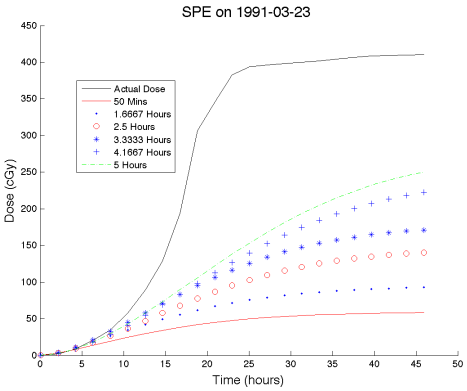
SPE on 1991-03-23
Actual Dose
50 Mins
1.6667 Hours
2.5 Hours
3.3333 Hours
4.1667 Hours
5 Hours
Dose (cGy)
Time (hours)

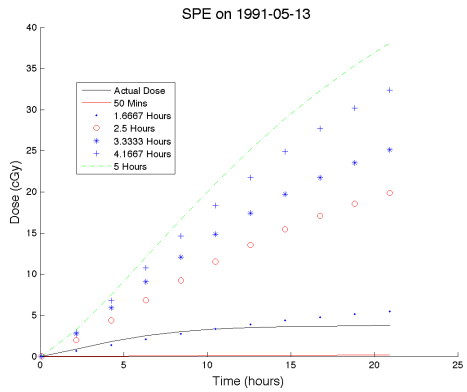
SPE on 1991-05-13
Actual Dose
50 Mins
1.6667 Hours
2.5 Hours
3.3333 Hours
4.1667 Hours
5 Hours
Dose (cGy)
Time (hours)

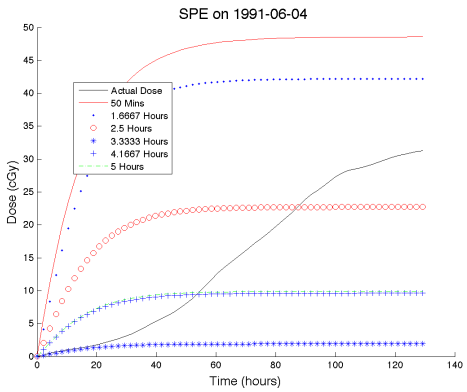
SPE on 1991-06-04
Actual Dose
50 Mins
1.6667 Hours
2.5 Hours
3.3333 Hours
4.1667 Hours
5 Hours
Dose (cGy)
Time (hours)

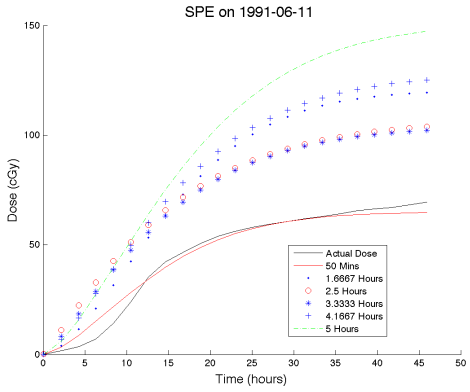
SPE on 1991-06-11
Dose (cGy)
Time (hours)
Actual Dose
50 Mins
1.6667 Hours
2.5 Hours
3.3333 Hours
4.1667 Hours
5 Hours

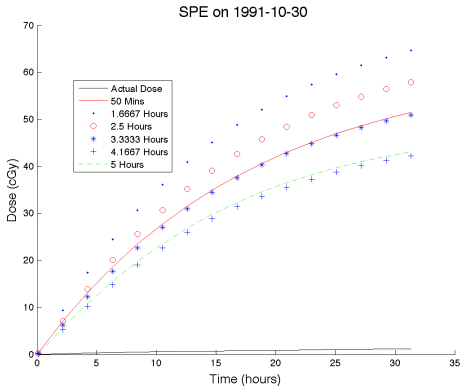
SPE on 1991-10-30
Dose (cGy)
Time (hours)
Actual Dose
50 Mins
1.6667 Hours
2.5 Hours
3.3333 Hours
4.1667 Hours
5 Hours

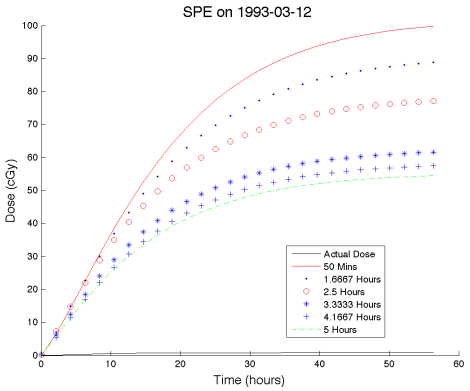
SPE on 1993-03-12
Dose (cGy)
Time (hours)
Actual Dose
50 Mins
1.6667 Hours
2.5 Hours
3.3333 Hours
4.1667 Hours
5 Hours

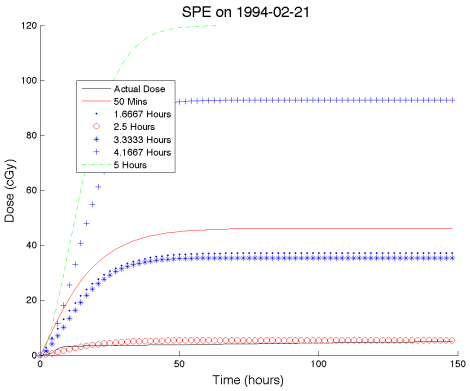
SPE on 1994-02-21
Dose (cGy)
Time (hours)
Actual Dose
50 Mins
1.6667 Hours
2.5 Hours
3.3333 Hours
4.1667 Hours
5 Hours

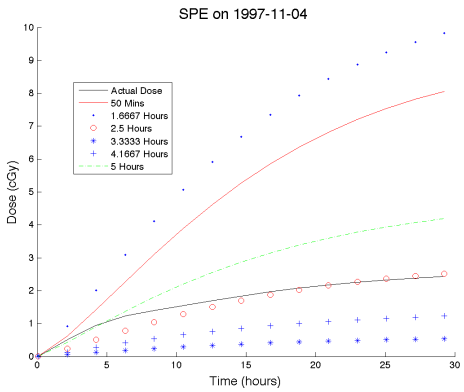
SPE on 1997-11-04
Dose (cGy)
Time (hours)
Actual Dose
50 Mins
1.6667 Hours
2.5 Hours
3.3333 Hours
4.1667 Hours
5 Hours

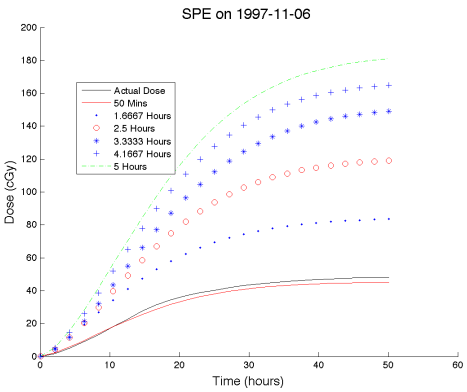
SPE on 1997-11-06
Dose (cGy)
Time (hours)
Actual Dose
50 Mins
1.6667 Hours
2.5 Hours
3.3333 Hours
4.1667 Hours
5 Hours

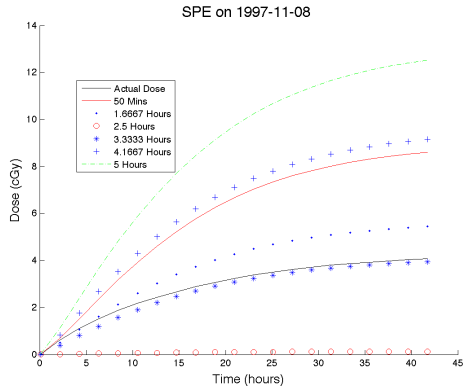
SPE on 1997-11-08
Actual Dose
50 Mins
1.6667 Hours
2.5 Hours
3.3333 Hours
4.1667 Hours
5 Hours
Dose (cGy)
Time (hours)

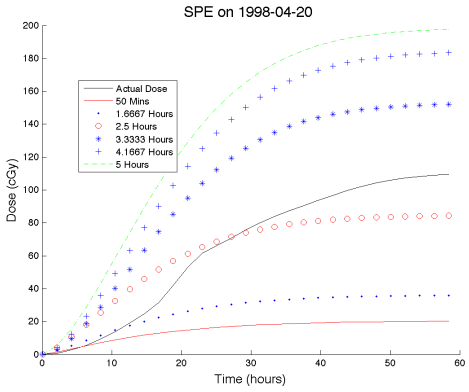
SPE on 1998-04-20
Actual Dose
50 Mins
1.6667 Hours
2.5 Hours
3.3333 Hours
4.1667 Hours
5 Hours
Dose (cGy)
Time (hours)

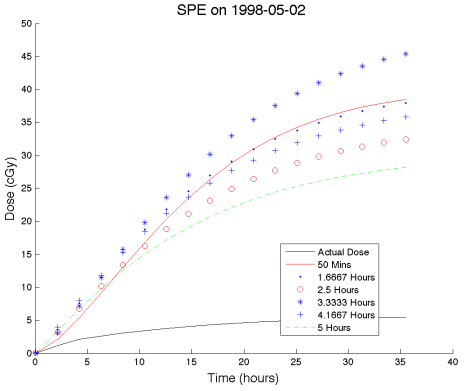
SPE on 1998-05-02
Actual Dose
50 Mins
1.6667 Hours
2.5 Hours
3.3333 Hours
4.1667 Hours
5 Hours
Dose (cGy)
Time (hours)

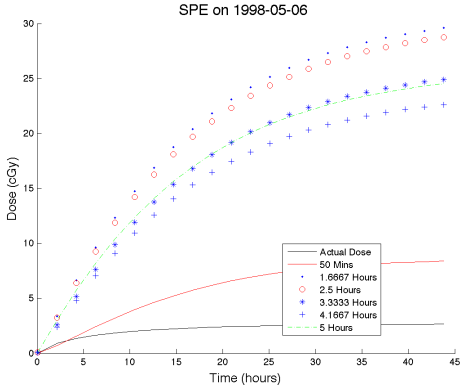
SPE on 1998-05-06
Actual Dose
50 Mins
1.6667 Hours
2.5 Hours
3.3333 Hours
4.1667 Hours
5 Hours
Dose (cGy)
Time (hours)

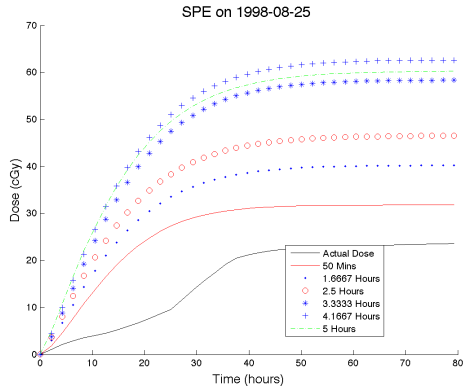
SPE on 1998-08-25
Actual Dose
50 Mins
1.6667 Hours
2.5 Hours
3.3333 Hours
4.1667 Hours
5 Hours
Dose (cGy)
Time (hours)

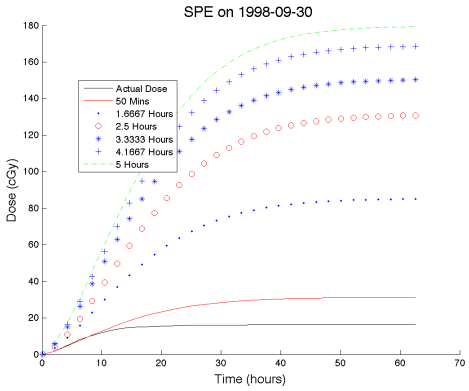
SPE on 1998-09-30
Actual Dose
50 Mins
1.6667 Hours
2.5 Hours
3.3333 Hours
4.1667 Hours
5 Hours
Dose (cGy)
Time (hours)

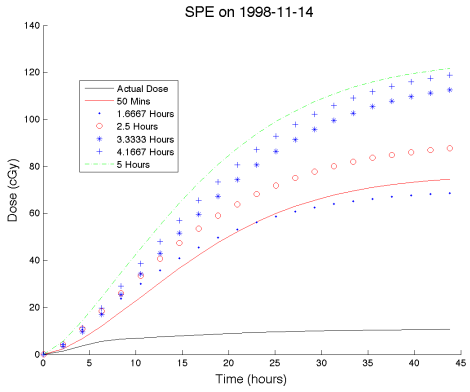
SPE on 1998-11-14
Dose (cGy)
Time (hours)
Actual Dose
50 Mins
1.6667 Hours
2.5 Hours
3.3333 Hours
4.1667 Hours
5 Hours

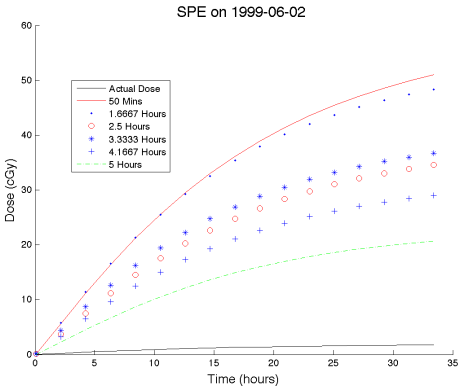
SPE on 1999-06-02
Dose (cGy)
Time (hours)
Actual Dose
50 Mins
1.6667 Hours
2.5 Hours
3.3333 Hours
4.1667 Hours
5 Hours

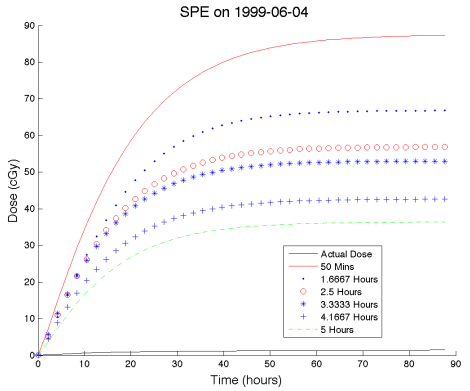
SPE on 1999-06-04
Dose (cGy)
Time (hours)
Actual Dose
50 Mins
1.6667 Hours
2.5 Hours
3.3333 Hours
4.1667 Hours
5 Hours

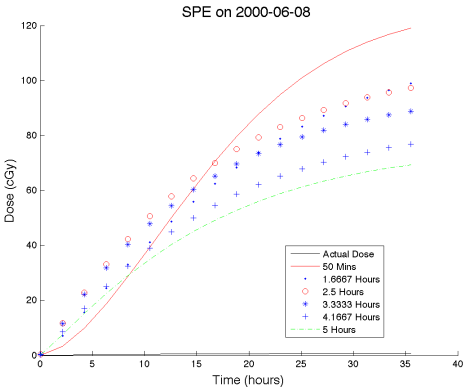
SPE on 2000-06-08
Dose (cGy)
Time (hours)
Actual Dose
50 Mins
1.6667 Hours
2.5 Hours
3.3333 Hours
4.1667 Hours
5 Hours

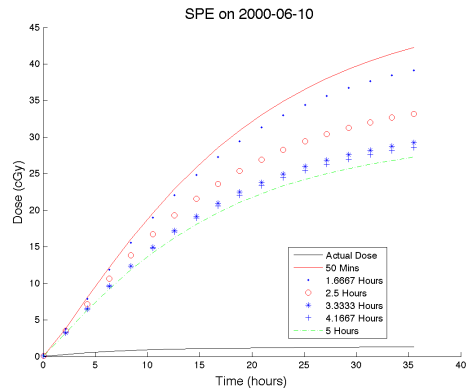
SPE on 2000-06-10
Dose (cGy)
Time (hours)
Actual Dose
50 Mins
1.6667 Hours
2.5 Hours
3.3333 Hours
4.1667 Hours
5 Hours

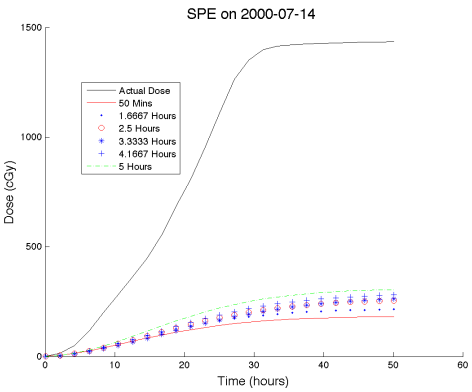
SPE on 2000-07-14
Dose (cGy)
Time (hours)
Actual Dose
50 Mins
1.6667 Hours
2.5 Hours
3.3333 Hours
4.1667 Hours
5 Hours

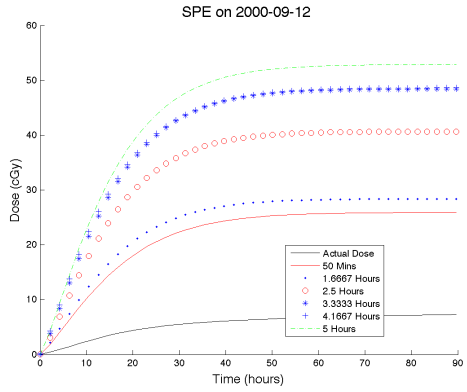
SPE on 2000-09-12
Dose (cGy)
Time (hours)
Actual Dose
50 Mins
1.6667 Hours
2.5 Hours
3.3333 Hours
4.1667 Hours
5 Hours

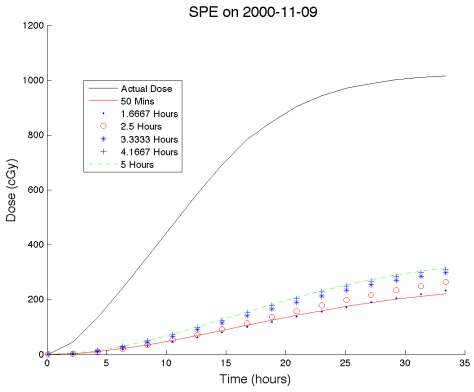
SPE on 2000-11-09
Dose (cGy)
Time (hours)
Actual Dose
50 Mins
1.6667 Hours
2.5 Hours
3.3333 Hours
4.1667 Hours
5 Hours

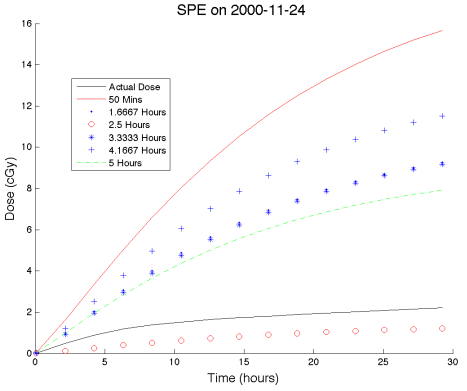
SPE on 2000-11-24
Dose (cGy)
Time (hours)
Actual Dose
50 Mins
1.6667 Hours
2.5 Hours
3.3333 Hours
4.1667 Hours
5 Hours

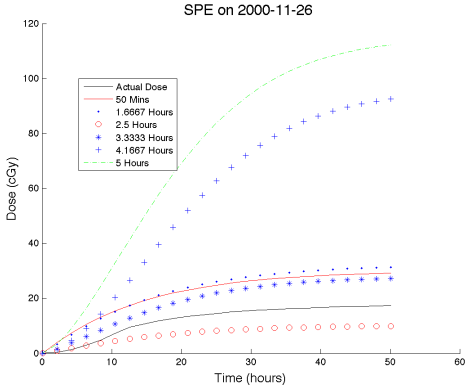
SPE on 2000-11-26
Dose (cGy)
Time (hours)
Actual Dose
50 Mins
1.6667 Hours
2.5 Hours
3.3333 Hours
4.1667 Hours
5 Hours

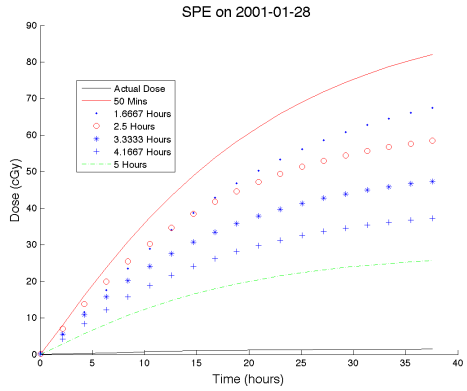
SPE on 2001-01-28
Dose (cGy)
Time (hours)
Actual Dose
50 Mins
1.6667 Hours
2.5 Hours
3.3333 Hours
4.1667 Hours
5 Hours

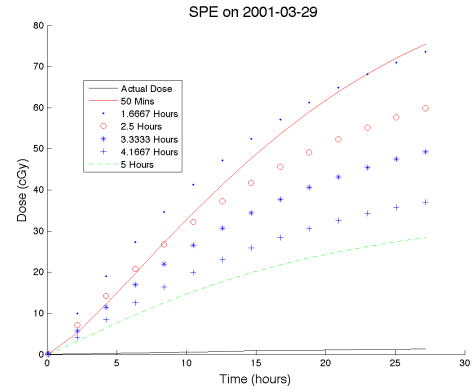
SPE on 2001-03-29
Dose (cGy)
Time (hours)
Actual Dose
50 Mins
1.6667 Hours
2.5 Hours
3.3333 Hours
4.1667 Hours
5 Hours

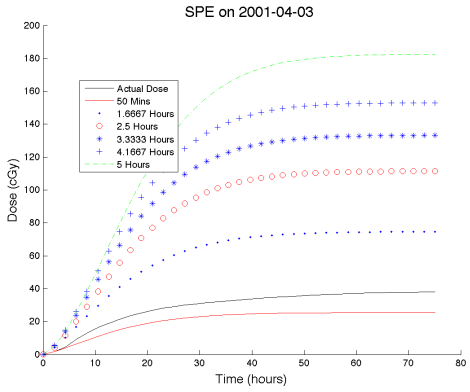
SPE on 2001-04-03
Actual Dose
50 Mins
1.6667 Hours
2.5 Hours
3.3333 Hours
4.1667 Hours
5 Hours
Dose (cGy)
Time (hours)

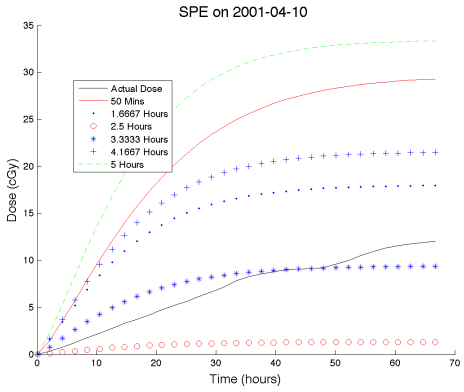
SPE on 2001-04-10
Actual Dose
50 Mins
1.6667 Hours
2.5 Hours
3.3333 Hours
4.1667 Hours
5 Hours
Dose (cGy)
Time (hours)

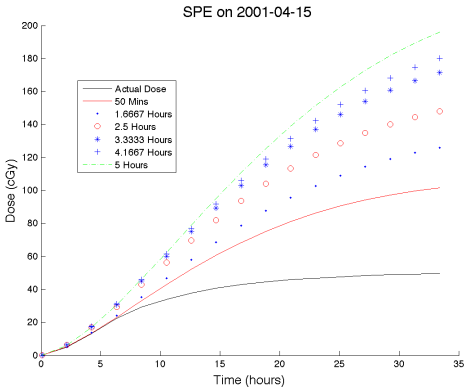
SPE on 2001-04-15
Actual Dose
50 Mins
1.6667 Hours
2.5 Hours
3.3333 Hours
4.1667 Hours
5 Hours
Dose (cGy)
Time (hours)

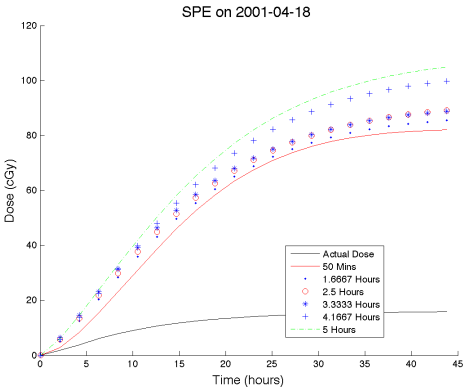
SPE on 2001-04-18
Actual Dose
50 Mins
1.6667 Hours
2.5 Hours
3.3333 Hours
4.1667 Hours
5 Hours
Dose (cGy)
Time (hours)

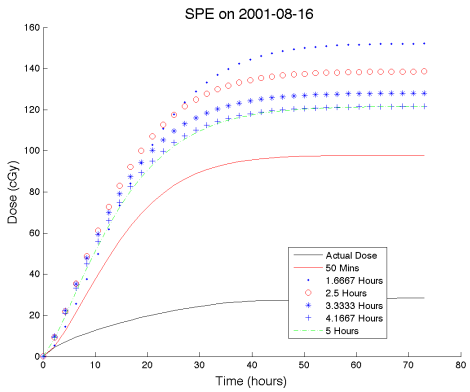
SPE on 2001-08-16
Actual Dose
50 Mins
1.6667 Hours
2.5 Hours
3.3333 Hours
4.1667 Hours
5 Hours
Dose (cGy)
Time (hours)

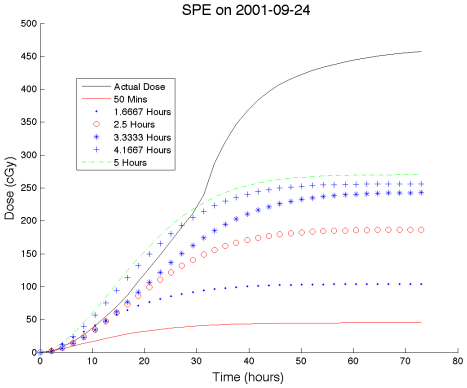
SPE on 2001-09-24
Actual Dose
50 Mins
1.6667 Hours
2.5 Hours
3.3333 Hours
4.1667 Hours
5 Hours
Dose (cGy)
Time (hours)

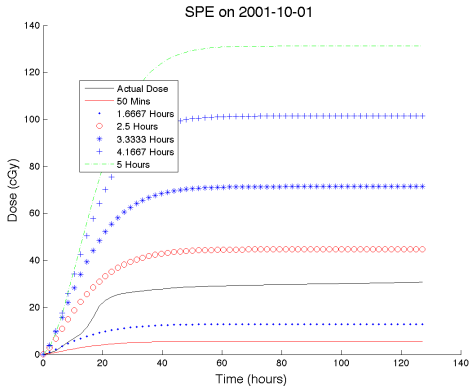
SPE on 2001-10-01
Dose (cGy)
Time (hours)
Actual Dose
50 Mins
1.6667 Hours
2.5 Hours
3.3333 Hours
4.1667 Hours
5 Hours

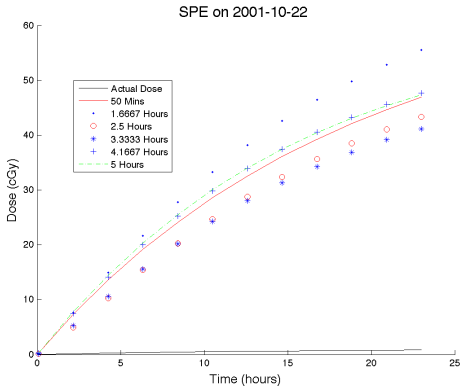
SPE on 2001-10-22
Dose (cGy)
Time (hours)
Actual Dose
50 Mins
1.6667 Hours
2.5 Hours
3.3333 Hours
4.1667 Hours
5 Hours

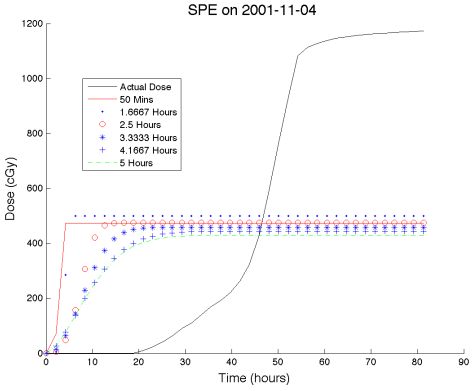
SPE on 2001-11-04
Dose (cGy)
Time (hours)
Actual Dose
50 Mins
1.6667 Hours
2.5 Hours
3.3333 Hours
4.1667 Hours
5 Hours

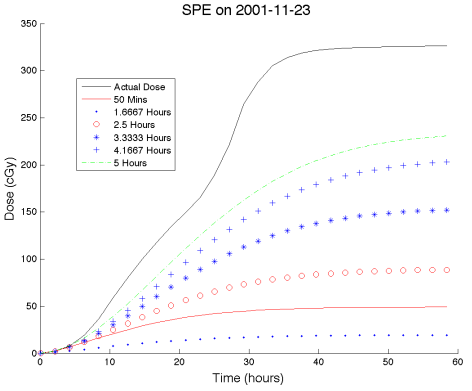
SPE on 2001-11-23
Dose (cGy)
Time (hours)
Actual Dose
50 Mins
1.6667 Hours
2.5 Hours
3.3333 Hours
4.1667 Hours
5 Hours

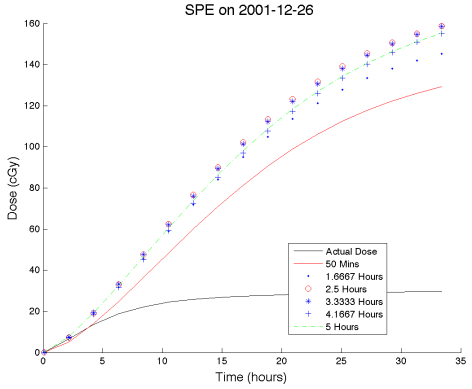
SPE on 2001-12-26
Dose (cGy)
Time (hours)
Actual Dose
50 Mins
1.6667 Hours
2.5 Hours
3.3333 Hours
4.1667 Hours
5 Hours

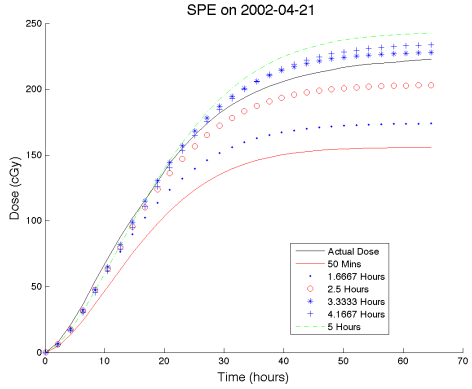
SPE on 2002-04-21
Dose (cGy)
Time (hours)
Actual Dose
50 Mins
1.6667 Hours
2.5 Hours
3.3333 Hours
4.1667 Hours
5 Hours

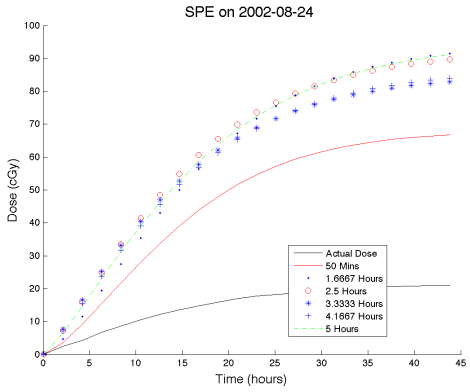
SPE on 2002-08-24
Dose (cGy)
Time (hours)
Actual Dose
50 Mins
1.6667 Hours
2.5 Hours
3.3333 Hours
4.1667 Hours
5 Hours

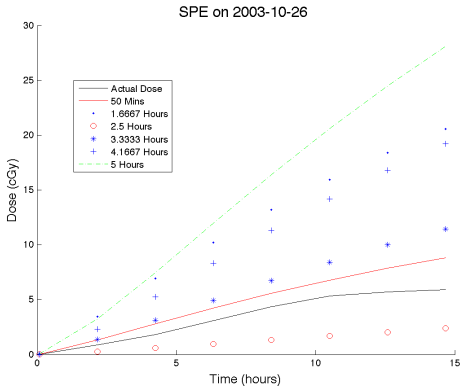
SPE on 2003-10-26
Dose (cGy)
Time (hours)
Actual Dose
50 Mins
1.6667 Hours
2.5 Hours
3.3333 Hours
4.1667 Hours
5 Hours

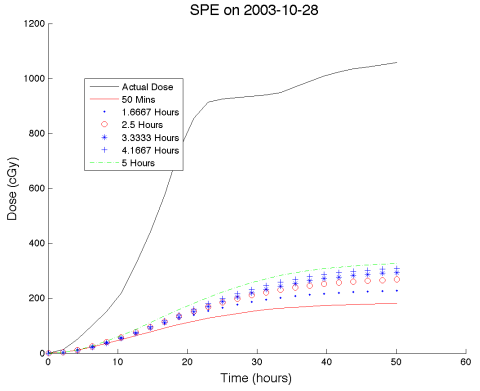
SPE on 2003-10-28
Dose (cGy)
Time (hours)
Actual Dose
50 Mins
1.6667 Hours
2.5 Hours
3.3333 Hours
4.1667 Hours
5 Hours

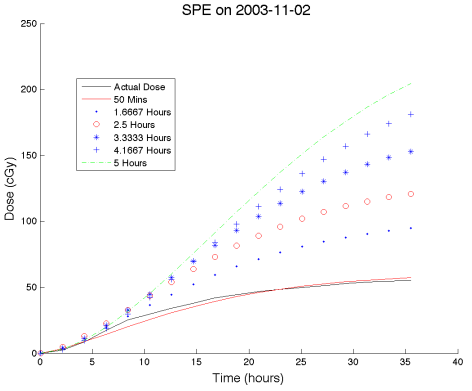
SPE on 2003-11-02
Dose (cGy)
Time (hours)
Actual Dose
50 Mins
1.6667 Hours
2.5 Hours
3.3333 Hours
4.1667 Hours
5 Hours

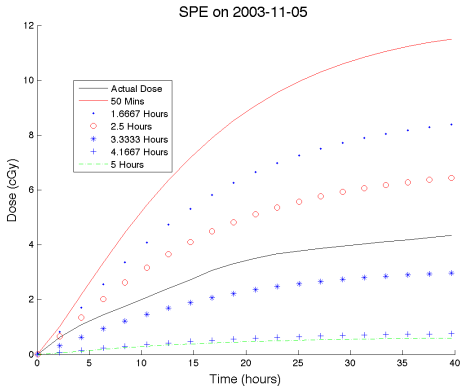
SPE on 2003-11-05
Dose (cGy)
Time (hours)
Actual Dose
50 Mins
1.6667 Hours
2.5 Hours
3.3333 Hours
4.1667 Hours
5 Hours

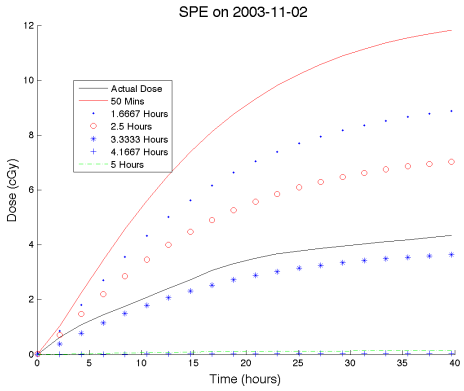
SPE on 2003-11-02
Dose (cGy)
Time (hours)
Actual Dose
50 Mins
1.6667 Hours
2.5 Hours
3.3333 Hours
4.1667 Hours
5 Hours

D Forecasts only for SPEs < 145 cGy

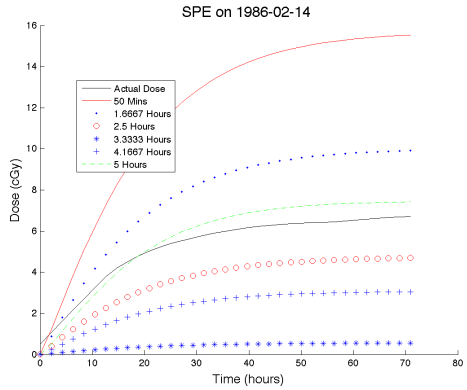

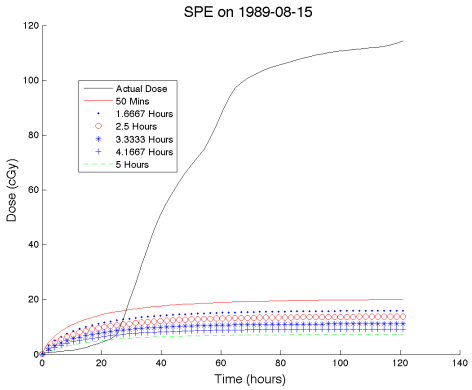

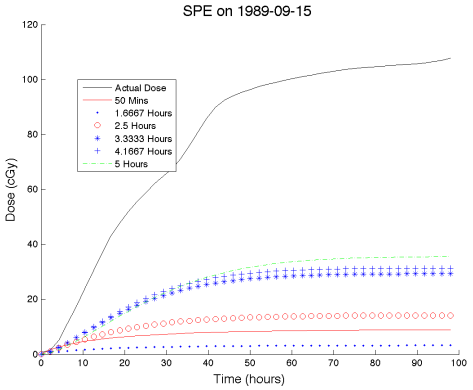

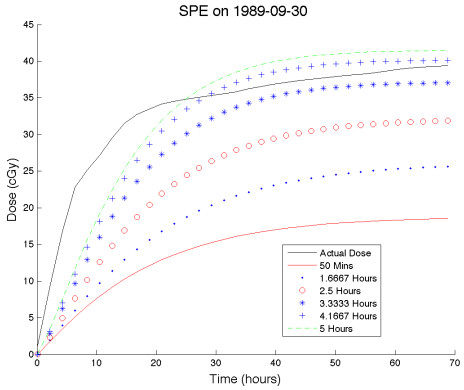

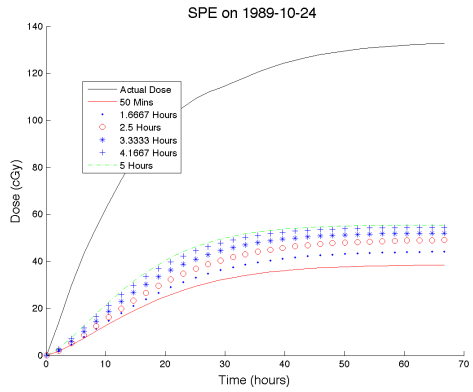

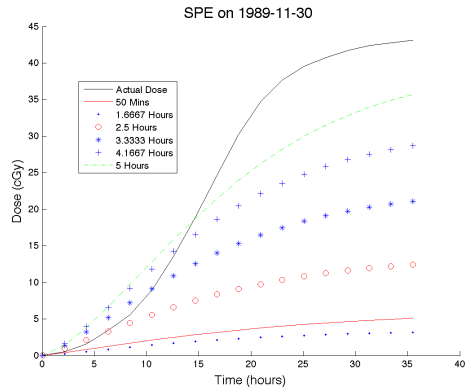

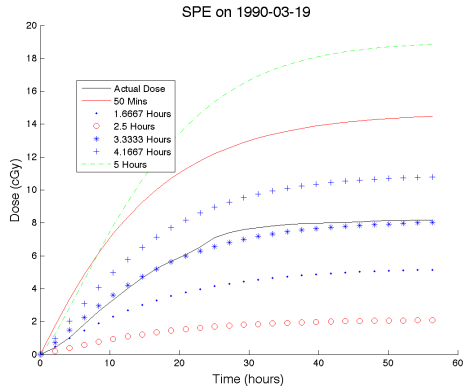
SPE on 1990-03-19
Actual Dose
50 Mins
1.6667 Hours
2.5 Hours
3.3333 Hours
4.1667 Hours
5 Hours
Dose (cGy)
Time (hours)

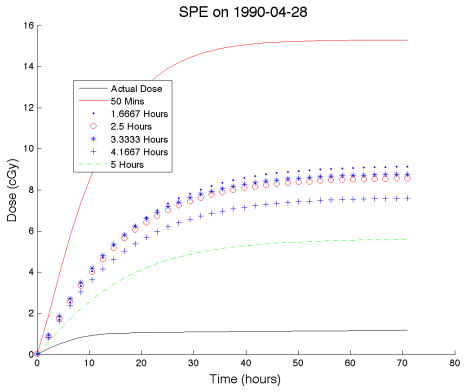
SPE on 1990-04-28
Actual Dose
50 Mins
1.6667 Hours
2.5 Hours
3.3333 Hours
4.1667 Hours
5 Hours
Dose (cGy)
Time (hours)

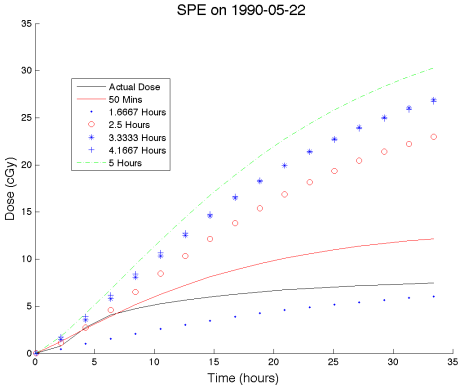
SPE on 1990-05-22
Actual Dose
50 Mins
1.6667 Hours
2.5 Hours
3.3333 Hours
4.1667 Hours
5 Hours
Dose (cGy)
Time (hours)

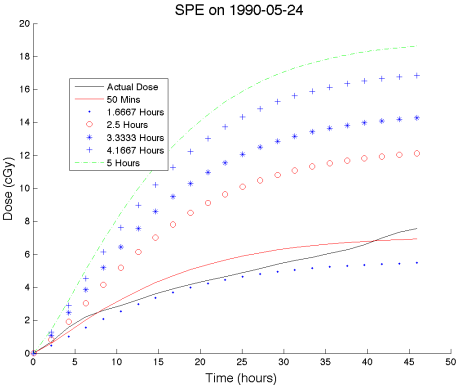
SPE on 1990-05-24
Actual Dose
50 Mins
1.6667 Hours
2.5 Hours
3.3333 Hours
4.1667 Hours
5 Hours
Dose (cGy)
Time (hours)

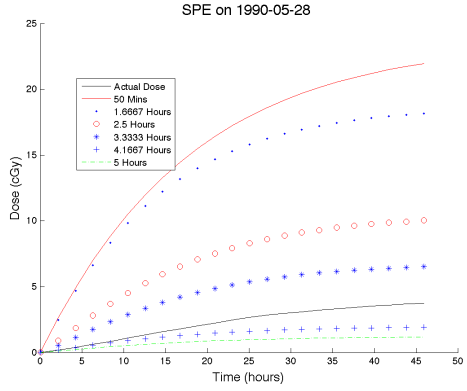
SPE on 1990-05-28
Actual Dose
50 Mins
1.6667 Hours
2.5 Hours
3.3333 Hours
4.1667 Hours
5 Hours
Dose (cGy)
Time (hours)

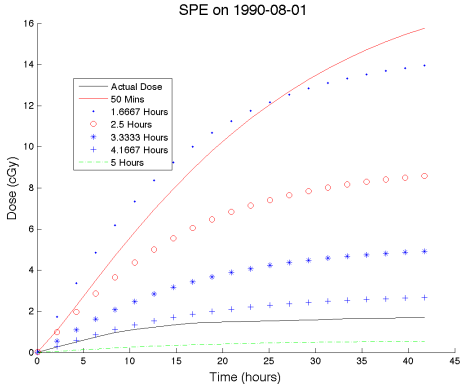
SPE on 1990-08-01
Actual Dose
50 Mins
1.6667 Hours
2.5 Hours
3.3333 Hours
4.1667 Hours
5 Hours
Dose (cGy)
Time (hours)

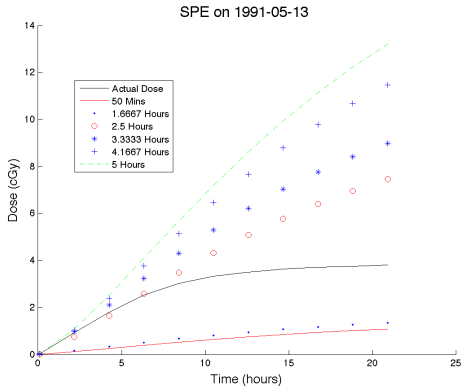
SPE on 1991-05-13
Actual Dose
50 Mins
1.6667 Hours
2.5 Hours
3.3333 Hours
4.1667 Hours
5 Hours
Dose (cGy)
Time (hours)

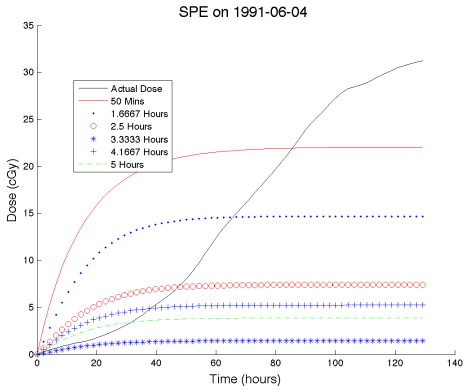
SPE on 1991-06-04
Actual Dose
50 Mins
1.6667 Hours
2.5 Hours
3.3333 Hours
4.1667 Hours
5 Hours
Dose (cGy)
Time (hours)

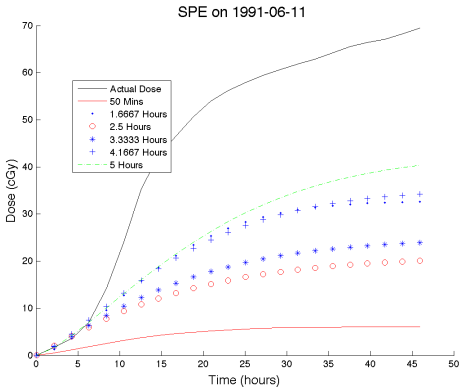
SPE on 1991-06-11
Actual Dose
50 Mins
1.6667 Hours
2.5 Hours
3.3333 Hours
4.1667 Hours
5 Hours
Dose (cGy)
Time (hours)

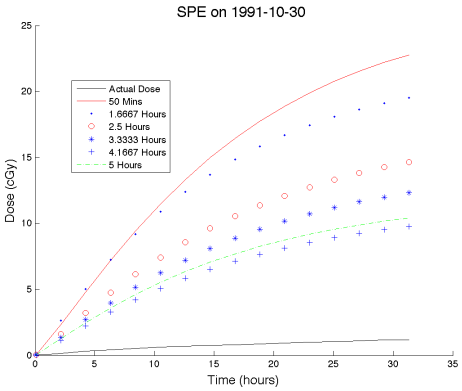
SPE on 1991-10-30
Actual Dose
50 Mins
1.6667 Hours
2.5 Hours
3.3333 Hours
4.1667 Hours
5 Hours
Dose (cGy)
Time (hours)

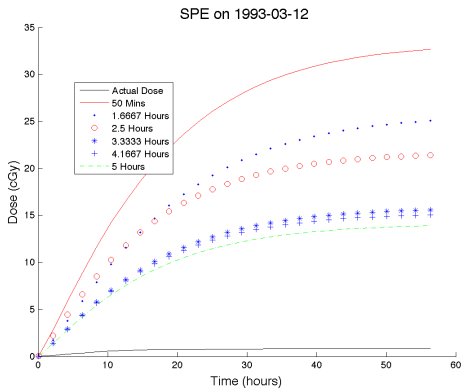
SPE on 1993-03-12
Actual Dose
50 Mins
1.6667 Hours
2.5 Hours
3.3333 Hours
4.1667 Hours
5 Hours
Dose (cGy)
Time (hours)

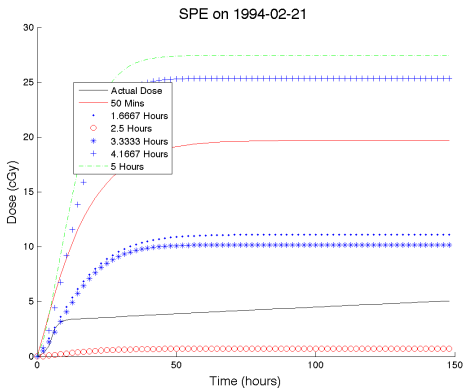
SPE on 1994-02-21
Actual Dose
50 Mins
1.6667 Hours
2.5 Hours
3.3333 Hours
4.1667 Hours
5 Hours
Dose (cGy)
Time (hours)

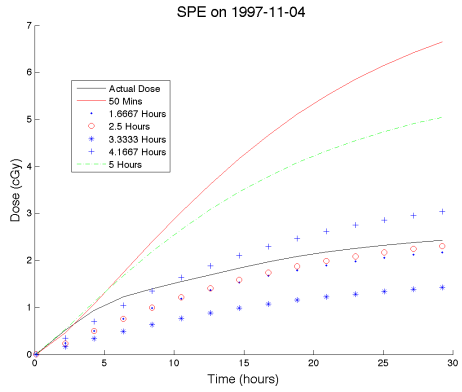
SPE on 1997-11-04
Actual Dose
50 Mins
1.6667 Hours
2.5 Hours
3.3333 Hours
4.1667 Hours
5 Hours
Dose (cGy)
Time (hours)

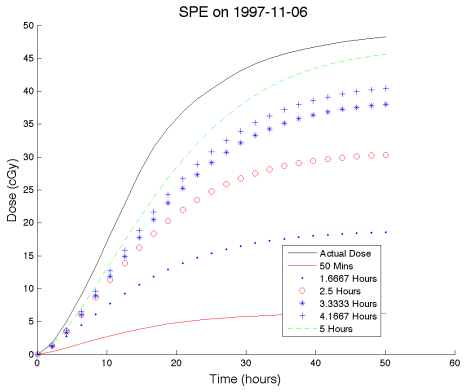
SPE on 1997-11-06
Actual Dose
50 Mins
1.6667 Hours
2.5 Hours
3.3333 Hours
4.1667 Hours
5 Hours
Dose (cGy)
Time (hours)

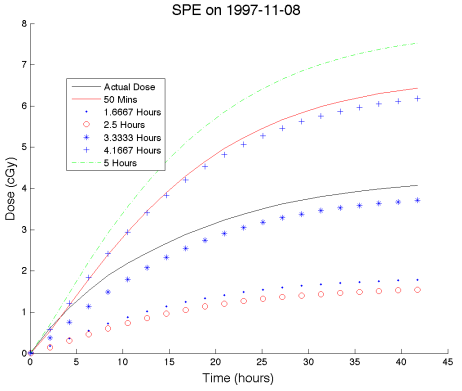
SPE on 1997-11-08
Actual Dose
50 Mins
1.6667 Hours
2.5 Hours
3.3333 Hours
4.1667 Hours
5 Hours
Dose (cGy)
Time (hours)

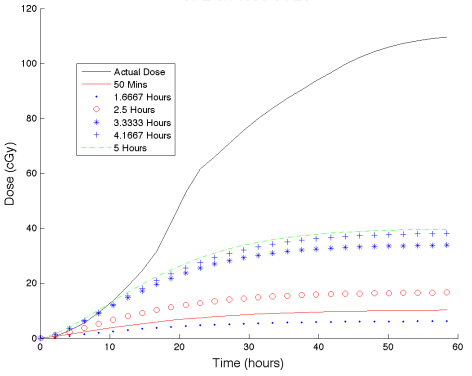
SPE on 1998-04-20
Actual Dose
50 Mins
1.6667 Hours
2.5 Hours
3.3333 Hours
4.1667 Hours
5 Hours
Dose (cGy)
Time (hours)

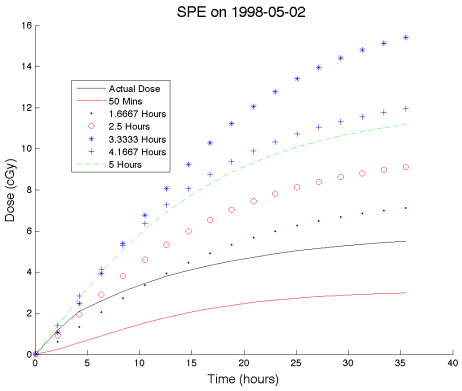
SPE on 1998-05-02
Actual Dose
50 Mins
1.6667 Hours
2.5 Hours
3.3333 Hours
4.1667 Hours
5 Hours
Dose (cGy)
Time (hours)

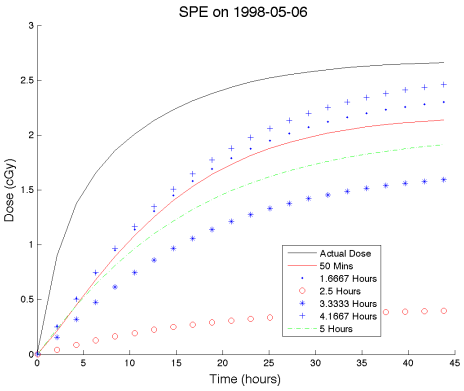
SPE on 1998-05-06
Actual Dose
50 Mins
1.6667 Hours
2.5 Hours
3.3333 Hours
4.1667 Hours
5 Hours
Dose (cGy)
Time (hours)

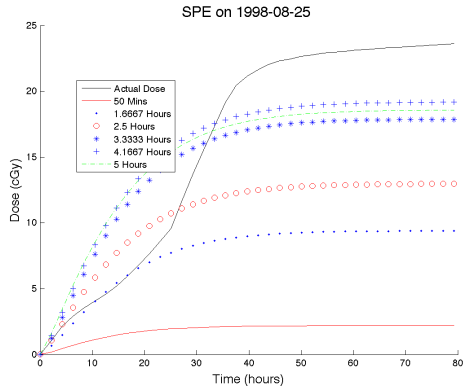
SPE on 1998-08-25
Actual Dose
50 Mins
1.6667 Hours
2.5 Hours
3.3333 Hours
4.1667 Hours
5 Hours
Dose (cGy)
Time (hours)

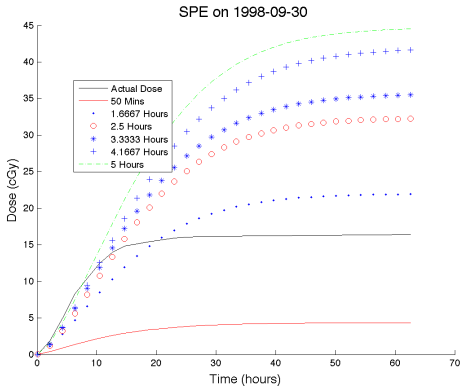
SPE on 1998-09-30
Actual Dose
50 Mins
1.6667 Hours
2.5 Hours
3.3333 Hours
4.1667 Hours
5 Hours
Dose (cGy)
Time (hours)

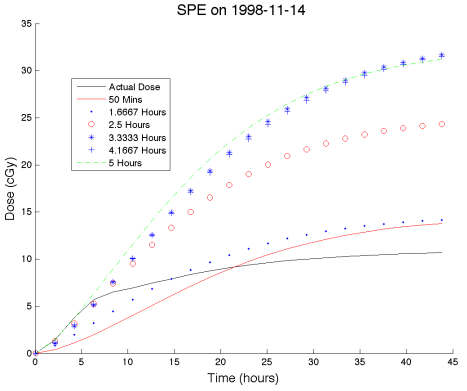
SPE on 1998-11-14
Actual Dose
50 Mins
1.6667 Hours
2.5 Hours
3.3333 Hours
4.1667 Hours
5 Hours
Dose (cGy)
Time (hours)

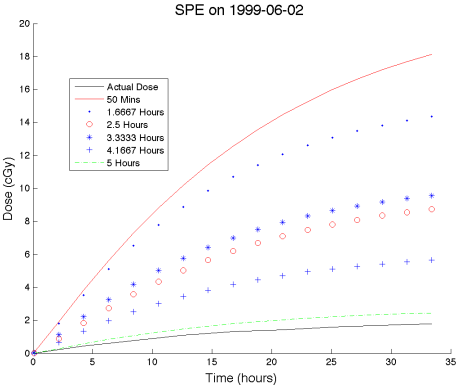
SPE on 1999-06-02
Actual Dose
50 Mins
1.6667 Hours
2.5 Hours
3.3333 Hours
4.1667 Hours
5 Hours
Dose (cGy)
Time (hours)

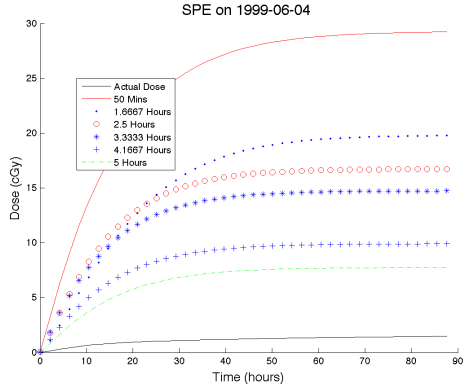
SPE on 1999-06-04
Actual Dose
50 Mins
1.6667 Hours
2.5 Hours
3.3333 Hours
4.1667 Hours
5 Hours
Dose (cGy)
Time (hours)

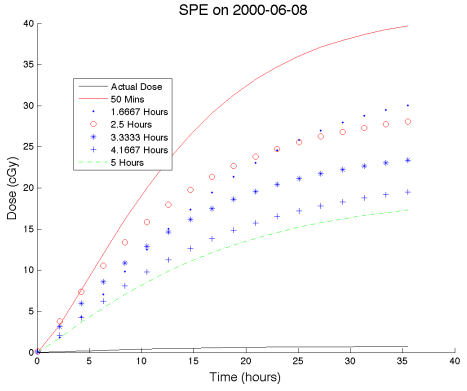
SPE on 2000-06-08
Actual Dose
50 Mins
1.6667 Hours
2.5 Hours
3.3333 Hours
4.1667 Hours
5 Hours
Dose (cGy)
Time (hours)

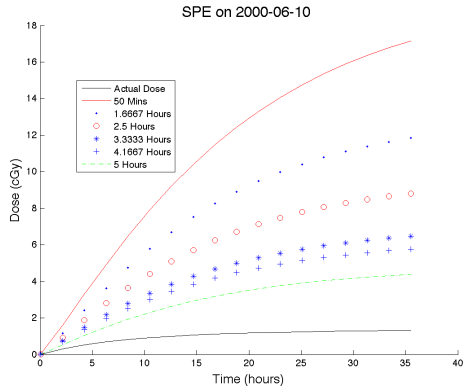
SPE on 2000-06-10
Actual Dose
50 Mins
1.6667 Hours
2.5 Hours
3.3333 Hours
4.1667 Hours
5 Hours
Dose (cGy)
Time (hours)

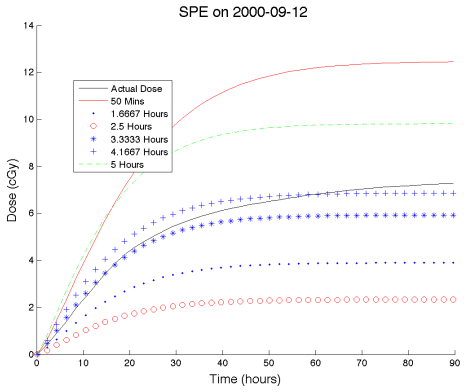
SPE on 2000-09-12
Actual Dose
50 Mins
1.6667 Hours
2.5 Hours
3.3333 Hours
4.1667 Hours
5 Hours
Dose (cGy)
Time (hours)

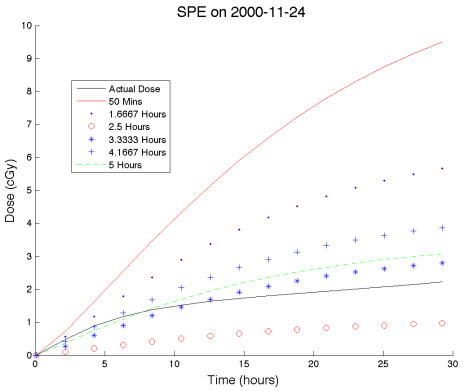
SPE on 2000-11-24
Actual Dose
50 Mins
1.6667 Hours
2.5 Hours
3.3333 Hours
4.1667 Hours
5 Hours
Dose (cGy)
Time (hours)

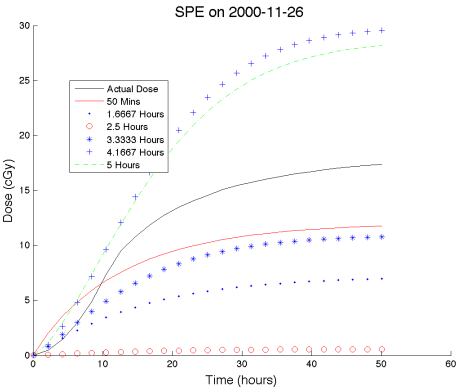
SPE on 2000-11-26
Actual Dose
50 Mins
1.6667 Hours
2.5 Hours
3.3333 Hours
4.1667 Hours
5 Hours
Dose (cGy)
Time (hours)

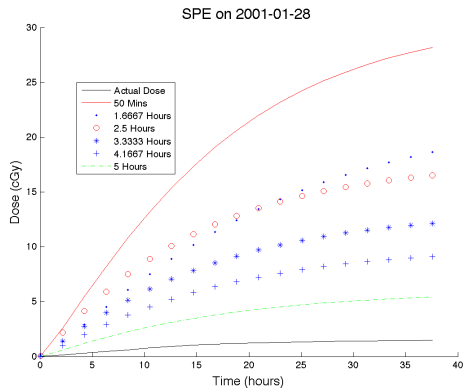
SPE on 2001-01-28
Actual Dose
50 Mins
1.6667 Hours
2.5 Hours
3.3333 Hours
4.1667 Hours
5 Hours
Dose (cGy)
Time (hours)

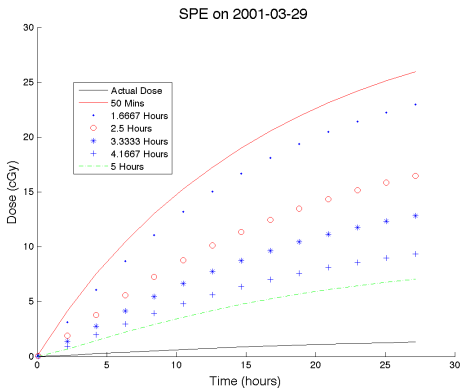
SPE on 2001-03-29
Actual Dose
50 Mins
1.6667 Hours
2.5 Hours
3.3333 Hours
4.1667 Hours
5 Hours
Dose (cGy)
Time (hours)

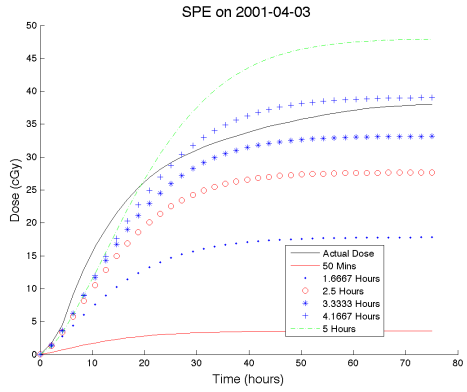
SPE on 2001-04-03
Dose (cGy)
Time (hours)
Actual Dose
50 Mins
1.6667 Hours
2.5 Hours
3.3333 Hours
4.1667 Hours
5 Hours

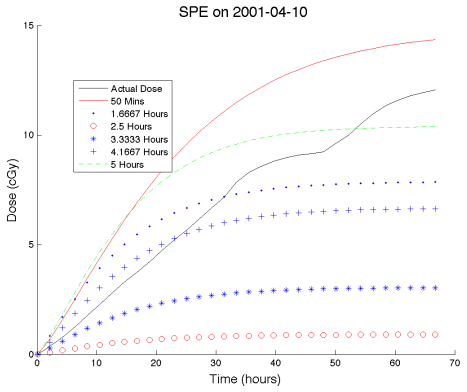
SPE on 2001-04-10
Dose (cGy)
Time (hours)
Actual Dose
50 Mins
1.6667 Hours
2.5 Hours
3.3333 Hours
4.1667 Hours
5 Hours

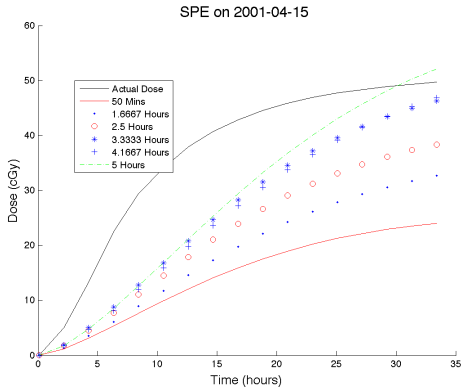
SPE on 2001-04-15
Dose (cGy)
Time (hours)
Actual Dose
50 Mins
1.6667 Hours
2.5 Hours
3.3333 Hours
4.1667 Hours
5 Hours

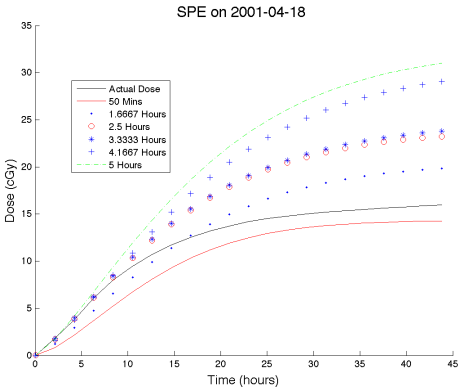
SPE on 2001-04-18
Dose (cGy)
Time (hours)
Actual Dose
50 Mins
1.6667 Hours
2.5 Hours
3.3333 Hours
4.1667 Hours
5 Hours

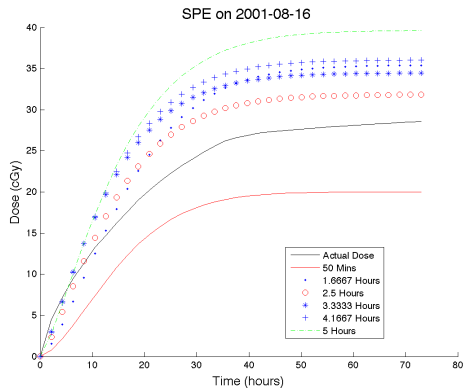
SPE on 2001-08-16
Dose (cGy)
Time (hours)
Actual Dose
50 Mins
1.6667 Hours
2.5 Hours
3.3333 Hours
4.1667 Hours
5 Hours

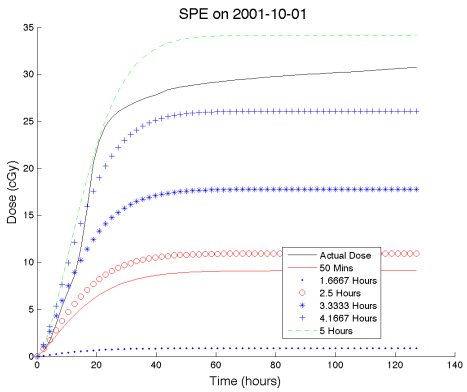
SPE on 2001-10-01
Dose (cGy)
Time (hours)
Actual Dose
50 Mins
1.6667 Hours
2.5 Hours
3.3333 Hours
4.1667 Hours
5 Hours

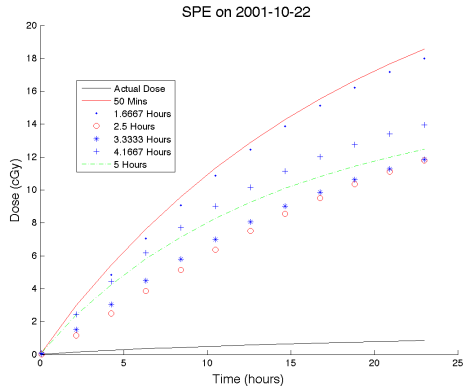
SPE on 2001-10-22
Actual Dose
50 Mins
1.6667 Hours
2.5 Hours
3.3333 Hours
4.1667 Hours
5 Hours
Dose (cGy)
Time (hours)

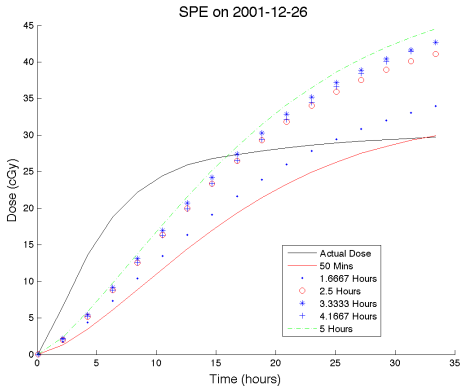
SPE on 2001-12-26
Actual Dose
50 Mins
1.6667 Hours
2.5 Hours
3.3333 Hours
4.1667 Hours
5 Hours
Dose (cGy)
Time (hours)

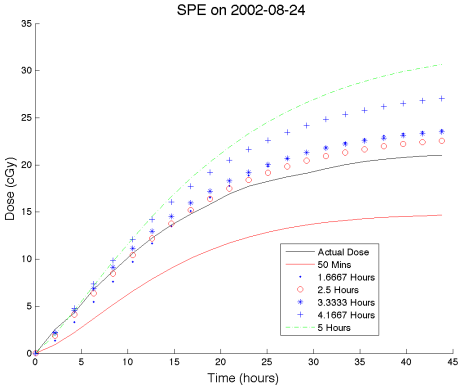
SPE on 2002-08-24
Actual Dose
50 Mins
1.6667 Hours
2.5 Hours
3.3333 Hours
4.1667 Hours
5 Hours
Dose (cGy)
Time (hours)

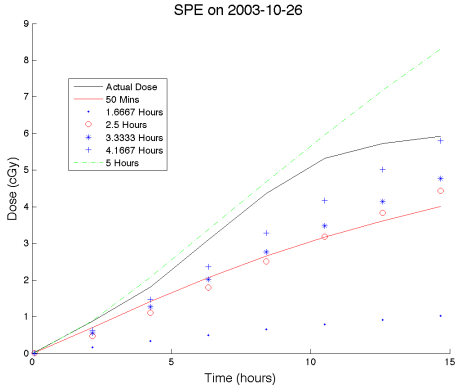
SPE on 2003-10-26
Actual Dose
50 Mins
1.6667 Hours
2.5 Hours
3.3333 Hours
4.1667 Hours
5 Hours
Dose (cGy)
Time (hours)

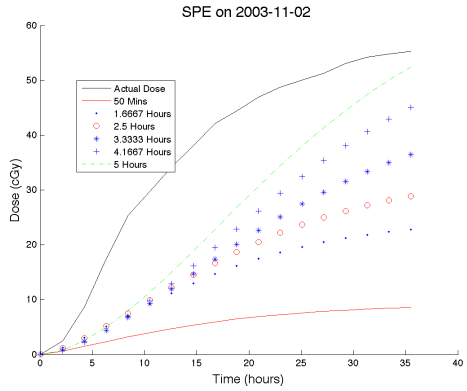
SPE on 2003-11-02
Actual Dose
50 Mins
1.6667 Hours
2.5 Hours
3.3333 Hours
4.1667 Hours
5 Hours
Dose (cGy)
Time (hours)

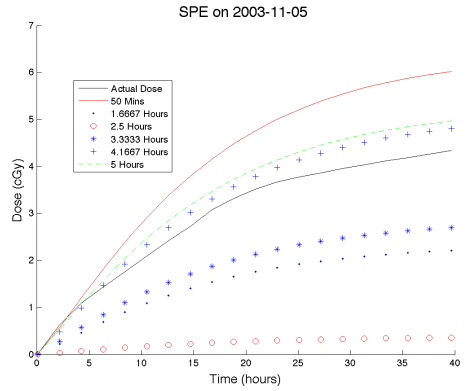
SPE on 2003-11-05
Actual Dose
50 Mins
1.6667 Hours
2.5 Hours
3.3333 Hours
4.1667 Hours
5 Hours
Dose (cGy)
Time (hours)

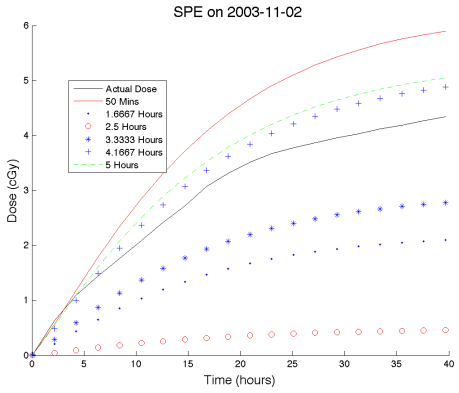
SPE on 2003-11-02
Actual Dose
50 Mins
1.6667 Hours
2.5 Hours
3.3333 Hours
4.1667 Hours
5 Hours
Dose (cGy)
Time (hours)
0
1
2
3
4
5
6
0
5
10
15
20
25
30
35
40

Vita

Theodore Franklin Nichols was born on January 28, 1980 in Memphis, Tennessee. His family moved to Knoxville, Tennessee in the summer of 1986. He attended West High School in Knoxville. In 1996 Theodore was awarded the Eagle Scout award from the Boy Scouts of America. He rowed crew in both high school and for his freshman year of college. The fall of 1998 he enrolled at the University of Tennessee where he majored in Physics. He was president of the Student Physics Society from fall of 2001 to the spring of 2002. May of 2002 he was received a bachelors degree in Physics. The fall of 2002 he entered the Master of Science program for Nuclear Engineering. Theodore received a Master of Science in Nuclear Engineering in August 2005 and the title of his thesis is "Using Artificial Intelligence Methods To Predict Doses From Large Solar Particle Events In Space". After completing his Master of Science, Theodore enrolled in the Ph. D. program for Nuclear Engineering. August of 2006 he took and passed the Ph. D. qualifying exam. On June 30, 2007 he married Stacey J. Horn, who is an English teacher.